Control of Carbon Nanotube Stiffness via Tunable Fabrication Process Parameters that Determine CNT Geometry

by

Michael A. Cullinan

B.S., Engineering (2006)
B.A., Economics (2006)

Swarthmore College

Submitted to the Department of Mechanical Engineering
in Partial Fulfillment of the Requirements for the Degree of
Master of Science

at the

Massachusetts Institute of Technology

February 2008

Signature of Author.....
Department of Mechanical Engineering
January 17, 2008

Certified by.....
Martin L. Culpepper
Associate Professor of Mechanical Engineering
Thesis Supervisor

Accepted by.....
Lallit Anand
Professor of Mechanical Engineering
Graduate Officer

Control of Carbon Nanotube Stiffness via Control
of Fabrication Process Parameters that Determine CNT Geometry

by

Michael A Cullinan

Submitted to the Department of Mechanical Engineering
on January 17, 2008 in Partial Fulfillment of the
requirements for the Degree of Master of Science

ABSTRACT

This paper presents tunable process parameters that may be used to control the geometry of multi-walled carbon nanotubes (MWCNTs). The results may be used to grow MWCNTs with desired stiffness properties. This is important to devices that rely on the compliance of MWCNTs in order to achieve specific performance requirements, e.g. deflection or stiffness. Examples of these types of devices include relays, resonators and flexural bearings for small-scale actuators. It is necessary to control the stiffness of these mechanisms because the force, stroke, and device bandwidth depend upon the stiffness of the constituent MWCNTs. For a given length MWCNT, the stiffness is controlled by the MWCNT diameter and the number of walls in the MWCNT. Herein we present a growth model that was generated via statistical and experimental analysis. The diameter and number of walls are controlled by adjusting several growth parameters – temperature, catalyst film thickness, and hydrocarbon concentration. The model is then used to design a growth process for specific applications. The results of these growths show that the geometry of the CNTs can be accurately controlled to within 6% of the desired geometry. Based on the measured geometries, it was estimated that the stiffness and natural frequency can be accurately controlled to within 1.5% of the desired values.

ACKNOWLEDGEMENTS

I would like to thank Professor Martin Culpepper for giving me an opportunity to work on this project and Karl Chang for providing funding for this project through the MIT Karl Chang Innovation Grant. I would also like to thank Neil Pappalardo for providing my funding for the first year through the Pappalardo Fellowship. I would especially like to thank Christopher DiBiasio for all his help on this project in setting up the CNT furnace. Finally, I would like to thank Robert Panas for proof reading this thesis.

Table of Contents

List of Figures

List of Tables

Chapter

1

Introduction

1.1 Introduction

The purpose of this research is to generate the knowledge – a method and process – that is required to manufacture carbon nanotubes that posses desired stiffness characteristics. This will enable the engineering of nano-scale compliant mechanisms that could be used to create nanomechanical relays, resonators, and flexural bearings. It is important to control the stiffness of such mechanisms because the force, stroke, and bandwidth are dependent upon the stiffness. Therefore, by controlling the stiffness of the CNTs, we should be able to design and manufacture CNT-based compliant mechanisms with the desired performance characteristics for many high-speed and high-stroke applications.

A good example of a CNT-based compliant mechanism is the linear flexural bearing shown in Figure 1. This ubiquitous nanomechanical building block is envisioned for use in emerging applications such as CNT-based non-volatile memory, force-displacement transducers and high speed probes for nano-scale research and manufacturing applications. The unique physical properties of CNTs make these applications possible. We must be able to design such devices to satisfy specific functional requirements such as range, resolution and speed in order to be able to make such devices practical for use in nanoelectromechanical systems (NEMS).

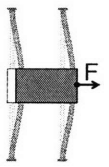

Figure 1.1. Carbon nanotube based linear flexural bearing.

For example, the flexural bearing in Figure 1.1 could be used to guide a probe for electric discharge machining at the nanometer scale (nano-EDM) [1]. Nano-EDM is a promising application because it will enable the creation of sub-micron features at high frequencies (> 1 GHz). In order to do this we must be able to accurately control the distance between the probe and the surface. For a force-based actuator, this distance is controlled by the force produce by the actuator and the stiffness of the flexural elements which in this case are the CNTs. The displacement resolution of the device is also affected by the stiffness of the flexural CNTs as seen in Equation 1.1 where the force resolution is set by the force-based actuator. The stiffness is a function of the CNT geometry; therefore the displacement resolution may be set by altering the diameter and wall thickness of the CNT. The results that will be presented in this thesis show that the CNT geometry can be controlled to within about 6% of the desired geometry. This allows for accurate control over the stiffness of CNT based devices. For example, it is estimated that the stiffness of the devices presented in Figure 1 can be controlled to within 1% of the desired stiffness.

$$\text{Displacement Resolution} = \frac{\text{Force Resolution}}{\text{Stiffness}} \tag{1.1}$$

The frequency at which the nano-EDM can write features is directly related to the stiffness of the flexural CNTs as seen in Equation 1.2 [2], where k is the stiffness of the CNTs, m is the mass of the positioning stage plus the mass of the probe, and f is the natural frequency in Hertz.

$$f = \frac{1}{2\pi}\sqrt{\frac{k}{m}} \tag{1.2}$$

We must, therefore, be able to control the stiffness of the CNTs in order to produce the desired resolution and speed requirements of the nano-EDM. Again, the stiffness is a function of the geometry of the CNT. Relationships between the CNT growth process parameters and the final CNT geometry must, therefore, be determined in order achieve

the desired resolution and frequency requirements of specific applications. The results in this thesis show that the frequency of CNT based resonators, switches, and flexural bearings can be controlled to within about 1.5%.

The speed at which CNT-based switches and resonators may be actuated is also dependent upon the stiffness of the CNT, as well as the mass of the CNT. Therefore, it is critical to be able the control the size of the CNT in order to reach the desired device bandwidth. An example of a CNT based switch may be seen in Figure 1.2. This switch uses the lateral bending of three vertical MWCNTs to create electrical contacts. The outermost CNTs have opposite potentials applied to them. When the central CNT has a potential applied to it, it feels an attractive electrostatic force to one of the outer CNTs. This attractive force between the CNTs causes them to come into contact, making an electrical connection and turning the switch on.

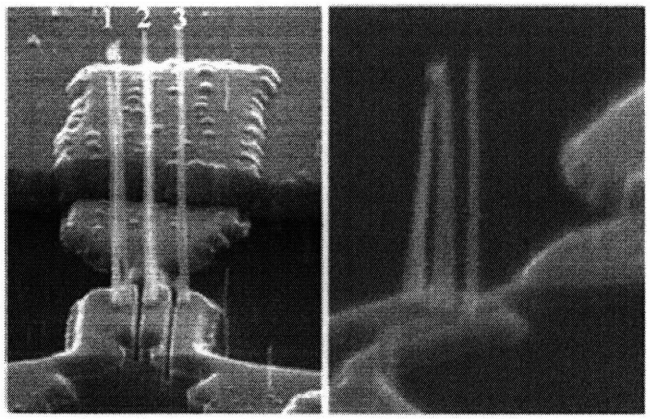

Figure 1.2. CNT-based Switch [3].
Reprinted with permission from the American Institute of Physics Copyright 2005

As may be seen in Equation 1.3 [2], the natural frequency of a cantilever switch is

$$\omega = \frac{\beta^2}{2\pi}\sqrt{\frac{EI}{mL^4}} = \frac{\beta^2}{8\pi L^2}\sqrt{\frac{\left(D^2+\left(D-2t\right)^2\right)E}{\rho}} \tag{1.3}$$

where β is a constant equal to 1.875 for a cantilever, E is the elastic modulus of the CNT, L is the length of the switch, D is the outside diameter of the CNT, t is the CNT wall thickness, and ρ is the density of the CNT. CNTs are ideal for high speed switches due to

their small mass and high elastic modulus. These unique properties allow them to operate with a bandwidth of over 10 GHz [4].

Similarly, the physical properties of CNTs make them ideal for high-bandwidth resonators. Such resonators are typically used as frequency determining elements in signal processing devices. An example of a CNT-based nanomechanical resonator is shown in Figure 1.3.

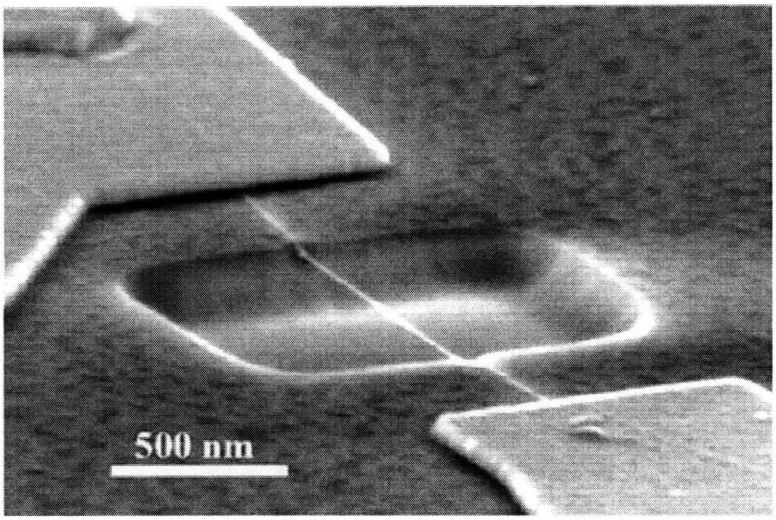

Figure 1.3. CNT-based Resonator [4].
Reprinted with permission from the American Chemical Society Copyright 2006

The natural frequency of the doubly-clamped resonator is given by Equation 1.3, with β equal to 4.73 for a doubly-clamped beam. Therefore, in order to control the resonators frequency it is necessary to be able to control the outside diameter and wall thickness of the CNT. Based upon Equation 1.3, a resonator that is 100 nm in length would be capable of operating at over 200 GHz depending on the diameter and wall thickness of the CNT. This is a vast improvement over silicon based MEMs resonators which typically operate in the 30-300 MHz range [5].

The rest of this chapter will focus on the structure and growth of CNTs as well as some applications which incorporate CNTs. Section 1.1 will provide an overview of the structure of CNTs and discuss how this structure affects the electrical and mechanical properties of the CNT. Section 1.2 will discuss why nanomechanical devices are important and how CNTs could be used to improve their performance. Section 1.3 will

give an overview of the different techniques that may be used to grow CNTs. Finally, Section 1.4 will explain the previous attempts to control CNT geometry as well as give an overview of the types of devices that have been created using CNTs.

1.2 What are CNTs

CNTs are carbon molecules that are a member of the fullerene structural carbon family. They may be thought of as rolled up sheets of graphene. Graphene is a single planer sheet carbon atoms whose lattice consists of carbon atoms arranged in a hexagonal structure. This hexagonal structure means that each carbon atom is bonded aromatically to its neighboring atoms via sp^2 hybridized bonds with a bond length of 0.142 nm. The C-C sp^2 bond configuration is one of the strongest found in nature which gives CNTs excellent mechanical properties. In the CNT structure, each carbon atom is bonded to three other carbon atoms by σ bonds with 120° of spacing. The carbon atom's fourth valence shell electron forms a delocalized π bond which is oriented perpendicular to the plane of carbon-carbon σ bonding.

A single-walled CNT (SWCNT) may be thought of as graphene sheet rolled along some chiral vector, $\vec{C}$, as shown in Figure 1.4. The chiral vector is a linear combination of two base vectors, $\vec{a}_1$ and $\vec{a}_2$, which are oriented 60° from each other.

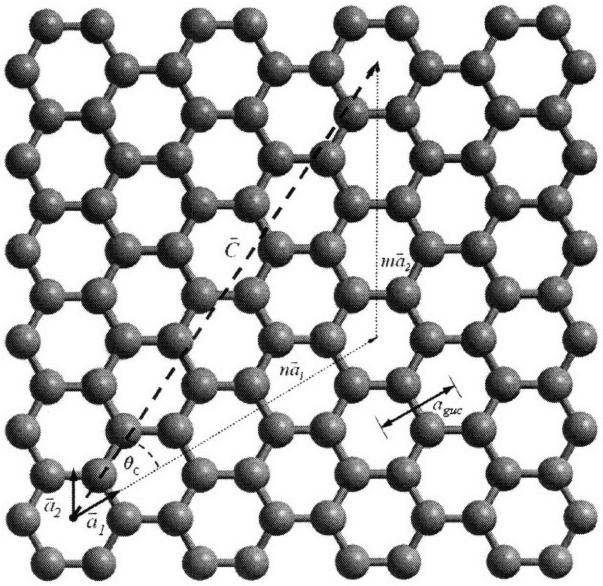

Figure 1.4. Chiral vector definition on a graphene sheet [6].

The chiral vector may be used to define the diameter of a SWCNT, d_{cnt}, of a carbon nanotube, as shown in Equation 1.4 [7] where a_{guc} is the distance between the centers of two unit cells and n and m are the lengths of the basis vectors.

$$d_{cnt} = a_{guc} \frac{\sqrt{n^2 + nm + m^2}}{\pi} \tag{1.4}$$

The energy per atom required to roll a graphene sheet into a CNT, U_r, is inversely proportional to the square of the CNT diameter [7], as shown in Equation 1.5 where E_g is the elastic modulus of graphene and t_g is the thickness of a graphene sheet.

$$U_r = \frac{\sqrt{3} E_g t_g^3 a_{guc}^2}{24 d_{cnt}^2} \tag{1.5}$$

In general, CNTs may be classified into three types: 1) zig-zag, 2) armchair, and 3) chiral. The zig-zag and armchair types are shown in Figure 1.5.

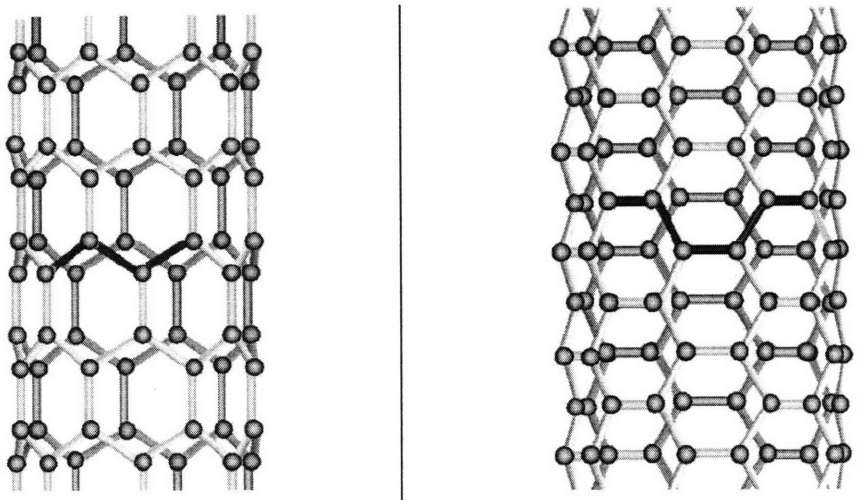

(a) (b)

Figure 1.5. Zig-zag (a) and armchair (b) carbon nanotube chiralities [8].
Reprinted with permission from Elesvier Copyright 2003

Zig-zag CNTs have $m = 0$, leading to a wrapping angle of 0° and diameters that are directly proportional to n. Armchair nanotubes have $m = n$, leading to a wrapping angle

of 30° and diameters that are proportional to $\sqrt{3}n$. Chiral nanotubes thus have wrapping angles between 0° and 30°.

The structure of the CNT also has a large effect on the electrical properties of the CNT. For example, electrically conductive tubes or metallic tubes always have a difference of their basis indices equal to an integer, q, multiple of three, as shown in Equation 1.6 [7]. This means that armchair nanotubes are always conductive.

$$3q = |n - m| \qquad \text{where } q = 0, 1, 2,... \tag{1.6}$$

If the difference between the basis indices is not equal to an integer multiple of three then, the tube is semiconducting with a bandgap, U_{gap}, that is proportional to a hopping parameter, γ, as is shown in Equation 1.7 [9].

$$U_{gap} = a_{guc} \frac{\gamma}{d_{cnt}} \tag{1.7}$$

For multi-walled CNTs (MWCNT) each wall may be treated as a resistor in parallel. This means that MWCNTs with many walls will likely be conducting because each shell has a one-in-three chance of being conductive.

1.3 CNT-based NEMS

1.3.1 NEMS Introduction

Nanoelectromechanical systems (NEMS) offer a promising area of research due to small size and potential to operate at high speeds. NEMS can operate in locations that larger machines can generally not fit into, such as inside the human body. Also, because of their size, NEMS can out perform their macro-scale counterparts in terms of speed and resolution. Microelectromechanical systems (MEMS) are already being used in a number of consumer applications such as accelerometers in car airbags, microphones in cell phones, ink jets in printers, and micromirrors in televisions. The ability of MEMS to accurately position fiber optics have also allowed for the creation of communication

systems that perform tasks were not previously possible at the macro-scale. MEMS have allowed devices to become smaller and lighter without reducing performance benefits. In fact, the MEMS have helped increase the resolution of ink jet printers and the picture quality of televisions that rely on digital light processing. Also, MEMS have helped reduce the cost of many devices due to their small materials costs and the ability to fabricate many MEMS devices at once. NEMS have the potential to build upon the benefits of miniaturization that were seen for MEMS by further increasing the performance and reducing the cost of such devices.

Most current NEMS devices, such as the one seen if Figure 1.6, are used as sensors because of the ability of nano-scale machines to sense small forces and displacements. Such sensors have made possible the measurement of small masses, on the order of the mass of nanoparticles and DNA. NEMS sensors have also been able to measure nano-scale forces, for instance van der Waals, forces that are not easily measured using macro-scale sensors. The ability of NEMS sensors to make these measurements is due in large part to the small mass of NEMS devices. This small mass increases the sensors sensitivity to the force and mass that is applied to the device.

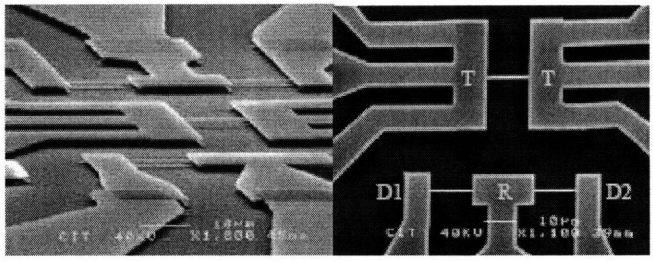

Figure 1.6. Side and Top views of a NEMS mass sensor [10].
Reprinted with permission from the American Institute of Physics Copyright 2004

The small mass of NEMS devices also allows such devices to operate at high frequencies. As was seen in Equation 2 in section 1.0, the natural frequency of the device is inversely proportional to the square root of the mass. Therefore, by reducing the mass of the device, the device may be run at much higher speeds. For example, while micro-scale devices typically run in the 10 kHz to 10 MHz range [11], NEMs devices can run at frequencies that are greater than 1 GHz [12]. This increased natural frequency can

improve signal processing speeds and increase the sensitivity of nano-scale sensors and transducers that rely on the resonance of a beam.

The small mass of NEMS devices also makes the amount of power dissipated by NEMS devices small, thus giving NEMS devices high quality or Q factors. The Q factor is defined in Equation 1.8 where ω is the angular frequency, m is the mass, K is the stiffness, and R is the mechanical resistance.

$$Q = \omega \times \frac{\text{Energy Stored}}{\text{Power Loss}} = \frac{\sqrt{mK}}{R} \tag{1.8}$$

The Q factor of NEMS devices may be hundreds of times better than similar high frequency electrical resonators [13]. NEMS are intrinsically low power devices due to these high Q factors. The fundamental power scale is defined by the thermal energy divided by the response time which is the Q factor divided by the natural frequency. For NEMS devices, this value is typically in the 10^{-18} watts range. Therefore, even if the NEMS device is only driven with a picowatt of power, the signal to noise ratio is still on the order of 10^6. The high Q factor of NEMS devices also means that they are sensitive to external damping. This is because the damping is directly proportional to the mechanical resistance as seen in Equation 1.9 where v is the velocity.

$$F_{damping} = -vR \tag{1.9}$$

Therefore, NEMS devices have the ability move with very high precision due to their high damping and signal to noise ratios.

Another major advantage of NEMS devices is that they eliminate the scale mismatch problem that is often seen when macro- and micro-scale devices are used to perform nano-scale tasks. In order for macro- and micro-scale devices to interact with nano-scale systems, it is typically necessary to de-amplify the motion of the macro- and micro-scale mechanisms because the displacement and force outputs of the macro- and micro-scale mechanisms are at least three orders of magnitude larger than the intended output motion for nano-scale systems. Flexures are commonly used to de-amplify force

and displacement outputs from an actuator, but in order to de-amplify an actuator displacement input, the flexure flexure's compliance must be a small fraction of the actuator's compliance. Unfortunately, adding a compliant flexure lowers the natural frequency of the system because the frequency scales with the square root of the system's effective spring constant. This may be a problem because it leads to an increase in the system's sensitivity to low frequency vibrations such as floor vibration, fan vibration in electronics, footsteps, and electrical noise. This sensitivity to low frequency vibrations can introduce large errors into the system (nanometers to microns) which can easily cause any nano-scale structures to fail. Fortunately, these vibration problems caused by scale mismatch may be avoided but using stiff nano-scale devices to perform nano-scale tasks. Overall, this elimination of the scale mismatch problem could allow nano-scale devices to have a large impact on a number of fields where nano-scale phenomenon are important such biology, chemistry, physics, and nano-fluidics by allowing machines to interact with individual molecules.

Another big advantage of NEMS is that they have a small footprint which should allow many devices to be packed into a small area, thereby increasing information density. For example, NEMS transistors, relays, and non-volatile memory could help increase how many processors may be fit on a chip. Such chips would also consume less power due to the high Q factor of NEMS and thus would not become as hot as current electronic processors allowing more processors to fit into the chip without the chip melting. Denser fiber optic interconnections could also be made using NEMS devices which would have a large impact on the communications industry.

1.3.2 Why CNT-based NEMS

Carbon nanotubes are ideally suited for NEMS devices because of their excellent mechanical and structural properties. CNTs have a high elastic modulus (~1 TPa[14]) which gives CNT-based devices the potential to operate at high speeds (> 100 GHz). CNTs also possess a large failure strain (~40% [15]) which could allow CNT-based nanomechanical devices to have a large range of motion compared with conventional silicon-based NEMS devices. Silicon is a brittle material and does not plastically deform,

therefore it becomes important to introduce a high factor of safety for practical designs so as to avoid beam fractures that would further decrease the device's range. The most relevant mechanical properties for MEMS/NEMS design are listed in Table 1.1 for silicon and CNTs [14, 16, 17].

Table 1.1: Mechanical Properties of Silicon and CNTs		
	Silicon	CNT
Elastic Modulus	190 GPa	~1 TPa
Failure Strength	7 GPa	150 GPa
Density	2300 kg/m^3	2240 kg/m^3

The inherent size of CNTs (1-100 nm in diameter) allows CNTs to be used to make nanomechanical devices at scales that are hard to reach with traditional photolithography. In photolithography, radiation (in the form of light, x-rays, ultraviolet light, etc.) is passed through a mask, exposing a pattern in the photoresist on the surface of a silicon wafer. The incoming radiation creates a chemical bond change in the resist. This chemical change allows the resist to be developed to produce a pattern in the resist by either removing the resist from the exposed regions for positive resists or removing the resist from the unexposed regions for negative resists. The patterns in the resist may then be transferred into the wafer using various etches. This process is shown in Figure 1.7.

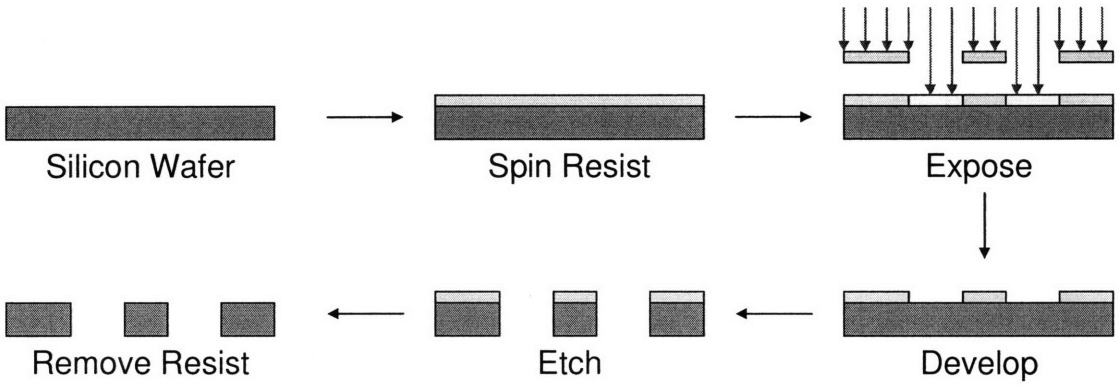

Figure 1.7. Photolithography Process Diagram

The resolution of photolithography is set by the diffraction limit of the incoming radiation. Therefore, it is typically hard to make nanometer-scale features via

photolithography. Equation 1.10 shows the relationship of minimum feature size, w_{min}, to both the radiation wavelength, λ, and numerical aperture, NA.

$$w_{min} = \frac{1}{2}\left(\frac{\lambda}{2NA}\right) \tag{1.10}$$

State-of-the-art photolithography systems use ArF lasers with a wavelength of 193 nm and can achieve numerical apertures of 0.9 using immersion lithography. Therefore, the minimum feature size under for current state-of-the-art systems is about 50 nm. This means that NEMS devices that utilize CNTs could be much smaller than silicon based NEMS since single-walled CNTs may be smaller than 1 nm.

There are other lithography systems that can compete with CNTs in terms size, but these systems are generally slower than standard photolithography systems. One system is electron-beam lithography (EBL). In EBL, an electron beam is focused onto a substrate that is coated with an electron-sensitive resist using a system of electromagnetic lenses. The wafer is broken up into 100μm squares over which the electron beam is scanned. The beam may be turned on and off at high speeds using a shutter which is placed in front of the electron source to expose some pixels while leaving others unexposed. Thus, the device geometry is transferred to the resist in a pixel-by-pixel fashion. Steps similar to photolithography are then used to develop resist and etch the pattern into the silicon wafer. With EBL, it is possible to produce features as small as 5 nm, but because of the pixel-by-pixel nature of the process, writing times may be very long. For example, in order to expose half of the pixels (4 nm^2 in size) in a 1 cm^2 area with each pixel requiring 100 electrons to be fully exposed, would take approximately three days. Therefore, EBL is not a good fabrication option if many devices are required.

Dip-pen nanolithography can also be used to produce features smaller than 20 nm, but it two suffers from being a slow process. In dip-pen nanolithography, a probe tip is used to transfer molecules to the surface of a substrate and define a pattern. An illustration of the process may be seen in Figure 1.8. Unfortunately, this process again suffers from being slow compared to photolithography because each feature has to be individually written, making the process impractical for mass manufacturing. Current dip-pen nanolithography research, however, is focusing on being able to use many probe

tips in parallel to write many features at once which would markedly increase the speed at which devices could be made.

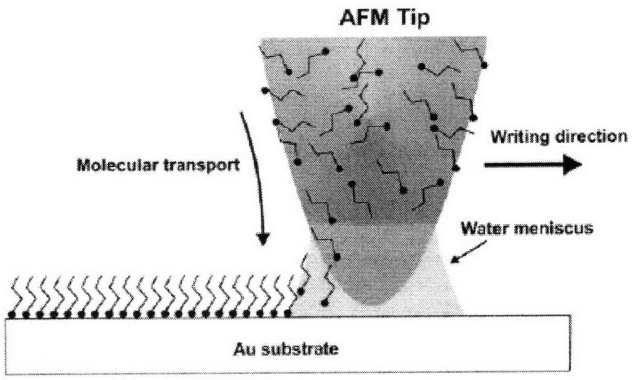

Figure 1.8. Dip-pen Nanolithography [18].
Reprinted with permission from AAAS Copyright 1999

Another alternative for nano-scale fabrication is nano-imprint lithography. In imprint lithography, a mold with nano-scale features is brought into contact with a wafer coated in resist. The resist flows around the mold, creating an imprint of the mold in the resist. The resist is then developed and etching is used to transfer the pattern to the silicon wafer. It has been shown that molds made from carbon nanotubes with diameters of only a few nanometers can create features in silicon with nanometer resolution [19], this is shown in Figure 1.9. Unfortunately, the contrast between the imprinted image and the background is typically not very high for such features. Therefore, when etches are performed to release the imprinted structures, the structures themselves are often destroyed. Nano-imprint lithography is impractical for making NEMS devices with a small number of defects.

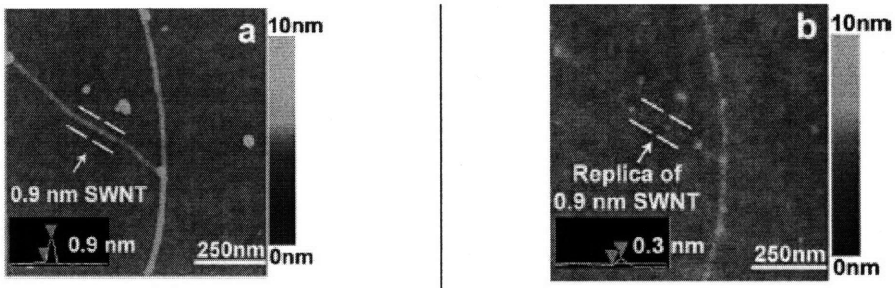

(a) (b)

Figure 1.9. (a) CNT Master (b) Nano-imprinted replica [19]
Reprinted with permission from the American Chemical Society Copyright 2004

One major advantage CNTs have over such top-down processes is that if the position and size of CNTs may be accuratly controlled, CNT-based nanomechanical devices could be produced by growing CNTs onto specific locations on prefabricated structures. In this case, the large silicon features could quickly be fabricated using photo lithography while the smaller features would be CNTs that are grown in place. This would allow CNT-based nanomechanical devices to be built more quickly than similar silicon-based nanomechanical devices that are produced by top-down approaches due to the massively parallel nature of the CNT growth process.

CNTs may be assembled into structures in one of two ways either pick-and-place or grow-in-place. In pick-and-place, a probe is brought into contact with a CNT which is attached the probe by van der Waals forces. The CNT may then be moved to the desired location and fixed in place by depositing a metal or amorphous carbon layer on top of the CNT thereby bonding it to the substrate. The probe may then be removed because the van der Waals forces are smaller than the bonding force. This method allows the CNTs to be placed accurately, but is slow.

The grow-in-place method is faster much harder to control. In general, attempts to control the location and direction of the CNT growth have focused on defining the location of the catalyst and the structure around the initial growth location. For example, it has been shown that by defining a series of pillars and depositing catalyst particles on top of the pillars, CNT may be made to grow between the pillars as seen in Figure 1.10.

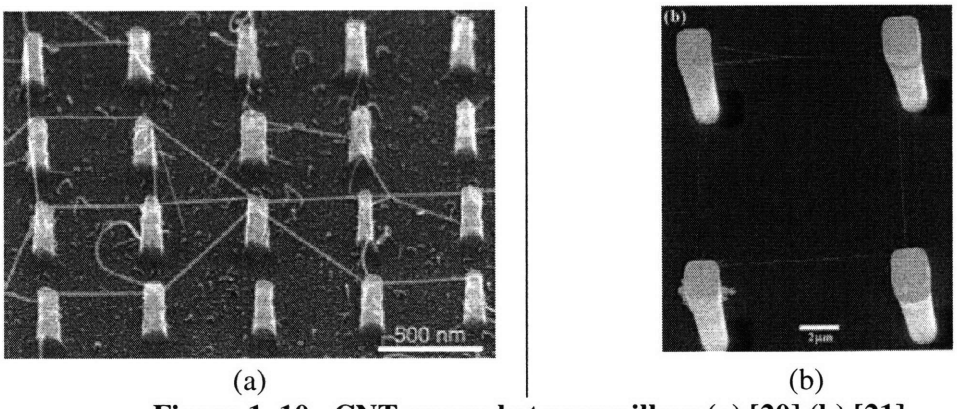

(a) (b)

Figure 1. 10. CNT grown between pillars (a) [20] (b) [21]

Reprinted with permission from the American Institute of Physics Copyright 2002 and the American Chemical Society 1999

Unfortunately, even with well-defined growth locations, it is hard to control exactly which direction the CNTs will grow. One way to overcome this is to use an electric field to direct the growth. The high polarizability of carbon nanotubes allows a large dipole moment to be induced in the carbon nanotube when the CNT is placed in an electric field. This dipole moment produces large aligning torques and forces on the nanotube, thereby causing the CNT to align in the direction of the electric field. The effects of the aligning torques may be seen in Figure 1.11.

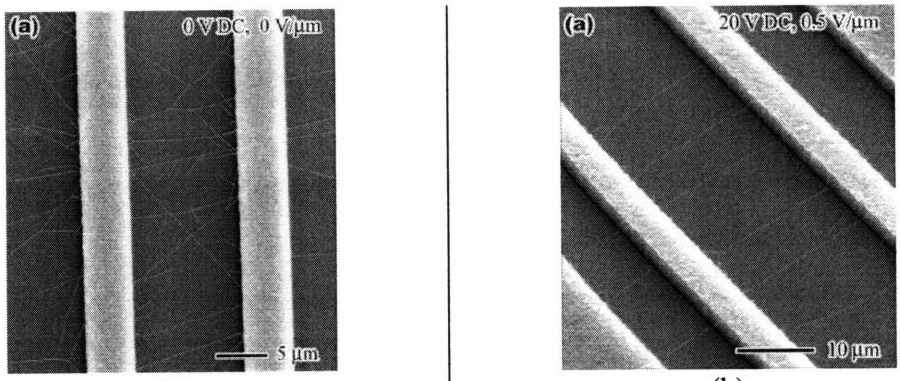

(a) (b)

Figure 1.11. (a) Growth without electric field (b) growth with 20 V electric field [22]
Reprinted with permission from the American Institute of Physics Copyright 2001

By producing an electric field between the place where the catalyst particles are deposited, and the place when the CNT is to be attached, the CNT may effectively be grown in place to create a nano-scale device. The CNT may then be fixed in place by depositing a thin metal film. Overall, this combination of top-down (photo-lithography to define the silicon structure) and bottom-up (CNTs grown-in-place) fabrication techniques could allow a large number of high quality CNT-based nanomechanical devices to be fabricated rapidly.

1.3.3 Controlling Stiffness and Speed

As may be seen in Equation 1.11 [23], the bending stiffness of a carbon nanotube, k, depends upon the elastic modulus E, the length of the tube, L, the outside diameter of the CNT, D, and the wall thickness, t, of the CNT.

$$k = \frac{3\pi E(D^4 - (D-2t)^4)}{64L^3} \tag{1.11}$$

The elastic modulus is a material property of the CNT and the length is usually set based upon the device size, therefore, the only independent way to control the stiffness is to change the outside diameter and wall thickness of the CNT. Similarly, as was shown in section 1.0, the natural frequency at which the CNT-based device vibrates depends on the elastic modulus, the length of the CNT, the outside diameter, the wall thickness, the device mass, and the device boundary conditions. Again, only the outside diameter and wall thickness are independent parameters because the elastic modulus is a material property, the length of the CNT is set by the device size, the device boundary conditions are set by the type of device and the mass is either set by the size of the stage if a stage is used as in the case of a linear flexural bearing or is a function of the diameter, and wall thickness of the CNT as in the case of CNT-based switches and resonators.

Fortunately, both the outside diameter and the wall thickness of CNTs grown by chemical vapor deposition (CVD) have been shown to be dependent on the conditions under which the CNTs are grown [24-26]. By controlling the growth parameters used to grow the CNTs, we should be able to extract equations that represent the causal relationship between the fabrication process parameters and the CNT diameter and wall thickness.

1.4 CNT growth

Carbon nanotubes are generally grown by one of three methods: (1) arc discharge, (2) lazar ablation, (3) chemical vapor deposition (CVD). In arc discharge, an arc is generated between two carbon electrodes which vaporizes the carbon atoms into a plasma at over 3000°C. This causes a carbon soot containing CNTs to be deposited on the negative electrode [7]. The major advantage of this process is that it is quick and simple. However, the CNTs produced by this method are generally relatively short (< 1μm) and unordered. Also, the soot has to be purified to separate the other carbon products from

the CNTs. Therefore, arc discharge synthesis is typically not used to produce CNTs for nanomechanical devices. A schematic of the arc discharge apparatus is shown in Figure 1.12.

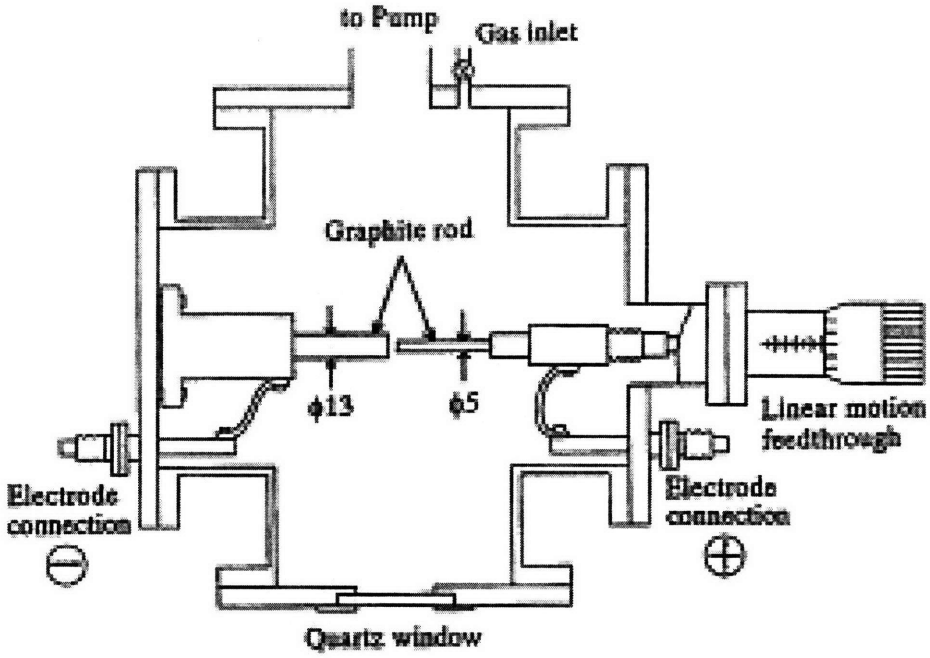

Figure 1.12. Cross-sectional view of a CNT arc discharge apparatus [27].
Reprinted with permission from JJAP Copyright 1993

In laser ablation, two sequenced laser pulses are used to evaporate a graphite target containing a small amount of a transition metal at a temperature of about 1200°C. The transition metal acts as a catalyst for CNT growth while the evaporated graphite acts as the carbon supply. Once the CNTs have been formed, flowing argon sweeps the CNTs away from the high temperature zone. Overall, the yield of the laser ablation process is 70%-90% [28] which eliminates some of the purification steps required for arc discharge. Laser ablation suffers from some of the same problems as CNTs grown by arc discharge. For example, CNTs grown from laser ablation are typically tangled and hard to separate. Therefore, CNTs grown by laser ablation may be hard to incorporate into nanomechanical devices. A schematic of the laser ablation method is shown in Figure 1.13.

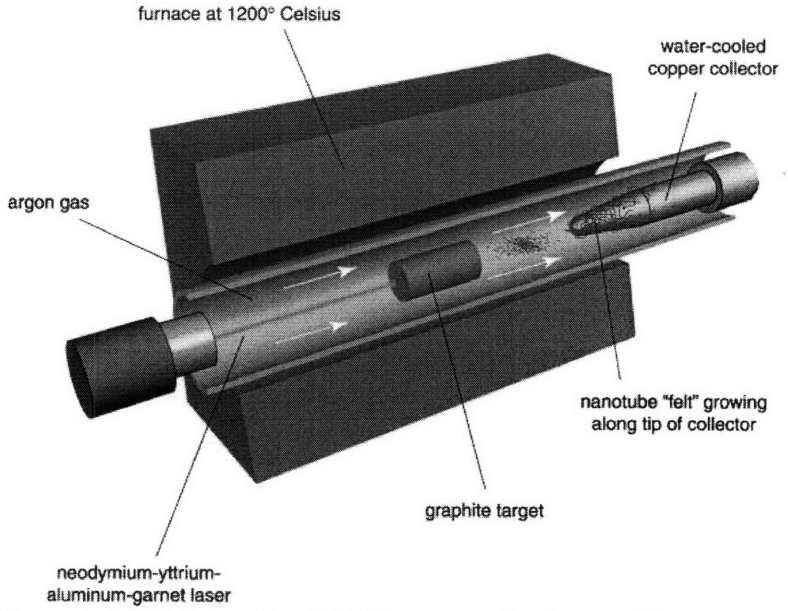

Figure 1.13. Schematic of CNTs grown by laser ablation [29].
Reprinted with permission from Sigma Xi Copyright 1997

CVD is the most commonly used method due to its scalability, low-cost, and its ability to control the position and orientation of the CNTs that are grown [30]. A schematic of a typical thermal CVD tube furnace is shown in Figure 1.14.

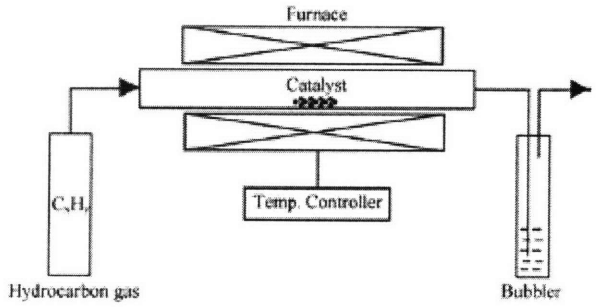

Figure 1.14. Thermal CVD tube furnace setup [31].
Reprinted with permission form Elsevier Copyright 2004

In thermal CVD growth of CNTs, a hydrocarbon gas such as methane or ethylene is flowed over a catalyst such as iron or nickel at an elevated temperature (700-1000°C). The hydrocarbon then decomposes on the surface of the catalyst and the carbon from the hydrocarbon is absorbed into the catalyst particle [32]. Finally, the carbon diffuses

through the catalyst particle and precipitates out as a carbon nanotube as may be seen in Figure 1.15. Growth from a substrate can precede either as base growth or tip growth depending on the adhesion forces between the catalyst particle and the substrate. A floating catalyst method, in which the catalyst is injected into the furnace as a vapor, is sometimes employed for high volume applications such as composites.

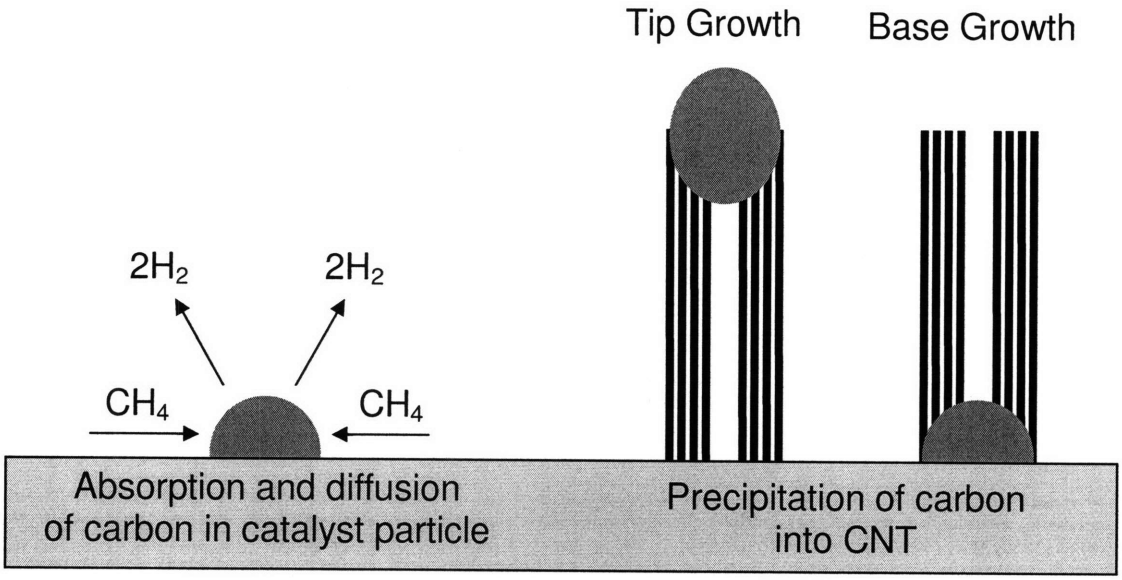

Figure 1.15. CNT Growth by CVD

Plasma-enhanced CVD (PECVD) is similar to thermal CVD except that high-energy electrons in the plasma are used to dissociate the precursor gas. This allows CNTs to be grown at lower temperatures because the thermal energy is no longer needed to dissociate the hydrocarbon. Growth temperatures as low as 120°C have been demonstrated using PECVD [33]. These low temperatures allow CNTs to be grown on many low temperature substrates and within microelectronic devices that require low temperatures. Unfortunately, the dissociation of the carbon precursor away from the catalyst particle may cause a large amount of amorphous carbon to build up on the outside of the catalyst thus poisoning the catalyst particle and stopping the growth of the CNT. Therefore, CNTs grown by PECVD are generally much shorter than CNTs grown by Thermal CVD. Also, as may be seen in Figure 1.16, the PECVD growth apparatus is more complicated than the thermal CVD apparatus. PECVD must be performed in a

vacuum which requires longer times between runs due to the pump down step. Also, the vacuum may be a problem when using substrate materials that out gas. Therefore, thermal CVD is generally the preferred growth method due to its lower cost and higher through put.

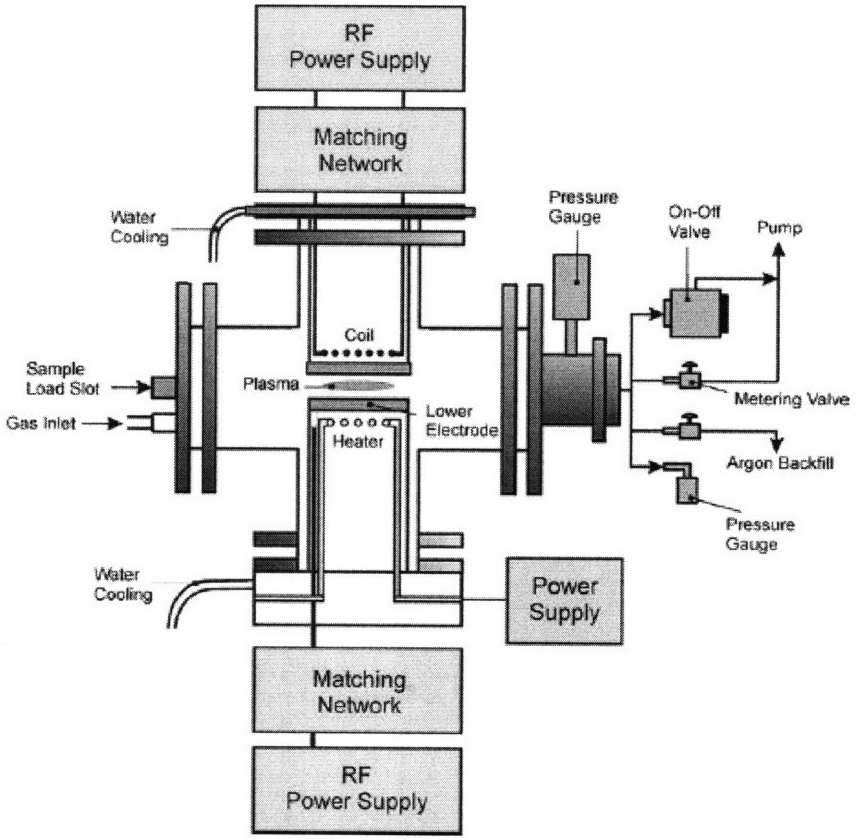

Figure 1.16. PECVD tube furnace setup [34].
Reprinted with permission of IOP Copyright 2003

1.5 Prior Art

1.5.1 Controlling CNT Growth

Attempts to control the size and geometry of carbon nanotubes have mainly focused on three process parameters: (1) the catalyst particle size, (2) the catalyst the growth temperature, and (3) the hydrocarbon concentration. The size of the catalyst particle used to promote the growth of the CNT has previously been shown to have a

direct positive correlation with the outside diameter of the CNT [32, 35-38] as may be seen in Figure 1.17. This is expected given the surface diffusion growth model because as the carbon diffuses through and precipitates out of the catalyst particle it will first precipitate out from the edges of the catalyst particle. Therefore, the size of the catalyst particle sets the outside diameter of the CNT. Experimental results suggest that the number of walls in the CNT increases as the catalyst particle size increases [32,39]. Unfortunately, there are not many studies on the effects of the growth process parameters on the number of walls in the CNT and, therefore, this result is not well-understood.

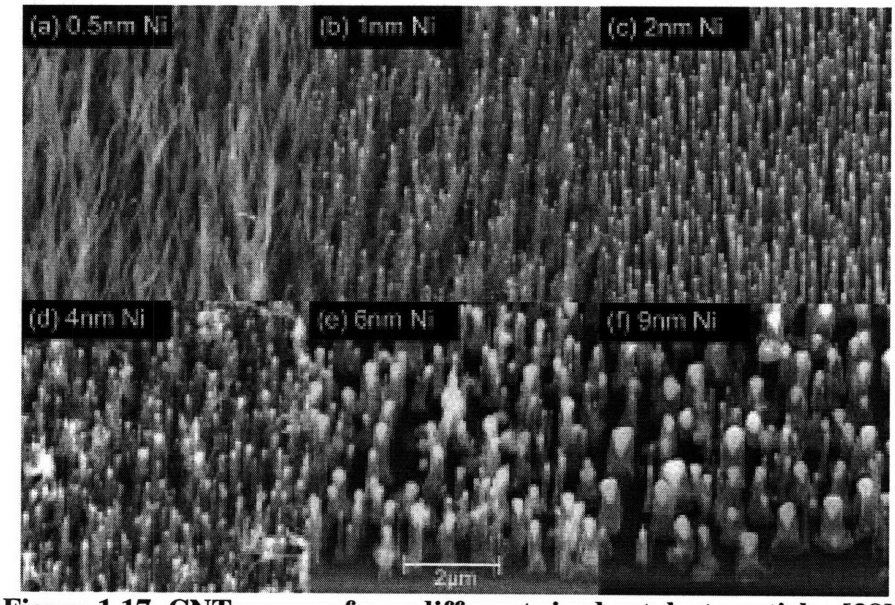

Figure 1.17. CNTs grown from different sized catalyst particles [38].
Reprinted with permission from the American Institute of Physics Copyright 2001

Increases in the growth temperature have also been shown to increase the outer diameter of CNTs grown through CVD [40-46] as may be seen in Figure 1.18. These increases are thought to be the result of the increased mobility of the catalyst particles on the substrate at higher temperatures. This increased mobility causes more collisions between catalyst particles, and thus more agglomeration, resulting in larger catalyst particles, which in turn increases the outside diameter of the CNTs [46]. The effect of temperature on the number of walls formed in the CNT is less clear, with some results suggesting that the number of walls in the CNT increases with temperature [41] and some results showing a decrease in the number of walls with an increase in temperature [40].

Therefore, more research needs to be done in order to determine the effect of temperature on the number of walls in a multi-walled CNT.

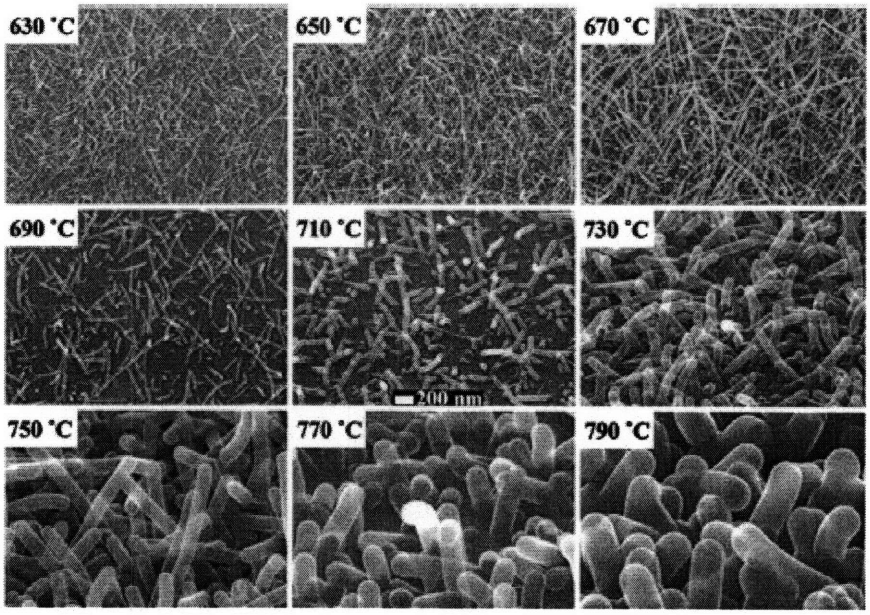

Figure 1.18. CNTs grown at different temperatures [43].
Reprinted with permission from the American Institute of Physics Copyright 2002

It has also been shown that for single-walled CNTs (SWCNT), increasing the concentration of the hydrocarbon precursor increases the outside diameter of the CNT [47]. The trend may be seen in Figure 1.19.

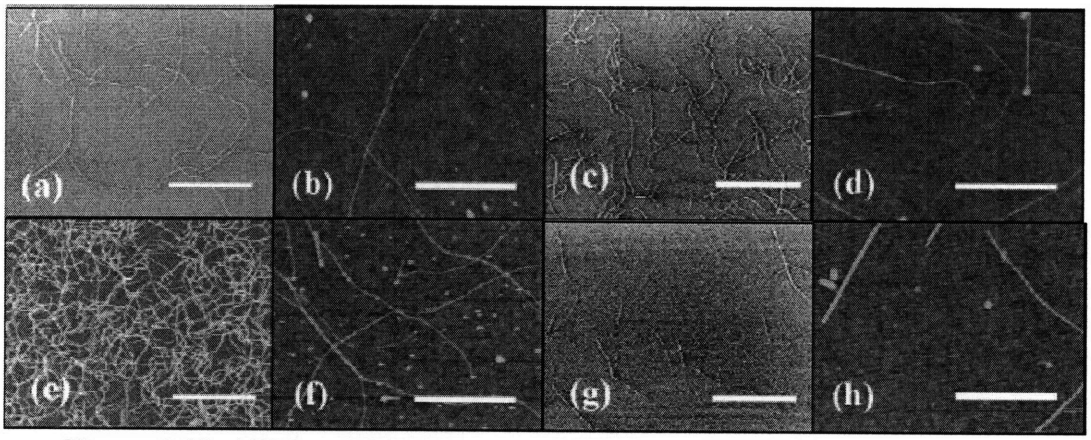

Figure 1.19. AFM and SEM images of CNTs grown with different ethane concentrations. (a,b) 140 ppm; (c,d) 1600 ppm; (e,f) 4200 ppm; (g,h) 14,400 ppm. Scale bar is 10 μm in left image and 1 μm in the right image of each pair [47].

This effect is thought to occur because there is an ideal particle size for the growth of a SWCNT for any given carbon feed rate. If the particle is too small, an amorphous layer of carbon forms on the outside of the catalyst particle which cuts off the carbon supply and stops and SWCNT from nucleating. If the catalyst particle is too big, not enough carbon diffuses into the catalyst particle to nucleate a CNT. The ideal size of the catalyst particle thus increases as the hydrocarbon concentration increases resulting in larger CNTs for higher flow rates. Unfortunately, similar research has not been performed to see the effects of hydrocarbon flow rate on the outside diameter of multi-walled CNTs or on the number of walls formed in the CNT.

1.5.2 CNT-based nanomechanical devices

There are many different types of nanomechanical devices where the incorporation of CNTs could substantially improve the device's performance. In order to be able to take full advantage of the outstanding mechanical properties of CNTs, we must be able to control the stiffness of the CNTs that are incorporated into the device. There are two major reasons the stiffness of CNTs of matters for CNT-based nanomechanical devices. First, the stiffness affects the bandwidth of the device. This is important for devices where a specific driving frequency might be required for specific signal processing applications. The natural frequency also affects the speed at which switches and relays can operate. For example, the relay in Figure 1.20a has a resonance frequency of 0.1 GHz and a stiffness of 0.1 nN/nm.

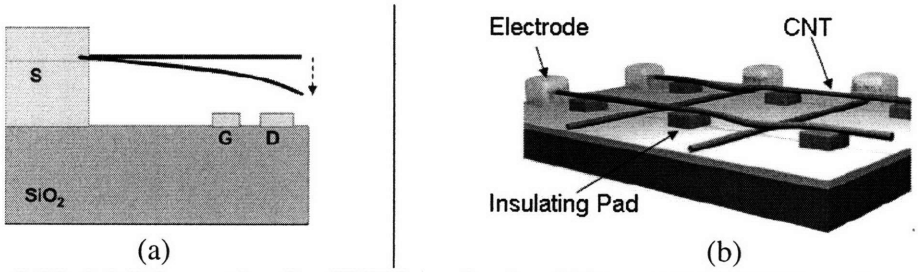

Figure 1.20. (a) Schematic of a CNT based relay [48] and (b) CNT based memory [49]. *Reprinted with permission from the American Chemical Society Copyright 2004 and AAAS Copyright 2000*

The relay works by using a voltage differential applied by the gate electrode (G) to deflect the CNT into contact with the drain electrode (D) which completes an electrical circuit between the source (S) and drain electrodes. Improvements in the control of the size and stiffness of the CNT enable the relay to operate at a higher natural frequency. Therefore, it is necessary to be able to control the stiffness of the CNTs in such devices in order to achieve the optimal device performance.

The ability to control the stiffness of CNTs could also help improve the speed of CNT-based non-volatile memory such as that shown in Figure 1.20b. The memory consists of a multi-layer grid of overlapping CNTs. The electrodes at the end of each CNT are used to apply voltages differences to different CNT pairs which will cause the overlapped CNTs to come into contact which turns on the memory node. Van der Waals attractive forces then hold the two CNTs in contact even without the presence of the potential difference, forming a non-volatile "ON" state. Simulation results suggest that this device could be operated at frequencies greater than 100 GHz depending on the stiffness of the CNTs used.

The sensitivity of CNT-based sensors, such as the mass sensor shown in Figure 1.21, is dependent on the resonance frequency of the system. The mass sensor is comprised of three electrodes with the two outer electrodes serving as the source and the drain for the CNT Bridge. The middle electrode is used to electrostaticly actuate the CNT. The mass on the CNT is then measured by measuring the shift in the natural frequency of the CNT when the mass is added. In this case, the mass sensor has a sensitivity of 0.66×10^{-21} g/Hz.

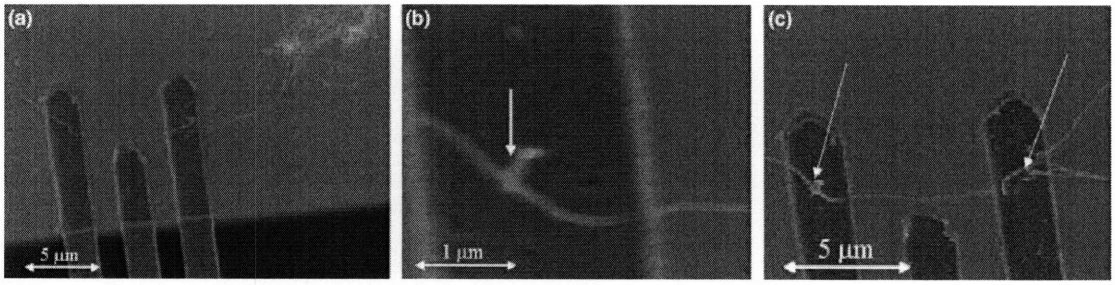

Figure 1.21. (a) CNT being attached to electrodes (b) CNT soldered to on electrode (c) Completed CNT-based mass sensor [50].
Reprinted with permission from Elesvier Copyright 2004

In general, sensors with higher natural frequencies make better mass sensors because, for a given mass, there is a greater frequency shift at higher frequencies. If the mass of the sensor becomes too large, its mass dominates the mass of the object being measured and it becomes difficult to measure the mass of the object. Thus, there is a tradeoff between the mass of the CNT and its stiffness in order to produce mass sensors with the best sensitivity to specific masses. It is necessary to be able to control the outside diameter and number of walls in the CNT in order to produce the optimal mass sensor.

The second reason why the stiffness of the CNT is important is that stiffness controls the force-displacement characteristics of CNT-based nanomechanical devices. For example, the resolution of a force-displacement transducer is set by the CNT stiffness. Also, the force needed to actuate devices that use CNTs as rotational or flexural bearings depends on the stiffness of the CNT. One example of this is the nano-scale pendulum shown in Figure 1.22(a) which uses the torsional deflection of a CNT as a rotational bearing [51-52]. The pendulum is suspended from a CNT which lays across two anchor pads, as may be seen in Figure 1.22(b). The bond between the CNT and an anchor is detailed in Figure 1.22(c). An external electric field is used to actuate the pendulum which is capable of 180° of rotation. In this case, the CNT bearing is single walled and has a diameter of 1.5 nm. Therefore, CNT bearing possess a spring constant of 2.86 nN·nm/rad and a resonance frequency of 0.1 MHz. By controlling the outside diameter and number of walls of the CNT bearing, a different spring constant and natural frequency could easily be achieved.

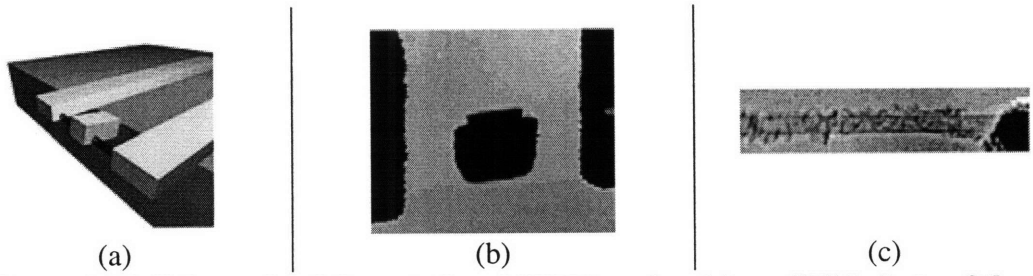

(a) (b) (c)

Figure 1.22. Schematic of the rotational CNT bearing (a), an SEM photo of the realized device (b), and a close-up of the CNT anchor (c) [51].

Reprinted with permission from AAAS Copyright 2005

1.6 Scope

This thesis focuses on how to control the geometry, the stiffness and the natural frequency of carbon nanotubes for nanomechanical and nanoelectromechanical devices. Chapter 1 introduces the topic and shows how being able to accurately control the structure of CNTs could be used to significantly improve the design and performance of NEMS devices. Chapter 2 shows how an experiment was designed to extract numerical relations between process parameters and the final CNT geometry. Chapter 3 presents the results of the experiment and shows how design equations may be extracted from the results. Chapter 4 shows how the growth process may be thermodynamically and kinetically modeled and examines how well these models match the experimental results. Chapter 5 uses the design equations presented in Chapter 3 to design several NEMS devices. Finally, Chapter 6 summarizes the findings of this thesis and provides a discussion of future work.

Chapter

2

Methods

2.1 Introduction

The carbon nanotubes for this research were grown using thermal chemical vapor deposition (CVD) in a resistively heated furnace. Thermal CVD was chosen as the growth method because CNTs may be grown directly onto the substrate. This process is suitable for monolithic device integration. Good control (< 3% variance) over process parameters may be achieved using thermal CVD. The rest of this chapter will discuss the experimental procedure, choice of process parameters, and the experimental design used in this study.

2.2 Setup and Procedure

The first step in the CNT growth procedure is to deposit catalyst onto a silicon substrate. Iron was chosen for the catalyst because it has been shown to be a high-quality catalyst for CNT growth when methane is used as the reacting gas [53]. The iron was deposited onto silicon wafers in thin films using electron beam deposition. A thin layer of aluminum oxide (Al_2O_3) was deposited between the iron layer and the silicon wafer to act as a diffusing barrier and to prevent iron silicides from forming during the high temperature annealing and growth steps. Electron beam deposition was chosen as the catalyst deposition method over liquid catalyst based methods because of its simplicity (1 step deposition), repeatability (~ 1 angstrom), and ability to make uniform deposits over the wafer.

Once the catalyst was deposited on the substrate, the substrate was placed in the furnace. The furnace was then purged for 5 minutes with argon flowing at 1000 sccm. This purge removed the oxygen from furnace and created an inert atmosphere. Argon was chosen as the carrier gas because of its high molecular mass as compared with air. A gas with a higher molecular mass will be better at displacing air. Anothor benefit is that argon is an inert gas and therefore will not become part of the CNT growth reaction. After the 5 minute purge, an annealing step was started when the temperature of the furnace was increased to 700 °C and held constant for 15 minutes. This annealing step allows the thin film of iron to dewet into nano-scale particles. The size of the nanoparticles used to catalyze the growth of the CNTs is therefore set by the catalyst film thickness because the parameters of the annealing process (time and temperature) are kept constant.

After annealing, the temperature was raised to the growth temperature (700-900°C) and methane was introduced into the system. Methane was chosen as the reacting gas because its simple molecular structure is easier to model for the purposes of this thesis. Also, methane has been shown to be a good hydrocarbon for growing high purity CNTs due to its high activation energy [54]. A high activation energy reduces the amount of amorphous carbon that forms during growth [54], allowing highly crystalline CNTs to form. Once the methane flow was turned on, the argon flow rate was adjusted to keep the total flow rate at 1000 sccm for another 20 minutes.

After the growth step was completed, the methane flow was shut off and the argon flow was increased back to 1000 sccm for 5 minutes to purge the system. The power was then slowly reduced over a 5 minute period, allowing the sample to slowly cool down to room temperature. The argon purge was continued for 5 minutes before the argon flow was turned off and the sample was removed.

The sample was then placed within a Scanning Electron Microscope (SEM) to quickly observe the growth results. A Transmission Electron Microscope (TEM) sample was then prepared using an ion mill. The ion mill was used to reduce the substrate thickness to less than 100 nm so that electrons could pass through the sample and an image could be taken via TEM. Most of the TEM work done in this thesis was performed in a Joel 200CX TEM which has a resolution of 0.4 nm. In the TEM, the

outside diameter and wall thickness were measured for thirty CNTs at different locations in the sample.

This procedure, which is outlined in Figure 2.1, was repeated for 15 different samples through the course of this investigation. A regression analysis was then applied to the results in order to extract equations that represent the causal relationship between fabrication process parameters, CNT diameter, and wall thickness. These equations were then used to design a fabrication process that was suitable for the creation of CNTs with specific properties.

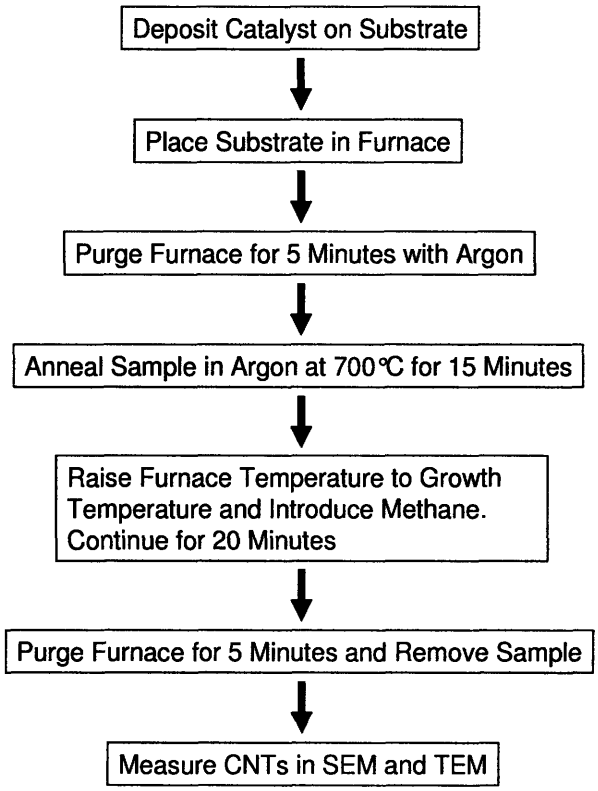

Figure 2.1. Growth Procedure

2.3 Choice of Experimental Parameter Ranges

There are three primary process parameters which are critical to the final geometry of the CNTs grown using CVD: (1) the catalyst particle size, (2) the temperature, and (3) the hydrocarbon concentration. There are, however, secondary

variables in the growth process such as the type of hydrocarbon, catalyst, carrier gas, and the total flow rate that must be set and held constant for the growth process to be repeatable. Limits on the ranges of the three experimental variables also must be set empirically in order to design an effective growth study.

The argon was mixed with the methane to keep the total flow rate at 1000 sccm. The methane concentration in the gas mixture was varied between 37% and 100%. The 37% limit was set because it was found from experimentation that the minimum methane flow rate at which CNTs would grow at a temperature of 800°C in this furnace setup was about 350 sccm, which is a concentration of 35%.

An iron film thickness range of 0.5 to 6 nm was chosen because the catalyst particles produced from such film thicknesses are between 10 and 100 nm in diameter. When film thicknesses of greater than 6 nm are used, the catalyst particles start to become large and as such are unable to fully separate from each other. This may be seen in Figure 2.2. The catalyst particles formed from films thicker than 6 nm tend not to be round and thus do not effectively catalyze the growth of CNTs.

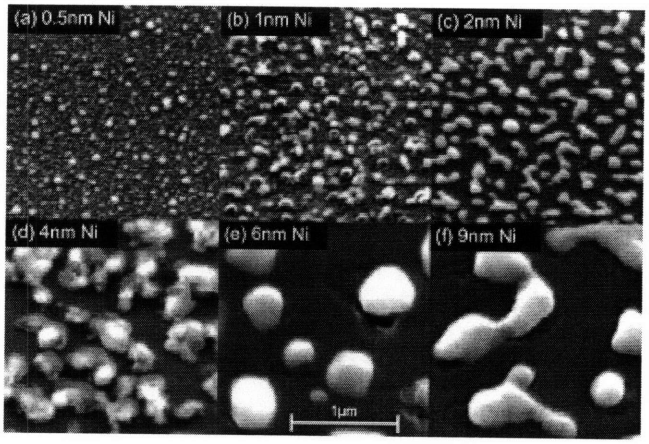

Figure 2.2. Dewetting of Catalyst Films of Different Thicknesses [38].
Reprinted with permission from the American Institute of Physics Copyright 2001

2.4 CNT Furnace Setup

The furnace for the CVD growth of the CNTs for this study was based on the resistive heating of a silicon platform [55]. This reactor is shown in Figure 2.3. The

silicon platform in this furnace was cleaved from a highly doped ($N_A > 10^{18}$), four inch, 600 μm thick silicon wafer. The platform is 2 inches long and 0.25 inches wide. It is clamped between two aluminum electrodes that act as heat sinks. When a current is passed through the silicon platform, the platform heats up due to collisions between the moving electrons and the ions in the silicon platform. This causes kinetic energy to be transferred from the electrons to the ions which must then be dissipated as heat. Using a 180 watt power supply, the platform may reach temperatures of over 900°C. The temperature of the substrate was set by adjusting the current flow through the silicon platform and was measured during the CNT growth using a K-type thermocouple. For The silicon substrate that was coated with catalyst film was placed on the silicon heater. The optical flatness (<300nm surface roughness) of the silicon platform and the silicon substrate ensured that (1) there was good thermal contact and (2) there was only a small temperature drop (< 10°C) between the platform surface and the reaction surface.

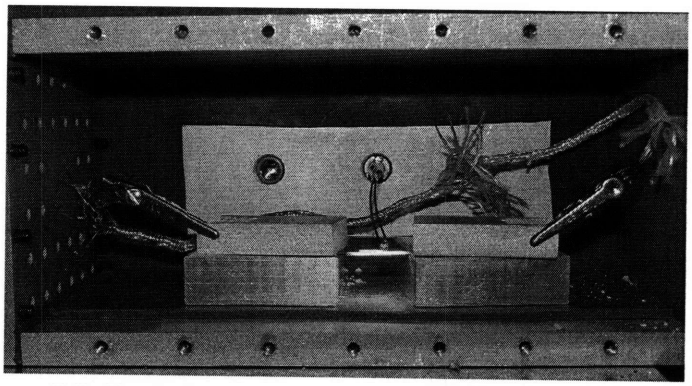

Figure 2.3. Resistively Heated Carbon Nanotube Furnace.

The hydrocarbon and carrier gasses enter the furnace through a diffuser plate as shown in Figure 2.4. The diffuser plate ensured that the flow is laminar at the entrance of the furnace. This is important because it ensured that the hydrocarbon concentration was uniform throughout the furnace. The laminar flow also provides a more stable environment for CNT growth, which helps to allow the hydrocarbons to come into contact with the catalyst particle surface long enough to breakdown and diffuse into the catalyst particle [55]. During the CVD growth process, the CVD chamber is sealed using gaskets. Bolts in the top and sides of the chamber, as shown in Figure 2.5, provide the

preload necessary for the gaskets to seal the chamber. The hydrocarbon and carrier gasses exit the CVD chamber through the exhaust port. The exhaust port is connected to a fume hood through an exhaust line as shown in Figure 2.5. This allows the waste products of the CVD reaction to be safely vented from the building.

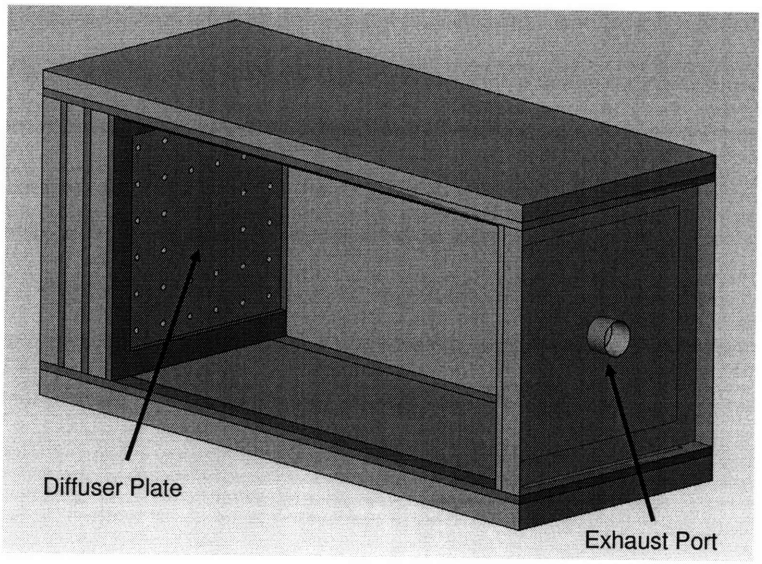

Figure 2.4. CAD Model of CVD Furnace.

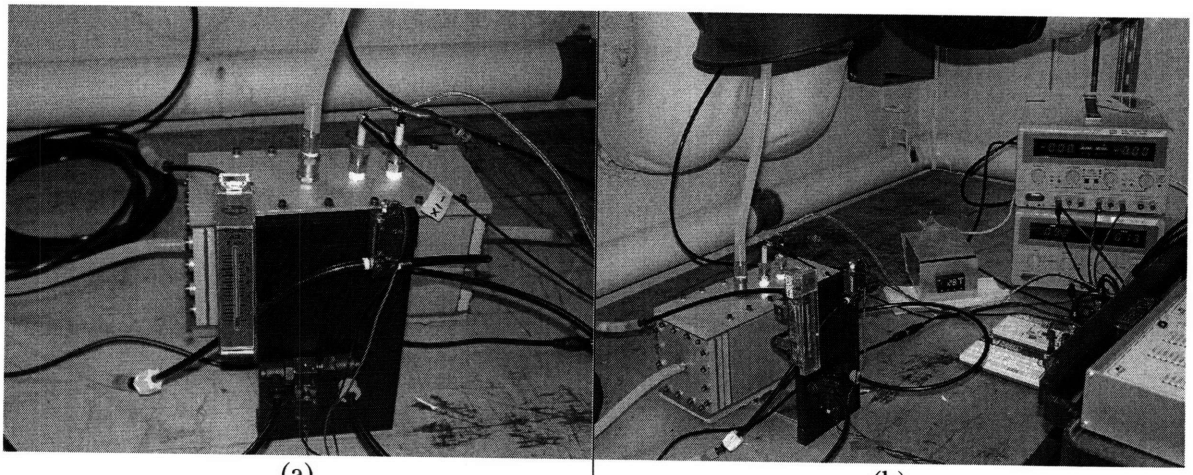

Figure 2.5. Exterior Furnace Setup

During the growth process, the flow rates of the methane, argon, and the temperature of the furnace are monitored using a LabVIEW. This program is archived in Appendix A. The flow rates are controlled using regulators on each of the tanks. These

regulators allow the flow rates to be controlled to within 10 sccm. The temperature is set using the power supply as shown in Figure 2.5b. This power supply allows the temperature to be controlled within 5°C of the desired value. Therefore, the control system allows both the flow rate and temperature to be set with less than 3% error.

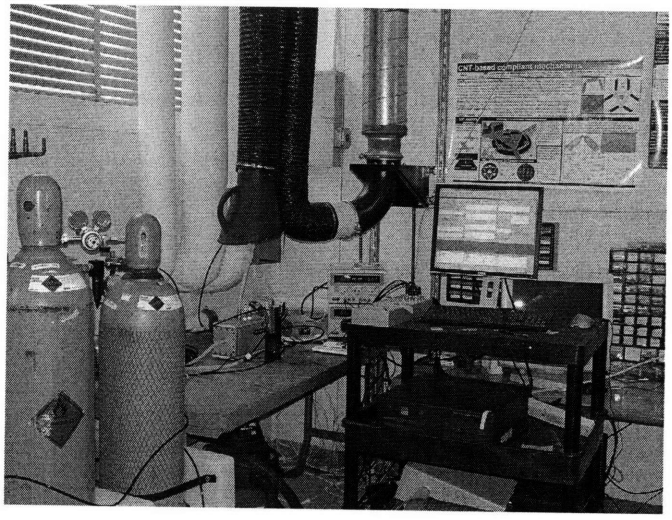

Figure 2.6. Furnace Control System.

A resistively heated CNT furnace has several advantages over traditional tube furnaces. First, the resistively heated furnace is less expensive and requires less setup time than a tube furnace. The prototype furnace build for this study cost less than $500 while tube furnaces may cost several thousands of dollars. Also, the resistively heated furnace may be heated faster than tube furnaces. The silicon platform may achieve slew rates of over 100 °C/s while tube furnaces can take over half an hour to heat up by 100°C [56]. High heating rate is important because it allows the preheat step to be separated from the growth step. With the resistively heated furnace, it takes only a few seconds to go from the preheat temperature to the growth temperature. With the tube furnace this may take over an hour. During this transitional step in the tube furnace, the catalyst particles on the substrate are free to move and agglomerate [46]. This means that the catalyst particles used for growth of CNTs in tube furnaces are typically larger. This causes the effect of the growth temperature on the CNT geometry to be exaggerated and therefore introduces unwanted sensitivity. In short, the resistively heated furnace

produces more accurate results that elucidate the effect of growth temperature on the structure of CNTs.

2.5 Experimental Design

Most experimental studies on the effect of process parameters on the diameter and number of walls in a CNT have focused on only one variable, such as temperature, catalyst particle size, catalyst composition, hydrocarbon source, or hydrocarbon flow rate. These studies are valuable in determining what parameters have a significant effect on the geometry of the CNTs grown through the CVD process. Unfortunately, these studies are unable to accurately access how much of an effect such parameters have and are therefore not very useful in the design of CNTs for specific applications. Such methods also miss any interactions between process parameters that might affect the final geometry of the CNT.

For this thesis, several multiple parameter experimental designs were studied and compared. A simple experimental design method that allows multiple parameters to be tested at once is the factorial design method [57]. In this method, a high and a low value of each parameter are chosen and tests are performed with both values of each parameter. Therefore, the total number of tests is equal to 2^n where n is the number of parameters. This means that if 3 parameters are tested, 8 tests must be run as shown in Table 2.1.

Table 2.1. Full Factorial Design Space.

Run	Parameter 1	Parameter 2	Parameter 3
1	Low	Low	Low
2	High	Low	Low
3	Low	High	Low
4	High	High	Low
5	Low	Low	High
6	High	Low	High
7	Low	High	High
8	High	High	High

Unfortunately, because only two levels of each parameter are being tested, this method does not provide full insight into the overall response of the system over the full

range of the parameters. The factorial design method is typically used to screen out unimportant variables so that more sophisticated experiments may be conducted without running hundreds of experiments. For example, Kuo et al. used a factorial design method to screen out the unimportant variables in their CVD growth process [58]. In their process, MWCNTs were synthesized using the floating catalyst method with $Fe(CO)_5$ as the catalyst precursor, methane as the reacting gas, and nitrogen as the carrier gas. Overall, they found that the reaction temperature, methane flow rate and chamber pressure had a statistically significant effect on the outside diameter of the CNTs grown while the nitrogen flow rate and the catalyst feed rate did not. Once these significant variables were determined, Kuo et al. were able to perform optimizations to find the growth conditions at which the maximum and minimum outside diameters of the CNT could be achieved.

A more sophisticated surface response design must be used in order to determine the effects of process parameters on the CNT geometry over the full range of the variables. A surface response design that is commonly used is the Box-Behnken design [57]. In this design, three levels are chosen for each variable and experimental tests were performed according to the settings in Table 2.2. In Table 2.2, +1 represents the high level, -1 represents the low level and 0 represents the medium level.

Table 2.2. Box-Behnken Experimental Design

Run	Parameter 1	Parameter 2	Parameter 3
1	-1	-1	0
2	1	-1	0
3	-1	1	0
4	1	1	0
5	-1	0	-1
6	1	0	-1
7	-1	0	1
8	1	0	1
9	0	-1	-1
10	0	1	-1
11	0	-1	1
12	0	1	1
13	0	0	0

Using the Box-Behnken design, it is possible to produce a response surface using a relatively small number of trials. The response surface produced by this method is generally not of the highest quality because most of the trials are performed on the edges of the parameter space with only one trial (run 13) located in the interior of the design space. This design method is, however, good for optimizations because the points near the edges of the parameter space as well as the center point are well known. For example, Kukovecz et al. used the Box-Brehnken design method to maximize the number of SWCNTs produced in a single CVD run [59]. In this experiment, the CNTs were grown using a fixed bed reactor with iron as the catalyst and acetylene as the reacting gas. The catalyst composition, reaction rate and flow rate were found to be the important variables using a factorial design analysis similar to that used by Kuo et al. The relation between the process parameters and the percentage of SWCNTs grown was determined using the Box-Brehnken design method. This result is given in Equation 2.1 where QDN is the quality descriptor number, *a* is the ratio of Fe to MgO in the catalyst, *b* is the reaction temperature, and *c* is the argon flow rate [59].

$$QDN = 5.163a + 0.1828b - 0.0007c + 1.1704a^2 - 0.0001b^2 - 0.0082ab - 0.0019ac - 80.22 \quad (2.1)$$

By using this equation, it was possible to optimize the SWCNT output by using the optimum values for the input parameters.

A better response may be created using a method that takes more points from the interior of the parameter space such as a central composite design [57]. In general, there are three types of central composite designs, the central composite face centered (CCF) design, the central composite circumscribed (CCC) design and the central composite inscribed (CCI) design. The CCF design is similar to the Box-Behnken design with the exception that more points are taken near the corners of the parameter space. This is indicated in Table 2.3. This design also lacks the interior points necessary to produce a high quality response surface.

Table 2.3. Central Composite Face-Centered Design.

Run	Parameter 1	Parameter 2	Parameter 3
1	-1	-1	-1
2	1	-1	-1
3	-1	1	-1
4	1	1	-1
5	-1	-1	1
6	1	-1	1
7	-1	1	1
8	1	1	1
9	-1	0	0
10	1	0	0
11	0	-1	0
12	0	1	0
13	0	0	-1
14	0	0	1
15	0	0	0

The CCC design is slightly different from the CCF design in that it uses five levels for every variable instead of three. Some of the points in the CCC design fall outside of the parameter space because it is a circumscribed design. This is indicated in Table 2.4. This results in an accurate surface response curve near the edges of the parameter space but it does not cover the center of the parameter space as well as desired.

Table 2.4. Central Composite Circumscribed Design.

Run	Parameter 1	Parameter 2	Parameter 3
1	-1	-1	-1
2	1	-1	-1
3	-1	1	-1
4	1	1	-1
5	-1	-1	1
6	1	-1	1
7	-1	1	1
8	1	1	1
9	-1.682	0	0
10	1.682	0	0
11	0	-1.682	0
12	0	1.682	0
13	0	0	-1.682
14	0	0	1.682
15	0	0	0

The CCI design is similar to the CCC design except that all of the sample values fall within the parameter space as may be seen in Table 2.5. This is important for sets of parameters that have specific limits which cannot be exceeded. The CCI design is also good at producing response surfaces around the center point because it takes multiple points from interior of the parameter space.

Table 2.5. Central Composite Inscribed Design.

Run	Parameter 1	Parameter 2	Parameter 3
1	-0.6	-0.6	-0.6
2	0.6	-0.6	-0.6
3	-0.6	0.6	-0.6
4	0.6	0.6	-0.6
5	-0.6	-0.6	0.6
6	0.6	-0.6	0.6
7	-0.6	-0.6	0.6
8	0.6	0.6	0.6
9	-1	0	0
10	1	0	0
11	0	-1	0
12	0	1	0
13	0	0	-1
14	0	0	1
15	0	0	0

A central composite inscribed design [57] was chosen for this study because some parameters, such as the methane concentration, had absolute limits that could not be exceeded. Therefore, a central composite circumscribed design could not be used to find the effect of each parameter on the output. Also, the central composite inscribed design is more accurate than other design at determining the effects of process parameters at most locations in the parameter space. Given the limits that were established on the parameter space that were established in Section 2.2, the parameters for each trial were calculated as described in the central composite inscribed design. Table 2.6 lists nominal values for each of the trials that were used in this study. Run 15 was repeated five times to determine the repeatability of the growth process. It was found that the variation between runs was not statistically significant.

Table 2.6. Central Composite Inscribed Design for Evaluating the Effect of Each Growth Parameter.

Run	Catalyst Film Thickness (nm)	Temperature °C	Methane Concentration (%)
1	1	740	55
2	1	860	55
3	5	740	55
4	5	860	55
5	1	740	82
6	1	860	82
7	5	740	82
8	5	860	82
9	3	700	68.5
10	3	900	68.5
11	0.5	800	68.5
12	6	800	68.5
13	3	800	37
14	3	800	100
15	3	800	68.5

2.6 Regression Analysis

Regression analysis is general method by which best-fit solutions may be determined for situations where there is more than one independent variable. This analysis may be used to determine the relationship between the input process parameters and the output CNT geometry.

There are several major assumptions made when using non-linear multiple regressions. First it is assumed that the errors between the predictions of the regression and the actual data are normally distributed. This is important because skewed variables may distort relations between the independent and dependent variables, and therefore create errors in the regression analysis [60]. As may be seen in Figure 2.7, the differences between the predicted and actual values of the CNT diameter approximately follow the normal distribution. Therefore, the first assumption is valid for this work.

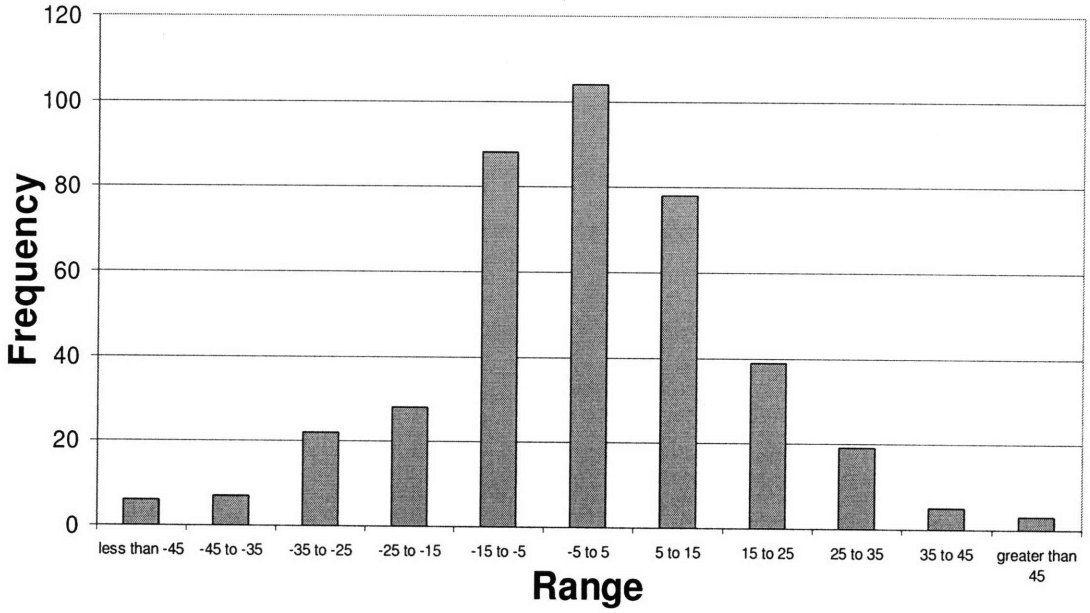

Figure 2.7. Histogram of Errors in the Growth Regression Model.

The second assumption is that the independent variables have low multicolinearity [60]. Multicolinearity is when one or more variables are a linear function of another variable. This condition is met in this growth study because the growth parameter variables (catalyst film thickness, temperature, and methane concentration) are independent of one another. If catalyst particle size was used in addition to the catalyst film thickness, temperature and methane concentration, this assumption would no longer be valid as the catalyst particle size is only a function of the film thickness, the temperature and the dewetting time.

It is also assumed in the regression model that there is homoscedasticity [60]. This means that the differences between the estimated value of the dependent variable and the actual value of the dependent value are independent of the magnitude of the dependent variable and are randomly distributed. Thus for the growth study, there should be no clear correlation between error in the value of the outside diameter estimated by the regression model and the actual value of the outside diameter. As may be seen in Figure 2.8, this condition is met. If the residual errors had been negative for smaller diameters and positive for larger diameters, then the regression model would clearly have had the incorrect functional form. Similarly, if the magnitude of the error values had started small and become larger, this homoscedasticity condition would not have been met and

different models would have had to been used for different diameter ranges. Fortunately, the data satisfies this homoscedasticity condition, and therefore a single regression model may be used to (1) describe the relationship between the independent and dependent variables over the full range of the data and (2) show that the correct functional form was likely chosen.

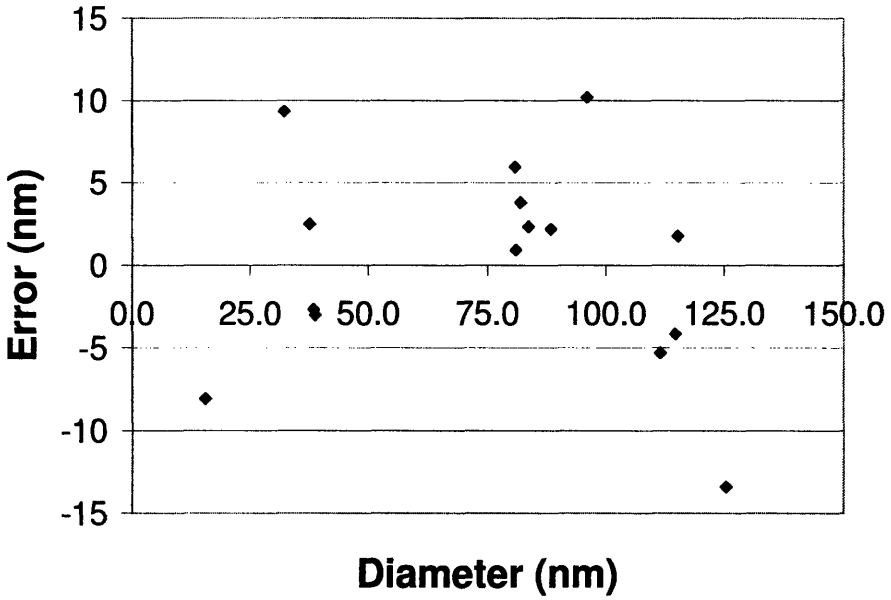

Figure 2.8. Error in Regression Model vs. CNT Diameter.

As all of the assumptions made in regression analysis are met in this growth study, regression analysis may be used to create relationships between the growth parameters and the geometry of the CNTs grown. The functional form of a multiple regression is presented in Equation 2.2 [60].

$$Y = a_0 + a_1 \hat{x}_1 + a_2 \hat{x}_2 + a_3 \hat{x}_3 + \ldots + a_k \hat{x}_k \qquad (2.2)$$

where $a_0 \ldots a_k$ are constants and $\hat{x}_1 \ldots \hat{x}_k$ are independent variables or are functions of independent variables. For example, if x_1 and x_2 are two independent variables then three possible $\hat{x}'s$ could be:

$$\hat{x}_1 = x_1$$
$$\hat{x}_2 = x_2$$
$$\hat{x}_3 = x_1 x_2$$

This is important because it allows the interactions between variables in the growth study to be accounted for in the regression analysis. Similarly, non-linearities may be included in the regression analysis by allowing the $\hat{x}'s$ to be non-linear functions of x_1 and x_2. For example, some possible $\hat{x}$ values could be:

$$\hat{x}_1 = x_1^2$$
$$\hat{x}_2 = \ln(x_2)$$
$$\hat{x}_3 = x_1 - x_2$$

Once the correct functional form has been determined, the values of the constants $a_0 \ldots a_k$ may be determined by minimizing the sum of the squares of the errors. For each data point, the error is by Equation 2.3 where y_i is the measured value of the dependent variable.

$$e = a_0 + a_1 \hat{x}_{1i} + a_2 \hat{x}_{2i} + a_3 \hat{x}_{3i} + \ldots + a_k \hat{x}_{ki} - y_i \tag{2.3}$$

The sum of the squares of the errors is then given by Equation 2.4.

$$E = \sum_{i=1}^{n} \left(a_0 + a_1 \hat{x}_{1i} + a_2 \hat{x}_{2i} + a_3 \hat{x}_{3i} + \ldots + a_k \hat{x}_{ki} - y_i \right)^2 \tag{2.4}$$

The sum of the errors may then be minimized by differentiating with respect to each $\hat{x}$ and setting the resulting equations to zero. This set of equations can then be solved simultaneously to determine the values of the constants $a_0 \ldots a_k$. Once these constants have been determined, they may be plugged into the multiple regression model and used

to determine the relationship between the growth process parameters and the CNT geometry.

In Chapter 3, the setup and procedures described in this chapter will be used to determine the effect of each of the process parameters on the CNT geometry. Each of the runs given by the Central Composite Inscribed experimental design will be tested. Regression analysis will then be used to determine the effect of each of the process parameters on the CNT diameter and wall thickness. The results of these regressions will then be used to design growths for specific applications in Chapter 5.

Chapter

3

Results and Discussion

3.1 Introduction

In order to determine the effect of each of the process parameters on the CNT geometry, several growths were performed using the central composite inscribed experimental design. The results of these growths are presented in this chapter along with the regressions used to determine the effect of each of the process parameters. Based upon the results of these regressions, a sensitivity analysis was also performed and is presented in this chapter.

3.2 CNT Outside Diameter Observations

3.2.1 Effect of Catalyst Particle Size on CNT Diameter

Previous work has suggested that the outside diameter of a carbon nanotube is set in-part by the size of the catalyst particle that is used to grow the CNT [61]. The size of the catalyst particle in this work is a function of the catalyst film thickness, the annealing time and the annealing temperature. Therefore, the size of the carbon nanotube should be a function of the catalyst film thickness. Figure 3.1 shows that an increase in catalyst film thickness yields an increase in the diameter of the CNT. For example, in sample A which has a 0.5 nm thick catalyst film, the average CNT diameter is 15.5 nm while in sample B which has a 1 nm thick catalyst film, the average CNT diameter is 38.5 nm. Similarly, the average CNT diameter continues to increase in C and D from 82 nm to 111.5 nm as the catalyst film thickness increases from 3 nm to 5 nm, respectively.

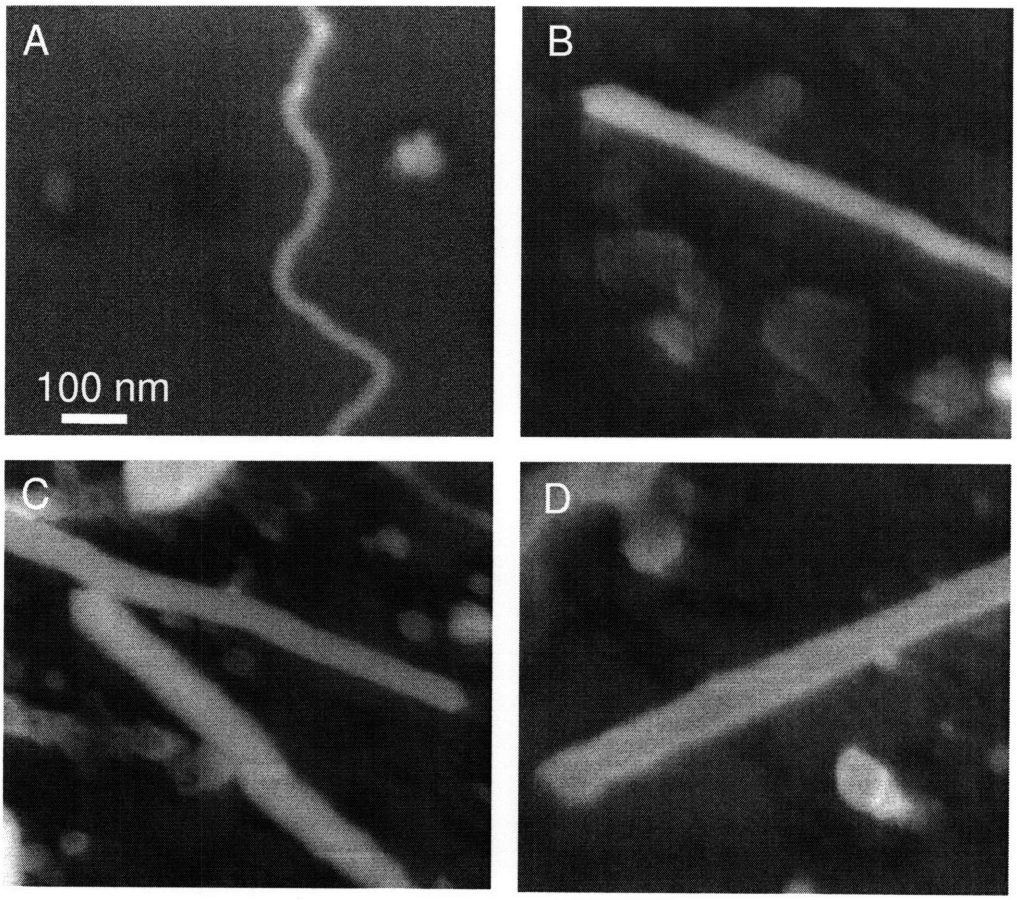

Figure 3.1. SEM images of CNTs Grown with Catalyst Film Thicknesses of (A) 0.5 nm (B) 1 nm (C) 3 nm and (D) 5 nm.

The outer diameters of the CNTs that were grown using the Central Composite inscribed method, as described in Chapter 2, are plotted against the catalyst film thickness in Figure 3.2. This figure shows that as the catalyst film thickness increases, the CNT outer diameter increases. This shows that there is a strong positive correlation between the catalyst film thickness and the outside diameter of the CNTs grown from that catalyst. This relationship, however, is not linear as might be expected. In fact, a logarithmic function best fits the data as shown by the high R^2 squared value. This R^2 value indicates that over 96% of the variance in the CNT diameter may be explained by the variance in the catalyst film thickness.

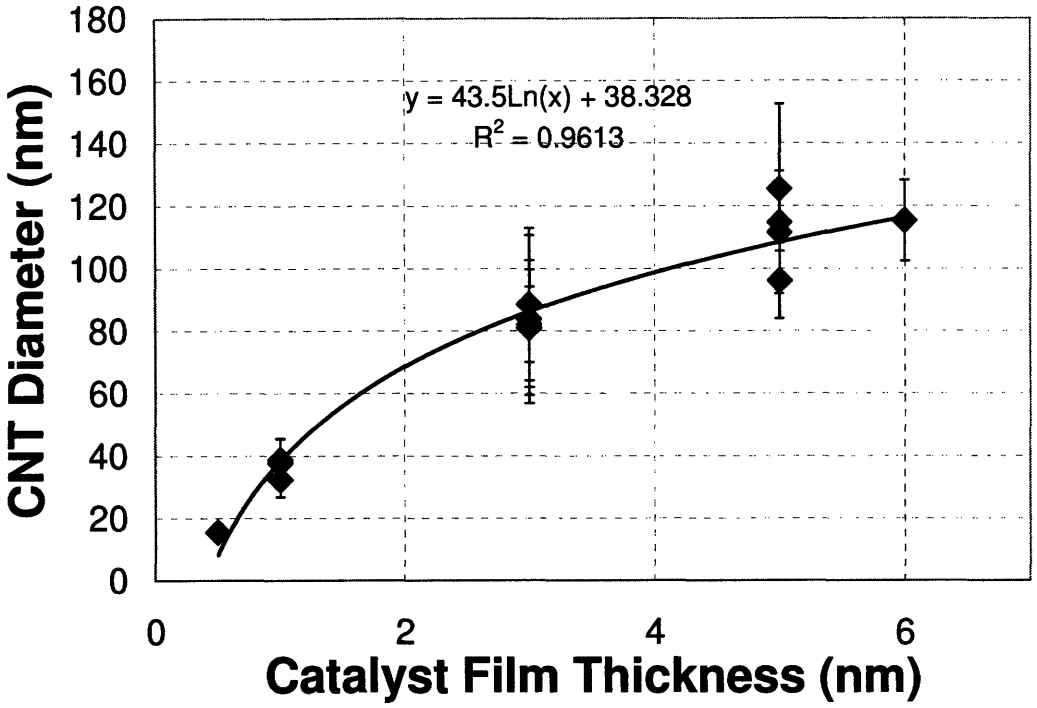

Figure 3.2. CNT Diameter vs. Catalyst Film Thickness.

The logarithmic dependence of the CNT diameter on the catalyst film thickness is caused by the differences in growth rates between catalyst particles of different sizes. Initially, when the catalyst particles are deposited, the size of the nucleated catalyst particles is proportional to the thickness of the catalyst film. During the annealing step in the growth process, these catalyst particles grow through the agglomeration of the iron particles that are diffusing along the substrate surface in a process known as Oswalt ripening. The rate of this process is inversely proportional to the radius of the catalyst particle as may be seen in Equation 3.1.

$$\frac{dr}{dt} = D(C - C_s)\frac{V_m}{r} \tag{3.1}$$

In Equation 3.1 r is the radius of the catalyst particle, D is the diffusion coefficient, C is the bulk concentration, C_s is the concentration on the solid surface and V_m is the molar volume of the nuclei [62]. Thus, as the radius of the catalyst particle increases, the growth rate should decrease.

Catalyst particle growth during the annealing process is a significant factor in the final size of the catalyst because a relatively long annealing time of 15 minutes was used in the growth process. This may be seen in the fact that in this growth study 0.5 nm and 1 nm thick films were used to grow CNTs with diameters between 15 and 40 nm while in other studies that do not have an annealing step, such films are used to grow single and double walled CNTs [63]. The difference in the final catalyst particle size between two different film thicknesses therefore decreases as the catalyst film thickness increases because the growth of the catalyst particles is significant and the growth rate inversely proportional to the radius of the catalyst particle. This may be seen in Equation 3.2 where δr is the difference in radius between two particles, r_0 is the initial radius, δr_0 is the initial radius difference, t is the annealing time and $k_D = 2D(C\text{-}C_s)V_m$.

$$\delta r = \frac{r_0 \delta r_0}{\sqrt{k_D + r_0^2}} \tag{3.2}$$

Therefore, as the catalyst film thickness increases, the rate of chance of the catalyst particle size decreases which causes the dependence of the catalyst particle size on the catalyst thickness to be logarithmic. This then causes the outside diameter of the CNTs to be logarithmically dependent on the catalyst film thickness because the outside diameter is directly proportional to the size of the catalyst particle used to grow the CNT.

3.2.2 Effect of Growth Temperature on CNT Diameter

As discussed in Chapter 1, there is generally thought to be a strong positive correlation between the growth temperature and the outside diameter of the CNTs grown. While this positive correlation was observed in this growth study, the dependence of the of the outside diameter of the CNTs on the growth temperature was found to be relatively week as may be seen in Figure 3.3. The R^2 value indicates that only about 1.3% of the variance in the CNT diameter may be explained by the variance in the temperature.

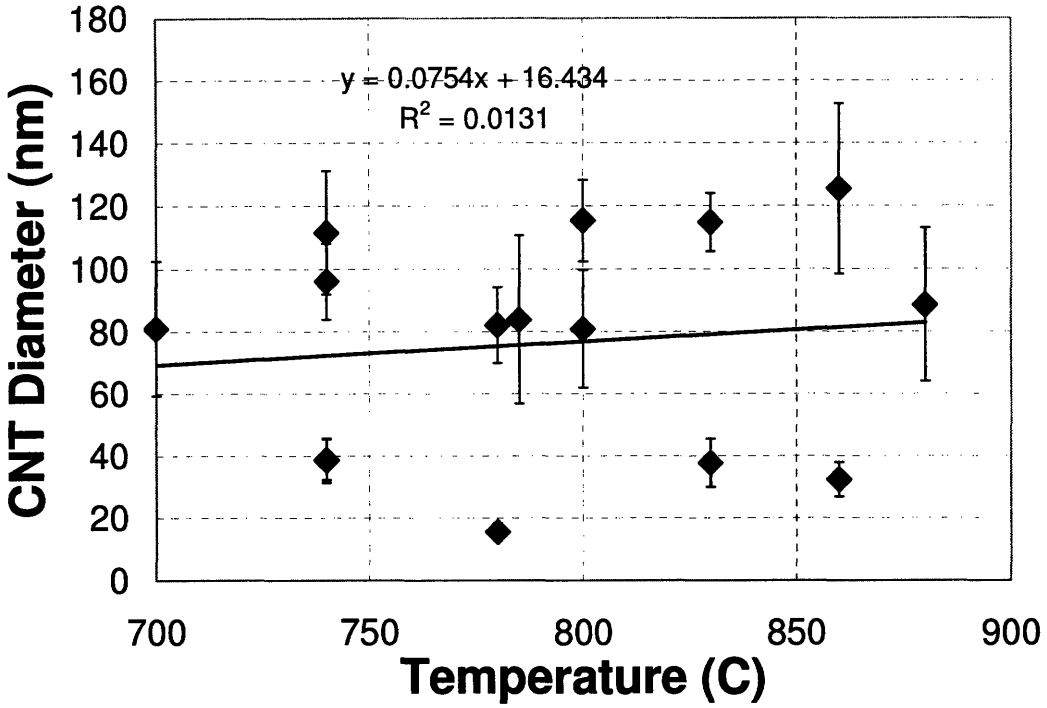

Figure 3.3. CNT Diameter vs. Growth Temperature.

The relatively weak dependence of the outside diameter of the CNTs on the growth temperature is likely due to catalyst growth between the end of the preheat step and the initiation of CNT growth. At higher temperatures, the catalyst particles should be able to diffuse along the surface of the substrate at a higher rate. This higher rate of diffusion would cause more catalyst particles to come into contact and agglomerate into larger particles. Therefore, the higher growth temperatures create larger catalyst particles which cause the outside diameter of the CNTs to increase.

The temperature effect in this work is weaker than has been reported in other work [43]. The difference is due to the fact that the time between the preheat step and the actual growth of the CNTs is much smaller (10's of seconds vs. 10's of minutes) for the resistively heated furnace used in this study than for tube furnaces used in previous studies. In the resistively heated furnace, it takes only a few minutes to heat the substrate to the growth temperature and to introduce the hydrocarbon gas, while in the tube furnace this process can take over an hour. Thus, the catalyst particles have less time to agglomerate into larger particles and the dependence of the outside diameter on the growth temperature is much lower in this study.

3.2.3 Effect of Methane Concentration on CNT Diameter

As shown in Chapter 1, previous research has suggested that there is a positive relationship between the hydrocarbon concentration and the CNT diameter for SWCNTs. This relationship was weak compared to the dependence of the outside diameter on the catalyst particle size. This type of causal relationship has never been demonstrated for MWCNTs. Figure 3.4 shows the relationship between methane concentration and CNT diameter for CNTs grown using the central composite inscribed method.

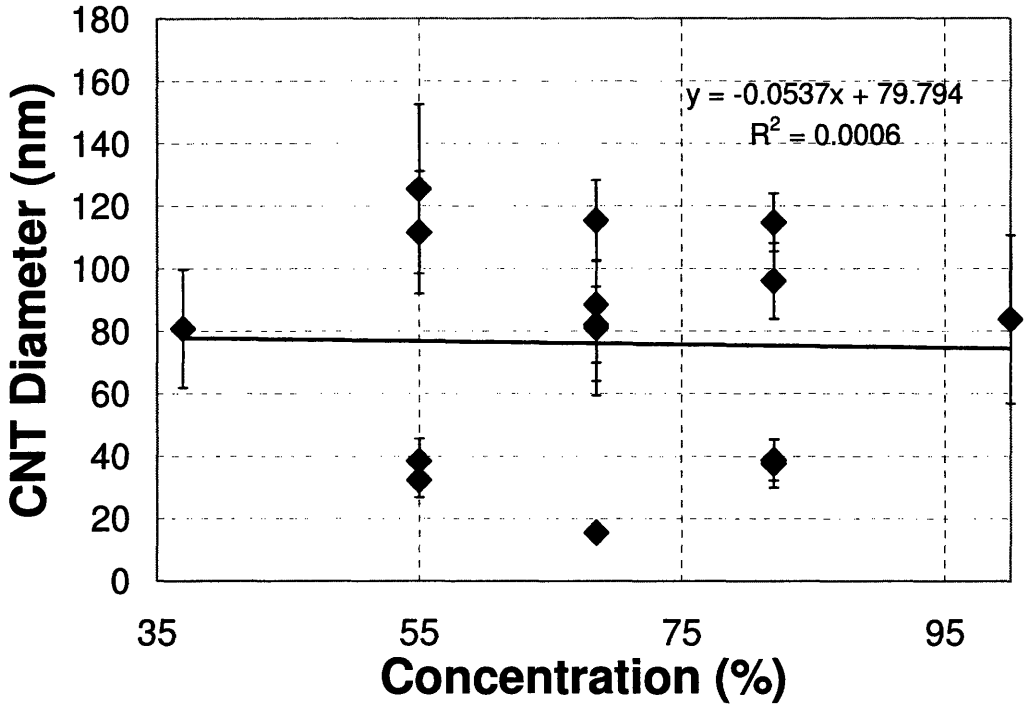

Figure 3.4. CNT Diameter vs. Concentration.

Figure 3.4 shows that there is a very weak (less than 3.5 nm change over the entire parameter space) negative correlation between the CNT diameter and the methane concentration. The variation in concentration, however, only explains about 0.06% of the variation in the CNT diameter. This low R^2 value and weak correlation between variables indicates that this result is probably not statistically significant and that the CNT diameter is independent of the methane concentration.

3.3 CNT Outside Diameter Regression Analysis

In order to determine the exact relationship between the growth process parameters and the outside diameter of the CNTs grown, a full regression analysis, with cross product terms, was performed. This regression analysis allows the independent effect of each process parameter to be examined. The results for this regression analysis are presented in Table 3.1.

Table 3.1. ANOVA Table for Full Regression Model.

	Coefficients	*Standard Error*	*t Stat*	*P-value*	*Lower 95%*	*Upper 95%*
Intercept	178.8	88.9	2.01	0.045	4.06	353
Film thickness	-10.91	9.22	-1.18	0.237	-29.0	7.21
Temperature	-0.231	0.111	-2.09	0.0376	-0.450	-0.0133
Concentration	-1.22	1.26	-0.965	0.335	-3.70	1.26
Temp * Concentration	0.00196	0.00159	1.23	0.218	-0.00116	0.00507
Thickness * Temp	0.0490	0.0105	4.66	0.00000	0.0283	0.0697
Thickness * Concentration	-0.121	0.0418	-2.88	0.00415	-0.203	-0.0383

From this full regression analysis, only the cross products of catalyst film thickness with temperature and concentration are statistically significant at a 99.9% confidence level as indicated by the P-value of less than 0.001. The catalyst film thickness and the temperature are not independently statistically significant as would be expected. Also, the adjusted R^2 value is only 0.785, which indicates that a better model probably exists. This poor fit is likely due to the lack of independence between variables. The cross product terms are not independent of the catalyst film thickness parameter because the catalyst film thickness is the dominant variable, as indicated by its presence in both the statistically significant cross product terms. Therefore, the model is over defined and no longer satisfies the requirements for regression analysis presented in Chapter 2.

In order to ensure the independence of each of the regression variables, the cross product terms were eliminated from the regression model. The results of this new linear regression model are presented in Table 3.2.

Table 3.2. ANOVA Table for Full Linear Regression Model.

	Coefficients	*Standard Error*	*t Stat*	*P-value*	*Lower 95%*	*Upper 95%*
Intercept	-15.69	14.48	-1.08	0.279	-44.2	12.77
Film thickness	19.72	0.535	36.9	5.70E-132	18.67	20.8
Temperature	0.0449	0.0169	2.66	0.0081	0.0117	0.0781
Concentration	-0.0338	0.0575	-0.588	0.557	-0.147	0.0792

The results of this full linear regression model match the results presented in Section 3.1 more closely than regression analysis that included the cross product terms. The catalyst film thickness and the temperature are significant at a 99% confidence level in this model. The y-intercept and the concentration are not statistically significant. Therefore, the model may be improved by removing these variables from the model. The results of this revised linear regression model are presented in Table 3.3.

Table 3.3. ANOVA Table for Modified Linear Regression Model.

	Coefficients	*Standard Error*	*t Stat*	*P-value*	*Lower 95%*	*Upper 95%*
Intercept	0	#N/A	#N/A	#N/A	#N/A	#N/A
Film thickness	19.63	0.531	37.0	1E-132	18.58	20.7
Temperature	0.0226	0.002188	10.34	2.04E-22	0.0183	0.0269

This model explains 95% of the variation of in the outside diameter of the CNT. The results of the catalyst film thickness and the temperature are highly statistically significant as indicated by the very high t-statistics for both variables. The results of this revised linear regression model indicate that for a 1 nm increase in the catalyst film thickness, the CNT diameter increases by 19.63 nm and that for a 10°C increase in temperature, the CNT diameter increases by 0.226 nm.

While this revised linear regression model is useful, a better fit may be achieved by including non-linear variables. As discussed in Section 3.1, there is a logarithmic dependence of the CNT outside diameter on the catalyst film thickness. Therefore, by introducing a logarithmic parameter for the catalyst film thickness into the regression model it should be possible to make a better fit to the data. The results of this non-linear model are presented in Table 3.4.

Table 3.4. ANOVA Table for Full Non-linear Regression Model.

	Coefficients	*Standard Error*	*t Stat*	*P-value*	*Lower 95%*	*Upper 95%*
Intercept	-1.99	13.94	-0.143	0.886	-29.4	25.4
Ln(Film thickness)	43.8	1.14	38.6	3.7E-138	41.6	46.0
Temperature	0.0545	0.0163	3.34	0.000907	0.0225	0.0866
Concentration	-0.0424	0.0555	-0.764	0.446	-0.152	0.0668

Again, both the y-intercept and the methane concentration are not statistically significant variables. Therefore, both these variables are eliminated from the model and a regression is performed on only the statistically significant variables. The results to this modified nonlinear regression are presented in Table 3.5.

Table 3.5. ANOVA Table for Modified Non-linear Regression Model.

	Coefficients	*Standard Error*	*t Stat*	*P-value*	*Lower 95%*	*Upper 95%*
Intercept	0	#N/A	#N/A	#N/A	#N/A	#N/A
Ln(Film thickness)	43.7	1.13	38.8	2.9E-139	41.5	45.9
Temperature	0.0484	0.00156	31.01	1.4E-109	0.0453	0.0515

This modified non-linear regression model fits the data extremely well. Both variables are statistically significant at over a 99.99% confidence level and the adjusted R^2 value is 0.953, indicating that over 95.3% of the variation in the CNT outside diameter may be explained by the natural *log* of the catalyst film thickness and the growth temperature. From this regression model, an equation may be derived to design a growth process to control the outside diameter of the CNTs as seen in Equation 3.3 where D is the CNT diameter in nm, F is the catalyst film thickness in nm, and T is the temperature in degrees Celsius.

$$D = 43.72\ln(F) + 0.0484T \tag{3.3}$$

This equation shows that for every 1 percent increase in the catalyst film thickness, the CNT outside diameter will increase by 0.435 nm and that for every 10° C increase in temperature, the CNT diameter will increase by 0.484 nm.

3.4 CNT Wall Thickness Observations

After the CNT diameter is set using Equation 3.3, the effect of the process parameters on the CNT wall thickness must be determined in order to set the geometry of the CNT as well as the stiffness and natural frequency of CNT-based compliant mechanisms. The wall thickness of a MWCNT is defined as the outside radius of the CNT minus the inside radius of the CNT as shown in Equation 3.4.

$$\text{CNT Wall Thickness} = \frac{\text{CNT Outside Diameter - CNT Inside Diameter}}{2} \qquad (3.4)$$

In this study, the typical wall thickness of the CNTs ranged from 4 nm to 40 nm depending on the growth conditions. Figure 3.5 shows a typical CNT grown in this study that is 96 nm in diameter and has a wall thickness of 33.3 nm. The arrows in the image show the edges of the CNT wall.

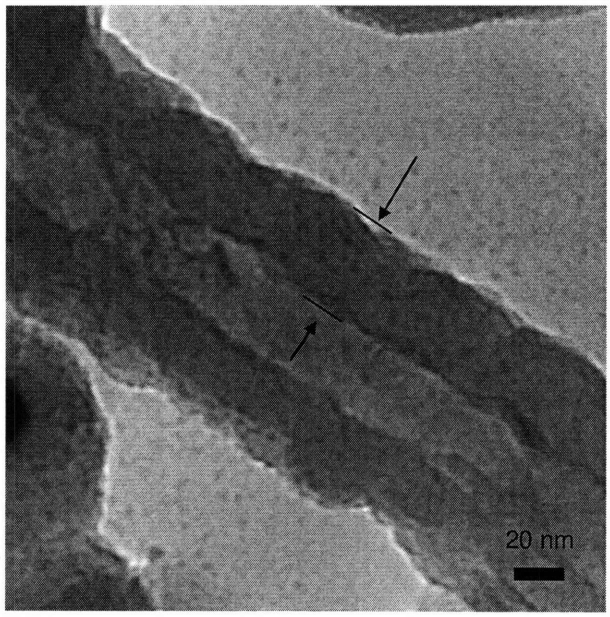

Figure 3.5. TEM Image of CNT with Wall Thickness Indicated by Arrows.

Given the wall thickness of the CNT, the number of individual shell walls that make up the CNT may easily be calculated by dividing the CNT wall thickness by the

shell wall thickness as may be seen in Equation 3.5. Previous experiments have shown that the shell wall thickness is equal to the spacing between graphene sheets in graphite which is 0.34 nm [64].

$$\text{Number of Walls} = \frac{\text{CNT Wall Thickness}}{\text{Shell Thickness}} = \frac{\text{CNT Wall Thickness}}{0.34} \qquad (3.5)$$

Based upon Equation 3.4, there is a clear correlation between the outside diameter of a CNT and its wall thickness. This correlation may be seen in Figure 3.6 where the CNT wall thickness increases linearly with the CNT diameter. This relationship is, however, not 1:2 as might be implied by Equation 3.4 because the inner diameter of the CNT also tends to increase as the outside diameter increases. In fact, Figure 3.6 implies that for every 1 nm increase in the CNT out side diameter, the wall thickness increases by about 0.3 nm. This is equivalent to an increase of about one shell wall for every one nanometer increase in the CNT diameter. Also, as may be seen by the R^2 value, the variance in the CNT outside diameter may be used to explain over 86 percent of the variance in the CNT wall thickness.

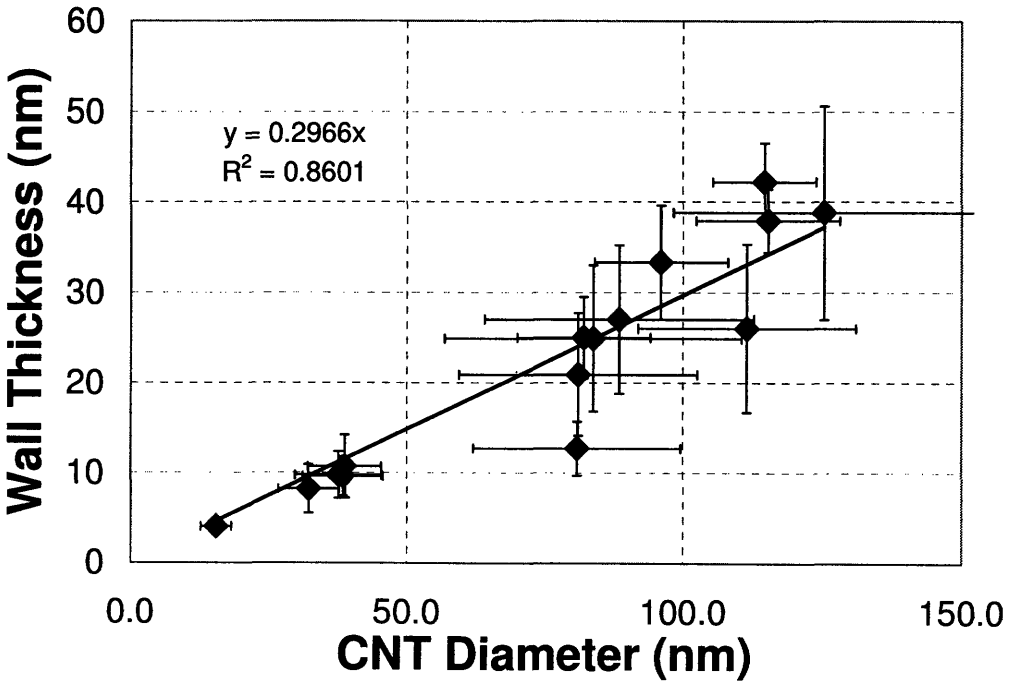

Figure 3.6. CNT Wall Thickness vs. CNT Outside Diameter.

Given this strong relationship between the wall thickness and the outside diameter of the CNT, there should be a similar relationship between the CNT wall thickness and the catalyst film thickness as the CNT outside diameter is highly dependent on the catalyst film thickness. This relationship may be seen in Figure 3.7. For every 1 nm increase in catalyst film thickness, the CNT wall thickness increases by about 7 nm. The R^2 value of this relationship is slightly lower than for the relationship between the CNT wall thickness and the CNT diameter because the CNT diameter is dependent on the growth temperature as well catalyst film thickness. The R^2 values are, however, very close, which indicates that the catalyst film thickness and the CNT outside diameter variables may be interchanged in the modeling of the effects of different process parameters on the CNT wall thickness.

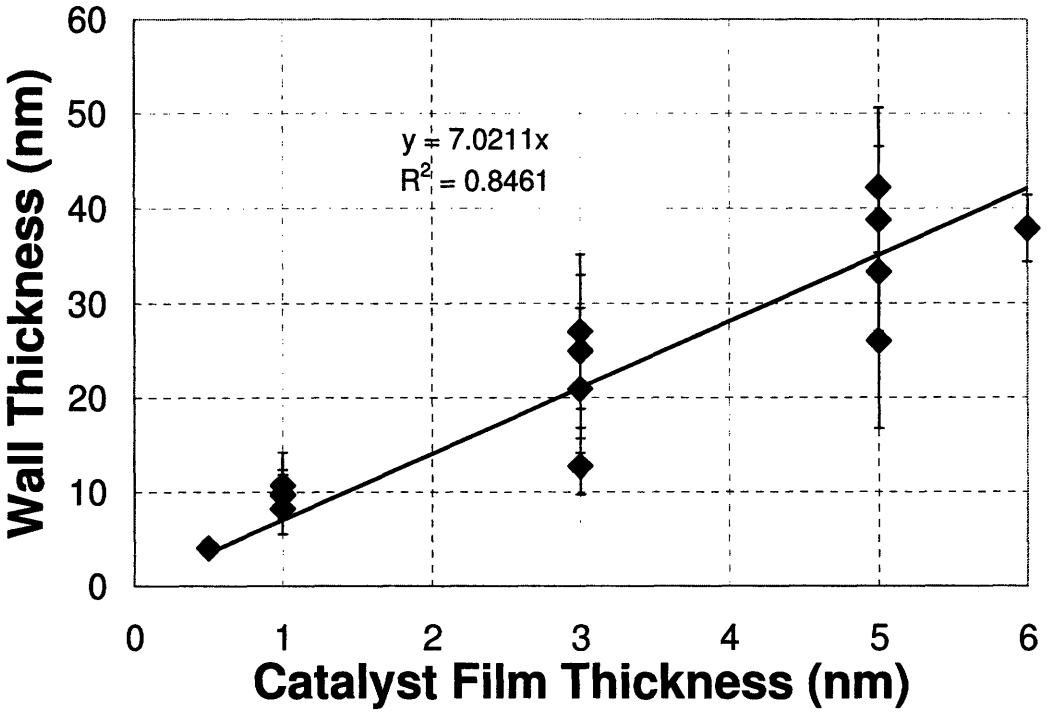

Figure 3.7. CNT Wall Thickness vs. Catalyst Film Thickness.

The growth temperature should also play an important role in the CNT wall thickness because the diffusion rate of carbon into the catalyst particle is dependent on temperature. As the temperature is increased, the diffusion rate should also increase, thereby allowing the carbon to diffuse further into the catalyst particle before it

precipitates out. This should cause the inner diameter of the CNTs to decrease and the overall wall thickness to increase. This expected result was experimentally verified in this study and may be seen in Figure 3.8. The results of this study show that a 10° C increase in the growth temperature will result in a 0.28 nm increase in the wall thickness. This shows that one new shell will be added to the CNT when the growth temperature is increased by about 12° C. The R^2 value for this result indicates that only about 3 percent of the variance in the CNT wall thickness may be explained by the variance in the growth temperature. This R^2 value is much smaller than the R^2 value for the relationship between the CNT wall thickness and the catalyst film thickness. This shows that the growth temperature has only a second order effect on the CNT wall thickness.

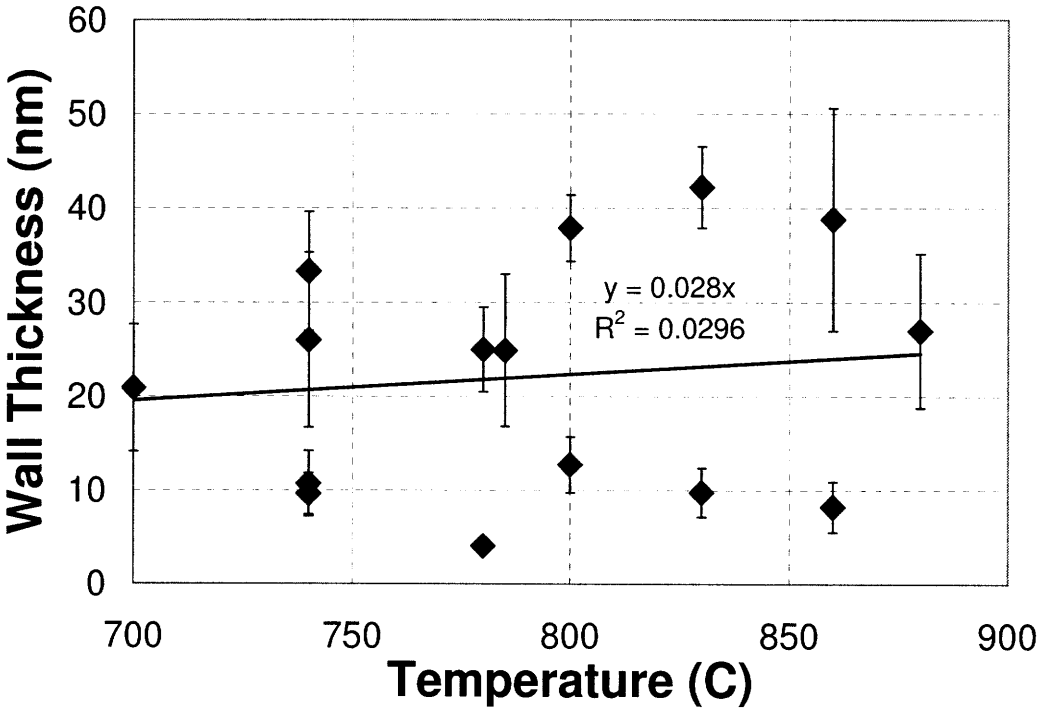

Figure 3.8. CNT Wall Thickness vs. Growth Temperature.

Similarly, the concentration of the methane gas present during the CNT growth will also have an effect on the diffusion rate of the carbon into the catalyst particle. Higher concentrations of methane should increase the rate at which carbon is able to diffuse into the catalyst particle due to the higher carbon concentration gradient between the surface and the center of the catalyst. This higher diffusion rate will allow the carbon

to diffuse further into the catalyst particle before it precipitates out and forms the CNT. This will result in an increase in the CNT wall thickness. This result may be seen in Figure 3.9. This figure shows that for every 1 percentage point increase in methane concentration, the CNT wall thickness will increase by 0.31 nm. This is equivalent to an increase of almost one shell in the CNT for each 1 percentage point increase in concentration. The R^2 value is, however, low indicating that only about 0.5 percent of the variance in the CNT wall thickness may be explained by the changes in methane concentration. This result implies that the methane concentration is less important than catalyst film thickness or the CNT outside diameter when predicting the CNT wall thickness. This result might still have a statistically significant effect on the CNT wall thickness and, therefore, was included in the regression model for the CNT wall thickness.

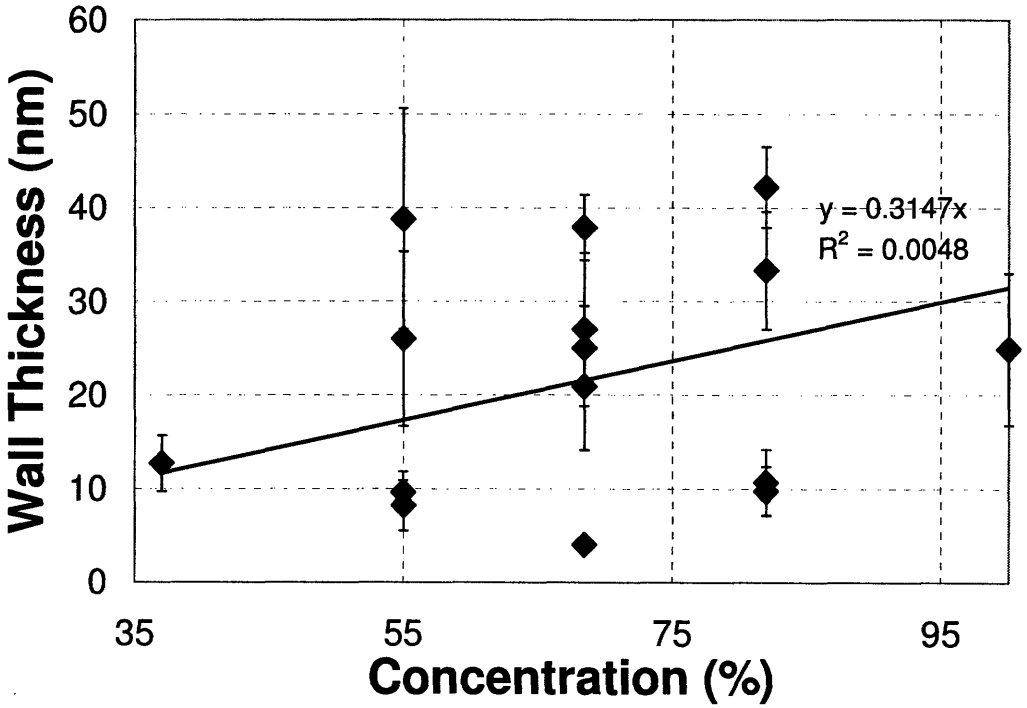

Figure 3.9. CNT Wall Thickness vs. Methane Concentration.

3.5 CNT Wall Thickness Regressions

Now that the general effects of each of the process parameters on the CNT wall thickness have been determined, regression analyses must be performed in order to determine an empirical relationship between the process parameters and the CNT wall thickness that may be used to design CNTs. As with the regression model for the outside diameter, it is helpful to start with a complete model that includes cross product terms in order to determine which variables must be included in the regression model. The results of the full regression model for the CNT wall thickness are presented in Table 3.6.

Table 3.6. ANOVA Table for Full Regression Model.

	Coefficients	*Standard Error*	*t Stat*	*P-value*	*Lower 95%*	*Upper 95%*
Intercept	42.1	33.3	1.26	0.207	-23.4	107.6
Film thickness	-19.44	3.43	-5.66	2.9E-08	-26.2	-12.7
Temperature	-0.0513	0.0414	-1.24	0.216	-0.133	0.0300
Concentration	-0.0754	0.491	-0.153	0.878	-1.04	0.891
Temp * Concentration	0.0282	0.00398	7.10	5.97E-12	0.0204	0.0360
Film Thickness * Temperature	0.000115	0.000611	0.188	0.851	-0.00109	0.00132
Film Thickness * Concentration	0.0528	0.0159	3.32	0.001	0.0215	0.0841

This table shows that only catalyst film thickness, the temperature/concentration cross product and the catalyst film thickness/concentration cross product are statistically significant. This implies that the catalyst film thickness is the dominant variable in the CNT wall thickness because it is statistically significant by itself. The growth temperature and methane concentration are likely only second order terms because they are only statistically significant as part of cross product variables. Unfortunately, the R^2 value for this regression is 0.766 meaning that only about 76.6 percent of the variation in the CNT wall thickness may be explained by the model. The occurs because not all of the variables are independent. Therefore, by moving to a simpler linear regression that contains only independent variables, it should be possible to improve the model. The results of this linear regression model are presented in Table 3.7

Table 3.7. ANOVA Table for Full Linear Regression Model.

	Coefficients	*Standard Error*	*t Stat*	*P-value*	*Lower 95%*	*Upper 95%*
Intercept	-42.1	5.53	-7.62	1.85E-13	-53.0	-31.3
Film thickness	6.51	0.206	31.58	1.9E-110	6.11	6.92
Temperature	0.0418	0.00648	6.46	3.12E-10	0.0291	0.0545
Concentration	0.169	0.0220	7.68	1.27E-13	0.126	0.213

With this linear regression model the catalyst film thickness, the growth temperature, and the methane concentration parameters are all statistically significant at over a 99.99% confidence level. This shows that each of the process parameters has a tangible effect on the CNT wall thickness. The value of the Y-intercept is also statistically significant and negative. This is due to the limits placed on some of the process parameters such as the growth temperature and the concentration. The minimum temperature at which CNTs will grow, under the process conditions described in Chapter 2, is 700 °C and the minimum methane concentration is 35%. As such, a negative Y-intercept must be introduced to force the CNT wall thickness to go to zero as the CNT diameter approaches zero.

The results of this linear regression indicate that a 1 nm increase in the catalyst film thickness will result in a 6.5 nm increase in the CNT wall thickness. Similarly, a 10° C increase in the growth temperature will result in a 0.4 nm increase in the CNT wall thickness and a 1% increase in the methane concentration will result in a 0.17 nm increase in the CNT wall thickness. Therefore, over the entire parameter space, the catalyst can change the CNT wall thickness by 35.8 nm, the growth temperature can have an effect of 8.4 nm on the CNT wall thickness, and the concentration can contribute about 11 nm to the change in CNT wall thickness.

While the linear regression model accurately reflects the effect of different process parameters on the CNT wall thickness, it is possible to increase the utility of the model in being able to design CNTs for specific applications by introducing the CNT outside diameter as a variable in the model. This would make it possible to select an outside diameter of the CNT and then to use that selection to identify the process parameters that are not included in the outside diameter model; such as the methane concentration. If both the CNT outside diameter and the catalyst film thickness are

included in the model, not all of the variables in the model will be independent because the CNT outside diameter and catalyst film thickness are highly correlated. Therefore, in order to include the CNT outside diameter in the model, the catalyst film thickness must be removed from the regression. The results of this design regression model are presented in Table 3.8.

Table 3.8. ANOVA Table for Design Model Regression.

	Coefficients	*Standard Error*	*T Stat*	*P-value*	*Lower 95%*	*Upper 95%*
Intercept	-38.3	3.99	-9.58	1.07E-19	-46.13	-30.42
CNT Outside Diameter	0.307	0.00667	46.1	5.5E-161	0.294	0.320
Temperature	0.0316	0.00475	6.67	8.85E-11	0.0223	0.0410
Concentration	0.166	0.0160	10.33	2.72E-22	0.134	0.197

In this design regression model each of the variables are statistically significant at over a 99.99% confidence level. Also, the R^2 value of 0.854 for this model is high indicating that over 85 percent of the variation in the CNT wall thickness may be explained by this model. This good fit and high R^2 value, indicate that any colinearity is small enough that it does not create a major source of error in the model. For example, the outside diameter of the CNTs has a weak, positive correlation with the growth temperature as may be seen in Equation 3.3. This correlation results in a small, but statistically significant reduction in the temperature coefficient when the CNT outside diameter is substituted into the model for the catalyst film thickness. This change in the temperature is about equal to the temperature coefficient from Equation 3.3 multiplied by the CNT outside diameter coefficient in Table 3.8. Therefore, if Equation 3.3 was substituted back into the design regression model, the dependence of the CNT wall thickness on the temperature would not be significantly different from the dependence of the CNT wall thickness on temperature from the linear regression model. Similarly, because the outside diameter is independent of the methane concentration, the dependence of the CNT wall thickness on the methane concentration is not statistically different for the linear regression and the design models.

Based upon the regression analysis presented in Table 3.8, a design formula for the CNT wall thickness may be created. This design equation is presented in Equation

3.6 where t_w is the wall thickness in nm, D is the CNT diameter in nm, T is the temperature in °C, and C is the methane concentration in percentage points.

$$t_w = -38.28 + 0.307D + 0.0316T + 0.166C \quad (3.6)$$

Equation 3.6 may be modified to determine the number of shell walls the MWCNT is composed of by dividing the CNT wall thickness by the thickness of an individual shell wall. This result is presented in Equation 3.7 where N_w is the number of walls.

$$N_w = -112.58 + 0.904D + 0.0931T + 0.487C \quad (3.7)$$

This equation shows that for every 1.1 nm increase in the CNT diameter, one new shell wall is added. Similarly, for every 10.7 °C increase in the growth temperature, one shell wall is added to the CNT and for every 2% increase in the methane concentration one shell wall is added. Therefore, using this design equation, it should be possible to create multi-walled carbon nanotubes with a specific number of walls. However, the accuracy of the number of walls is highly dependent on how tightly the process parameters can be controlled.

3.6 Sensitivity Analysis

In this section it is shown that the largest source of error in growing CNTs with an specific diameter and wall thickness is the dewetting of the catalyst film into nanoparticles. This process is hard to control because small variations in the initial film structure may result in large differences in the final nanoparticle size. This may be seen in the SEM image of a 1 nm thick film shown in Figure 3.10. In this figure, the average catalyst particle size is 37.6 nm with a standard deviation of 5.0 nm or about 13%. This percent standard deviation is about average for the catalyst films used in this study. The maximum standard diviation in the catalyst particle size was to be 15.7% for the 3 nm thick film and the minimum standard deviation was found to be 11.1% for the 5 nm thick

film. The average standard deviation in the catalyst nanopaticles for all the films tested was found to be 13.4% of the catalyst particle size. Therefore, this standard deviation was used to calculate the expected errors in the CNT diameter and wall thickness.

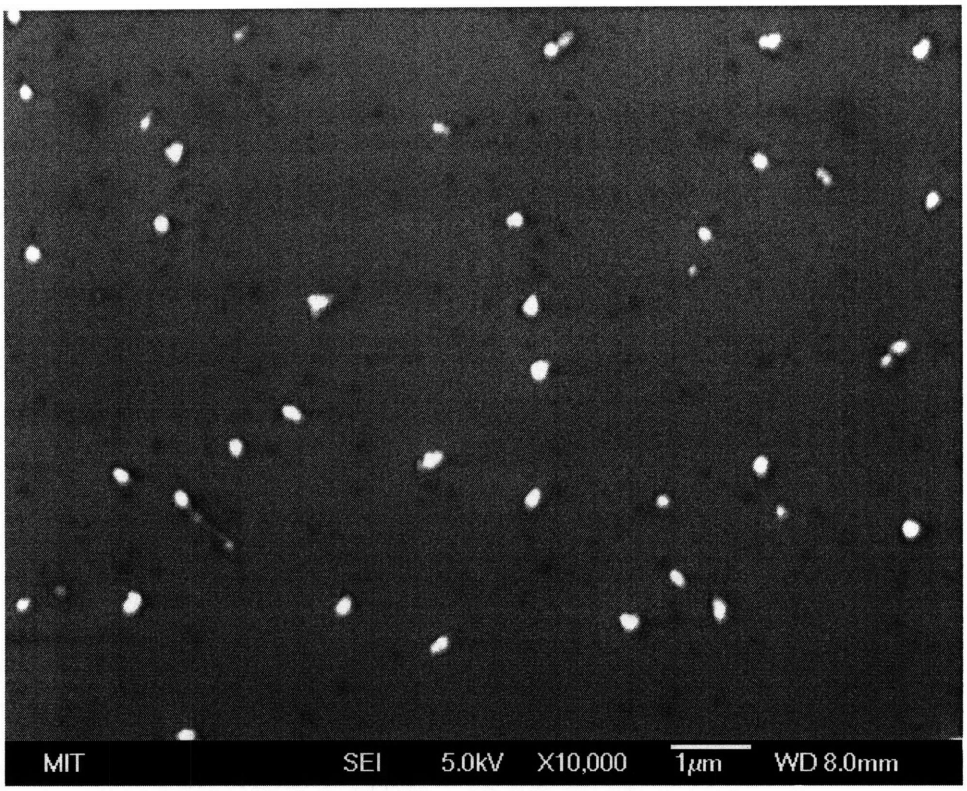

Figure 3.10. Deposited Catalyst Particles.

The error caused by the variation in the catalyst dewetting may be found by plugging the standard deviation of 13.4% into Equation 3.3 for the film thickness. This results in an error of 5.50 nm in the outside diameter of the CNT. This error may then be combined with the error caused by the variation in the temperature during the CNT growth process. Over the 20 minute growth time, the growth temperature can easily be controlled to with 10 °C. Plugging this temperature error into Equation 3.3, the error in the CNT outside diameter caused by the variation in temperature is 0.48 nm. Using equation 3.8, where S is the standard deviation, the total expected standard deviation in the CNT outside diameter is found to be 5.52 nm. This means that almost all of the variation in the CNT outside diameter is caused by the dewetting of the catalyst film. Therefore, better methods for creating uniform catalyst particles must be used in order

tightly control the diameter of CNTs grown through a CVD process. If the variation in the catalyst particle size may be reduce to 2%, the variation in the CNT outside diameter may be reduced to less than 1 nm.

$$S_{total} = \sqrt{S_{film}^2 + S_{temp}^2} \tag{3.8}$$

Using the expected standard deviation for the outside diameter of the CNT, it is possible to determine how much this uncertainty in the CNT diameter contributes to the uncertainty in the CNT wall thickness. Plugging the uncertainty value of 5.52 nm into Equation 3.6, the uncertainty in the CNT wall thickness due to the variance in the CNT diameter is determined to be 1.70 nm. This uncertainty value may then be added to the uncertainty values of the CNT wall thickness caused by variations in the growth temperature and methane concentration. Again the temperature may be controlled to within 10 °C so plugging this value into Equation 3.6, the uncertainty in the CNT wall thickness caused by variations in temperature was found to be 0.32 nm. The methane concentration can easily be controlled to within 1%. Therefore, the variation in the methane creates an uncertainty in the CNT wall thickness of 0.17 nm. The total expected standard deviation in the CNT wall thickness caused by variations in the CNT outside diameter, the growth temperature and the methane concentration is equal to 1.73 nm. This is equivalent to about 5 walls in the CNT structure. This value indicates that most of the error in the CNT wall thickness is caused by errors in the CNT outside diameter. Thus precisely controlling the CNT outside diameter will allow for very tight control over the number of walls in a multi-walled carbon nanotube. This means that in order to control both the CNT diameter and number of walls in the CNT, it is necessary to use catalyst deposition techniques that produce catalyst particles that are more uniform in size. Therefore, more research needs to be done on catalyst deposition techniques in order to improve the uniformity of CNTs grown through CVD processes.

Chapter

4

CNT Growth Theory

4.1 Introduction

In order to better understand the experimental results presented in Chapter 3, it is necessary to look at the theoretical basis for these results. The thermodynamics and kinetics of the CNT growth reaction play an important role in explaining the observed final geometry of the CNTs under different growth conditions. A better understanding of the theoretical basis for the experimental results in Chapter 3 will also be useful in selecting CNT growth specimens for specific device requirements. This is because by using CNT growth theory, it is possible to design growth specimens that minimize the spread of the values for the CNT's geometric characteristics and thereby minimizes the error in devices that are manufactured using this growth technique.

4.2 Thermodynamic CNT Growth Model

From the results given in Chapter 3, it is possible to design CNTs with a wide range of diameters and wall thickness. In CNT-based devices, however, the stiffness and/or natural frequency of the CNTs is what affects the device performance. Given that the mechanical properties, and not the geometry of the CNTs, are of concern to the device designer, there are numerous possible combinations of CNT diameters and wall thickness that could be used to satisfy the device requirements. In order to find the optimal CNT growth for a specific application, it is essential to find the CNT geometry that minimizes the Gibbs free energy of the CNT. This will cause the growth to be

centered on a thermodynamically stable point and thus minimize the variance between CNT geometries within the growth.

The Gibbs free energy is equal to the sum of the surface energy of the CNT, the strain energy of the CNT, and the change in the chemical potential energy of the formation of the CNT [65]. The surface energy of the CNT is the product of the surface energy density and the surface area. The surface area of the CNT encompasses the inner and outer surfaces of the CNT. The total surface area per unit length of the CNT is given by Equation 4.1 where r_o is the outside radius, r_i is the inside radius and dl is the incremental length.

$$Surface\ Area = 2\pi r_o dl + 2\pi r_i dl = 2\pi(r_o + r_i)dl \tag{4.1}$$

The total surface energy of the CNT per unit length is given by Equation 4.2 where σ is the energy required to form one unit area of the surface. The variable, σ, is equal to 77 ergs/cm^2 at 970°C [65].

$$Surface\ Energy = 2\pi(r_o + r_i)\sigma dl \tag{4.2}$$

The non-deformed strain energy of the CNT is the energy that is required to roll a graphene sheet into a CNT. In order to calculate the strain energy, each shell of the CNT may be treated as a curved beam. This model is shown in Figure 4.1.

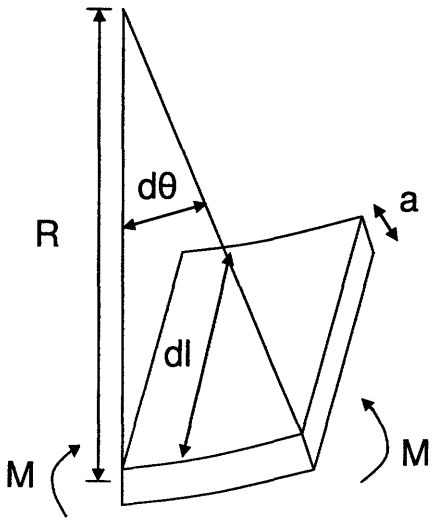

Figure 4.1. CNT Segment Treated as a Curved Beam.

From this model, the strain energy is given by Equation 4.3, where M is the moment and $d\theta$ is the wrapping angle [65]. For a tube the wrapping angle is equal to 2π.

$$Strain\ Energy = \frac{1}{2} M d\theta \tag{4.3}$$

For a curved beam, the moment is given by Equation 4.4, where E is the elastic modulus, I is the second moment of inertia, and R is the radius of curvature.

$$M = \frac{EI}{R} \tag{4.4}$$

The second moment of inertia for the wrapping of the graphene sheet is given by Equation 4.5 where L is the length of the beam and a is the shell thickness. For a beam composed of a single shell of a CNT, a is equal to the graphitic interplanar spacing which is 0.34 nm.

$$I = \frac{La^3}{12} \tag{4.5}$$

Therefore, the strain energy equation is

$$Strain\ Energy = \frac{\pi E a^3 dl}{12R} \tag{4.6}$$

and the strain energy per unit thickness of the CNT is

$$Strain\ Energy\ Per\ Unit\ Thickness = \frac{Strain\ Energy}{a} = \frac{\pi E a^2 dl}{12R}. \tag{4.7}$$

Thus, the total strain energy per unit length of the CNT may be found by integrating the strain energy per unit thickness from r_i to r_o as seen in Equation 4.8.

$$\begin{aligned} Total\ Strain\ Energy &= \int_{r_i}^{r_o} \frac{\pi E a^2 dl}{12R} dR \\ &= \frac{\pi E a^2 dl}{12} \ln\left(\frac{r_o}{r_i}\right) \end{aligned} \tag{4.8}$$

The change in the chemical potential energy is characterized by the precipitation of carbon atoms from the dissolved state. This may be seen in Equation 4.9 where μ_o is the change in the chemical potential per carbon atom and *dn* is the number of carbon atoms.

$$Chemical\ Potential\ Change = \Delta\mu_o dn \tag{4.9}$$

The number of carbon atoms that precipitate from the catalyst particle to the CNT, *dn*, is given by Equation 4.10 where Ω is the volume of a carbon atom in graphene.

$$dn = \frac{\pi\left(r_o^2 - r_i^2\right)dl}{\Omega} \tag{4.10}$$

The total Gibbs free energy of the formation of a CNT is given by Equation 4.11 [65].

$$\Delta G = 2\pi\left(r_o + r_i\right)\sigma dl + \frac{\pi E a^2 dl}{12}\ln\left(\frac{r_o}{r_i}\right) - \Delta\mu_o dn \tag{4.11}$$

It is generally more useful, however, to look at chemical reactions in terms of the change in the chemical potential that drives the precipitation reaction. The change in chemical potential, $\Delta\mu$, is given by Equation 4.12 [65].

$$\Delta\mu = -\frac{\Delta G}{dn} \tag{4.12}$$

The change in the chemical potential for the CNT growth process is given by Equation 4.13 [65].

$$\Delta\mu = \Delta\mu_o - \frac{2\sigma\Omega}{r_o - r_i} - \frac{Ea^2\Omega}{12\left(r_o^2 - r_i^2\right)}\ln\left(r_o / r_i\right) \tag{4.13}$$

In general, any CNT geometry with $\Delta\mu$ greater than zero will grow because this is the condition necessary for a spontaneous reaction to occur. CNTs with the highest $\Delta\mu$ will, however, be more likely to form and will grow the most rapidly [66]. Equation 4.13 shows that the chemical potential is highly dependent on the inside and outside radius

values. Given that the CNT outside radius is set by the catalyst particle size as shown in Chapter 3, the optimal inner radius may be found which maximizes $\Delta\mu$ by taking the derivative of the chemical potential with respect to the inner radius while holding the outer radius constant as shown in Equation 4.14.

$$\left[\frac{d(\Delta\mu)}{dr_i}\right]_{r_o} = 0 \tag{4.14}$$

Using this condition, the thermodynamically optimal inner diameter was calculated for each measured outer diameter in this growth study. These results are plotted in Figure 4.3 along with the measured data.

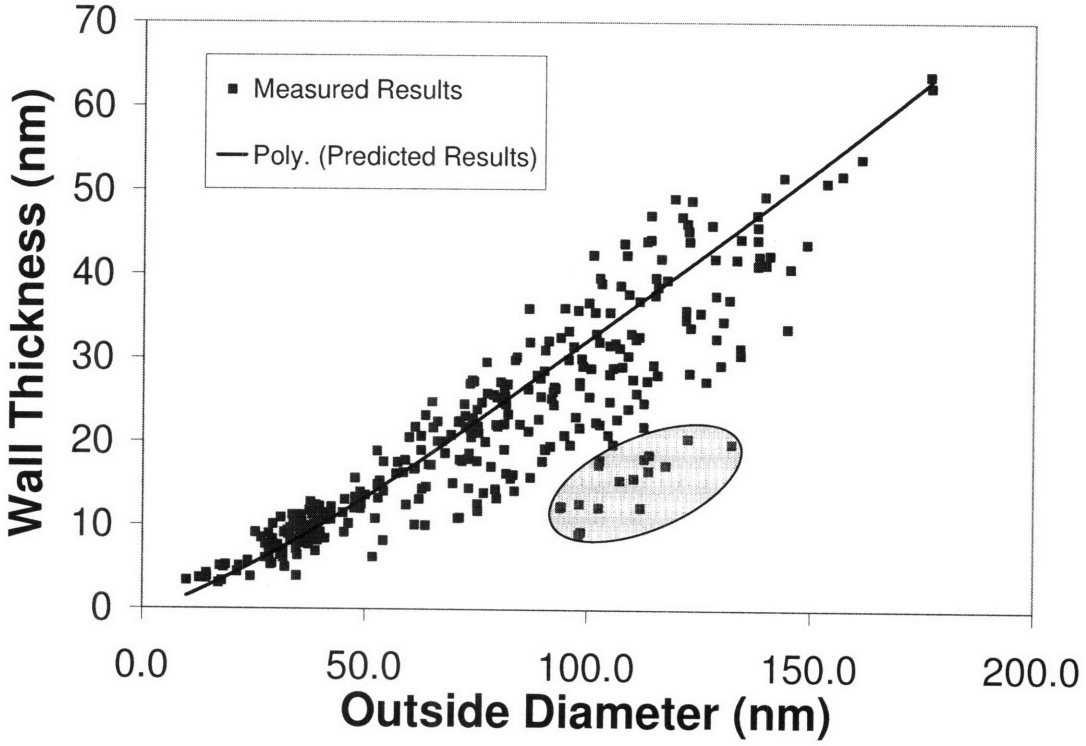

Figure 4.2. Results from Thermodynamics Model vs. Measured Results.

From this graph, it is clear that the reaction kinetics have a large effect on the wall thickness of the CNT. For example, the points in the shaded region that are far below the line are CNTs that were grown at low temperatures (Run 9) and low methane concentrations (Run 13). While the kinetic effects are significant, the thermodynamic

model may be used to help explain the general trend of the data as this outside diameter of the CNT increases. In fact, the R^2 value of this fit indicates that almost 79% of the variance in the CNT wall thickness may be explained by the thermodynamics model.

A regression analysis may be performed on the predicted results for each CNT growth in order to determine how the predicted results depend on the growth parameters. When this is done, it is found that neither the temperature nor the methane concentration is statistically significant. This result is expected because neither of these variables enters into the thermodynamics model. These variables were, therefore, eliminated from the regression model and the regression was repeated with the new variable set. The results of this regression are given in Table 4.1 and Equation 4.14 where D is the CNT diameter and t is the wall thickness.

Table 4.1. ANOVA Table for the Thermodynamics Model.

	Coefficients	*Standard Error*	*T Stat*	*P-value*	*Lower 95%*	*Upper 95%*
Intercept	0	#N/A	#N/A	#N/A	#N/A	#N/A
CNT Diameter	0.319	0.00138	232	0	0.316	0.321

$$t = 0.319D \tag{4.14}$$

At a 95% confidence level, the theoretical dependence of the wall thickness on the CNT diameter is not significantly different from the measured dependence given by Equation 3.6. This means that there is a good match between the measured and theoretically determined dependence of the CNT wall thickness on the CNT diameter. The kinetics of the reaction must yet be factored into theoretical model of the CNT wall thickness. This is because there is only a weak energy minimum at the optimal CNT inner radius, as may be seen in Figure 4.3. This figure shows that the optimal inner radius for a CNT with an outside radius of 20 nm is about 10 nm. The figure also shows that it is possible to produce CNTs with inner radii of between about 5 and 14 nm because the Gibbs free energy is negative for all of the inner radii between 5 and 14 nm. Thus, the kinetics of the reaction may be used to set the inner radius within these limits.

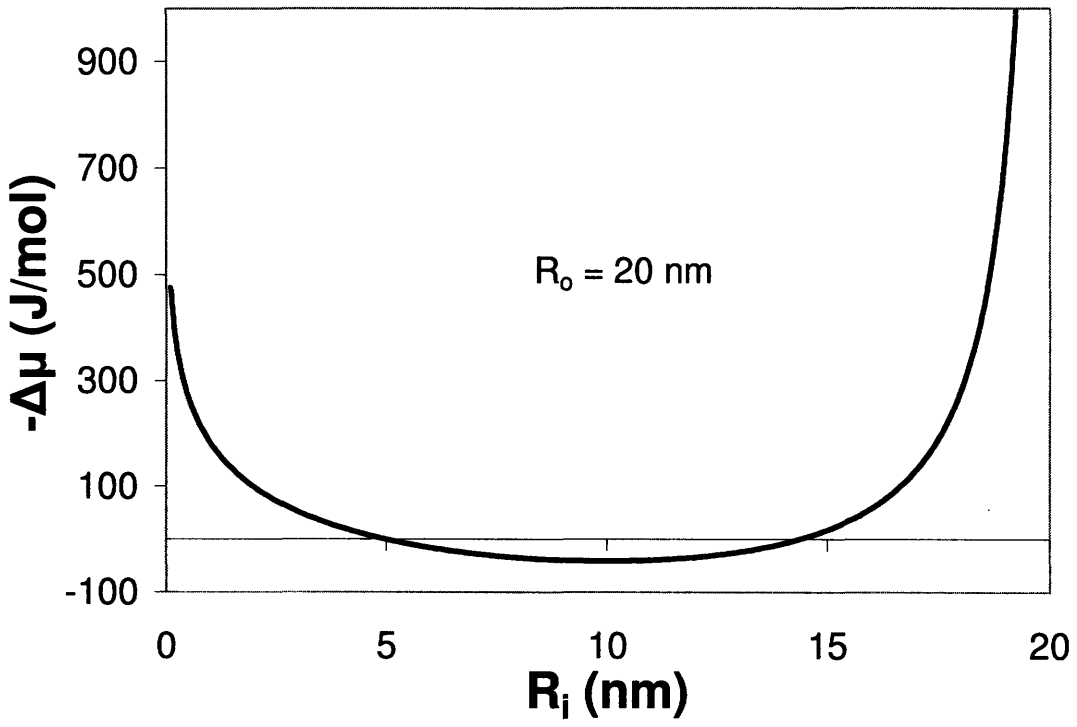

Figure 4.3. Chemical Potential vs. Inner Radius for a 20 nm Outside Radius CNT.

Near the optimal inner radius, the energy well is shallow meaning that not much work is needed to move the inner radius away from the optimal inner radius. As the inner radius is moved away from the optimal inner radius, the slope of the energy curve increases and more work is required to set the inner radius. This indicates two things:

(1) That the reaction kinetics will have a larger effect near the energy minimizing inner radius and

(2) That the most stable inner radius is the energy minimizing inner radius because there is no energy gradient pushing the growth away from that point.

The CNTs designed for mechanical devices should be designed, if possible, with inner radius values that are equal to the energy minimizing inner radiuses. This will reduce the spread in the CNT wall thickness over the sample due to the energy gradient. Also, as the kinetics of the reaction have a major effect on the inner radius near the

optimal point, the reaction kinetics need to be incorporated into the theoretical model in order to determine the size of this effect.

4.3 Kinetic CNT Growth Model

In order to understand the reaction kinetics of CNT growth, we first must understand the reaction mechanism. The first step in the CNT growth reaction is the absorption of the methane onto the catalyst surface. This is, in fact, the rate limiting step for the entire reaction [67]. The next step is the removal of the hydrogen from the methane through a series of reactions on the catalyst particle surface. This releases hydrogen back into the atmosphere and leaves the carbon on the surface of the catalyst particle. The carbon then dissolves into the catalyst particle and defuses through the particle before it finally precipitates out of the catalyst particle as part of the CNT. The overall activation energy for this process ranges from 60 kJ/mol to 236 kJ/mol depending on the type of catalyst that is used [67]. The full reaction mechanism is outlined in Figure 4.4.

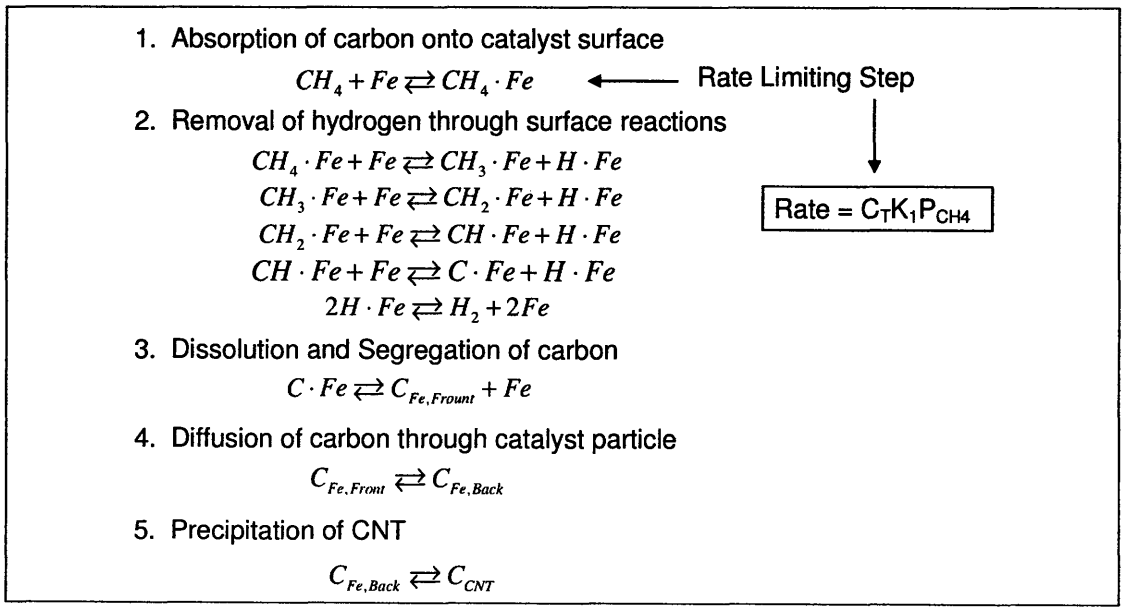

Figure 4.4. CNT Growth Mechanism.

From this reaction mechanism and from the surface melting model of CNT growth, it is possible to determine how much the reaction kinetics effect the CNT wall thickness. The surface melting model is a compromise between the vapor-liquid-solid (VLS) model [68] in which the catalyst particle becomes a molten liquid during the growth process and the solid catalyst model [69] where the catalyst particle remains a solid through out the growth process. In the surface melting model, a molten skin layer surrounds the solid crystalline core of the catalyst particle. The accuracy of this model is supported by (1) simulations that show that only the surface of the catalyst particle melts at the CNT growth temperatures [70] and (2) experiments that show the reshaping of the catalyst particle during the growth process [71]. A schematic of this surface melting model is given in Figure 4.5.

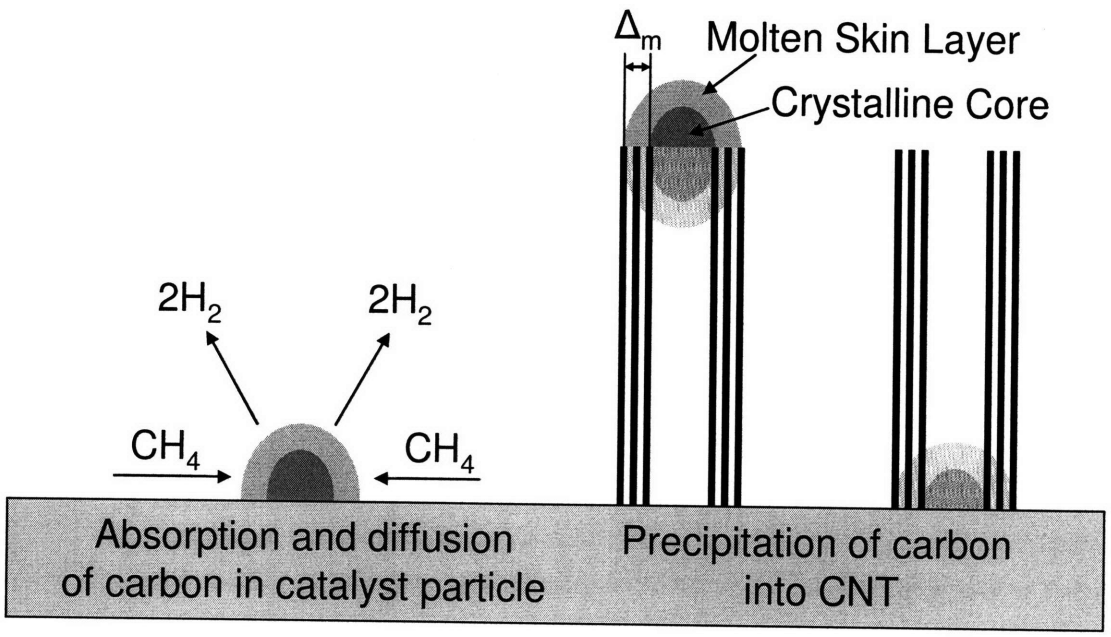

Figure 4.5. Surface Melting Model of CNT Growth.

As may be seen in Figure 4.5, the wall thickness of the CNT is set by the thickness of the molten skin layer. This is because the rate of carbon diffusion through the molten layer is much greater than diffusion through the ordered crystalline core so

that virtually all of the carbon that precipitates out of the catalyst particle and into the CNT comes from the molten layer of the catalyst particle [72]. The thickness of this layer may be found by determining the number of carbon atoms in this layer at steady state because the density of the carbon atoms in a CNT is known. This thickness is given by Equation 4.15 where Δ_m is the molten layer thickness, N_c is the number of carbon atoms in the molten layer, S_0 is the nanoparticle surface area, n_m is the density of a monolayer of carbon atoms which is equal to 10^{15} atoms/cm^2, t is the thickness of this monolayer which is 0.34 nm, and α is a scaling parameter equal to 0.3 [72].

$$\Delta_m = \frac{tN_c}{\alpha S_0 n_m} \tag{4.15}$$

The scalars α, t, and n_m are known constants and S_0 may be determined from the catalyst particle radius, R, using Equation 4.16.

$$S_0 = 4\pi R^2 \tag{4.16}$$

The only unknown in determining the molten layer thickness, and therfore the CNT wall thickness, is the number of carbon atoms in the molten layer, N_c.

At steady state, the rate of change in the number of carbon atoms in the surface layer should be zero. The flux of the carbon atoms onto the surface of the catalyst particle, F_C, is, therefore, equal to the flux of carbon atoms out of the surface layer, F_p. The flux of carbon atoms out of the surface layer is equal to the surface-bulk penetration rate, k_{sb}, multiplied by the number of carbon atoms in the surface layer, N_C. The flux of carbon atoms in the surface layer is therefore given by Equation 4.17.

$$\frac{d(N_c)}{dt} = 0 = F_c - k_{sb}N_c \tag{4.17}$$

In solving this equation for N_c one may obtain,

$$N_c = \frac{F_c}{k_{sb}} \tag{4.18}$$

The flux of carbon atoms onto the catalyst particle surface is equal to the flux of the carbon feedstock gas multiplied by the probability of a molecule from this gas coming into contact with and absorbing into the catalyst particle surface. This probability may be found using Equation 4.19 were E_a is the activation energy, k_B is the Boltzmann constant, T is the temperature in Kelvin and p_1 is a constant equal to 10^9 [72]. The activation energy, E_a, is the activation energy of the entire reaction because the absorption of carbon into the catalyst particle surface is the rate limiting step.

$$P_{absorption} = p_1 e^{\frac{-E_a}{k_B T}} \tag{4.19}$$

The flux of carbon onto the catalyst particle surface is given by Equation 4.20 where F_b is the flux of the carbon feedstock gas.

$$F_c = F_b p_1 e^{\frac{-E_a}{k_B T}} \tag{4.20}$$

The flux of the carbon feedstock gas is a function of the surface area of the catalyst particle, S_0, the density of the methane in the reaction atmosphere, n, and the velocity of the methane atoms. The flux of the carbon feedstock gas is given by Equation 4.21 [72] where m is the mass of a methane atom.

$$F_b = \frac{1}{4} S_0 n \left(\frac{k_B T}{2\pi m} \right)^{1/2} \tag{4.21}$$

Substituting this back into Equation 4.20, the flux of carbon onto the catalyst particle surface is

$$F_c = \frac{1}{4} S_0 n \left(\frac{k_B T}{2\pi m} \right)^{1/2} p_1 e^{\frac{-E_a}{k_B T}}. \tag{4.22}$$

Now that the flux of carbon atoms on to the surface of the catalyst particle has been determined, rate of the carbon surface-bulk penetration rate must be determined in order to find the number of carbon atoms in the molten surface layer. The surface-bulk penetration rate is the probability that an atom in the molten surface layer will leave the surface layer and enter CNT lattice structure. The surface-bulk penetration rate is given by Equation 4.23 [72] where E_{sb} is the activation energy of the surface-bulk penetration and B is a constant equal to 2 x 10^{14}. The surface-bulk penetration activation energy for carbon in iron is 2.2 eV [72].

$$k_{sb} = Be^{\frac{-E_{sb}}{k_B T}} \tag{4.23}$$

Substituting Equations 4.22 and 4.23 into Equation 4.18, the number of carbon atoms in the molten surface layer is

$$N_c = \frac{1}{4B} S_0 n \left(\frac{k_B T}{2\pi m}\right)^{1/2} p_1 e^{\frac{-E_a + E_{sb}}{k_B T}}. \tag{4.24}$$

Equation 4.24 may then be substituted back into Equation 4.15 to determine the wall thickness that is predicted by the CNT growth reaction kinetics. This result is given in Equation 4.25.

$$\Delta_m = \frac{t}{4\alpha B} \frac{n}{n_m} \left(\frac{k_B T}{2\pi m}\right)^{1/2} p_1 e^{\frac{-E_a + E_{sb}}{k_B T}} \tag{4.25}$$

This equation shows that the temperature and the methane concentration, as accounted for in the density of the methane in the reaction atmosphere, n, are factors in the CNT wall thickness that is predicted by the CNT growth reaction kinetics. The CNT outside diameter and the catalyst particle size, however, do not factor into the CNT wall thickness in this model. It is necessary, therefore, to combine this kinetic model with the thermodynamic model that was derived in Section 4.1 to produce the full theoretical

model for the CNT wall thickness. To combine these two models it is necessary to measure how much the reaction kinetics drive the CNT wall thickness away from its thermodynamically optimal state. This may be done by adding the wall thickness found from the thermodynamic model to the change in wall thickness caused by the reaction kinetics as shown in Equation 4.26 where t_p is the thermodynamic wall thickness, t_{thermo} is the thermodynamic wall thickness, Δ_m is the kinetic wall thickness and $\bar{\Delta}_m$ is the median kinetic wall thickness. The median kinetic wall thickness is the wall thickness predicted by the kinetic model at the mid-point of the parameter space. For this growth study the mid-point of the parameter space is a growth temperature of 800°C and a methane concentration of 68.5%.

$$t_p = t_{thermo} + \Delta_m - \bar{\Delta}_m \tag{4.26}$$

From this equation, the wall thickness was predicted for each of the CNT growths that were run for the central composite inscribed growth study presented in Chapters 2 and 3. The results of these predictions were then plotted against the measured results for each of the growths as seen in Figure 4.6. In this Figure, a 45° line used added to show where points with perfect agreement between the measured and predicted results would fall.

As may be seen in Figure 4.6, thirteen of the fifteen experimentally measured points fall within the error of their predicted values at a 95% confidence level. At a 99% confidence level, all fifteen of the experimental results fall within the error of the predicted results. Also, the R^2 value of 0.907 indicates that over 90% of the variation in the measured CNT wall thickness may be explained using the combined thermodynamic and kinetic growth model. This R^2 value for the theoretical model is very close to the R^2 value of 0.927 for the experimental regression model indicating that the theoretical model matches the experimental data almost as well as the empirical model.

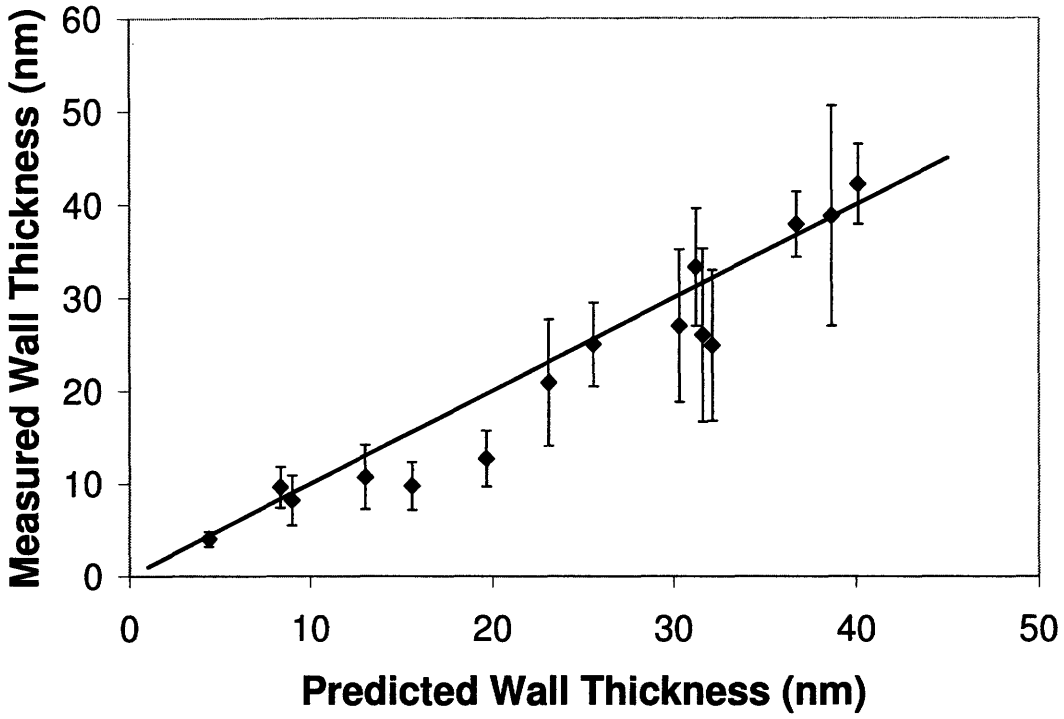

Figure 4.6. Results from Full Theoretical Model vs. Measured Results.

In order to measure how closely the full theoretical model of the combined thermodynamic and kinetic models matches the experimental regression model, the full theoretical model must be linearized so that the dependence of the CNT wall thicknesses on each of the process parameters in the theoretical model may be compared with the experimental regression model. This linearization may be done by performing a regression analysis on the predictions from the theoretical model for each of the data points collected. The results of this regression are presented in Table 4.2.

Table 4.2. ANOVA Table for Full Theoretical Model.

	Coefficients	*Standard Error*	*t Stat*	*P-value*	*Lower 95%*	*Upper 95%*
Intercept	-33.9	0.169	-200	0	-34.2	-33.5
CNT Outside Diameter	0.319	0.000282	1130	0	0.318	0.319
Temperature	0.0260	0.000201	129	0	0.0256	0.0264
Concentration	0.190	0.000678	280	0	0.188	0.191

As may be seen in Table 4.3, the coefficients for the y-intercept, the CNT outside diameter, the growth temperature, and the methane concentration are within the experimental error of the coefficients that were determined from the experimental regression model.

Table 4.3. Comparison of Experimental Results and Theoretical Model.

	Experimental		*Theoretical*	*Within Error?*
Intercept	-38.3	7.8	-33.9	Yes
CNT Outside Diameter	0.307	0.013	0.319	Yes
Temperature	0.0316	0.0093	0.0260	Yes
Concentration	0.166	0.031	0.190	Yes

The good match between the theoretical and experimental results shows that the theoretical model may be used to better understand the experimental results. The theoretical model may also be used to determine how other growth parameters, those that were not considered in this growth study, might effect the dependence of the CNT geometry on the catalyst film thickness, growth temperature and hydrocarbon concentration. For example, the theory shows that the dependence of the CNT wall thickness on the catalyst film thickness is solely due to the balance between the surface energy and the strain energy of the CNT. This means that there is little that may be done to change this dependence. Similarly, the dependence of the CNT wall thickness on the hydrocarbon concentration will not be affected by the type of hydrocarbon or catalyst that is used. The dependence of the CNT geometry on the growth temperature, however, will change depending on the type of catalyst or hydrocarbon used because the activation energies for the surface-bulk penetration, E_{sb}, and the overall reaction, E_a, will change. When E_a is greater than E_{sb}, as in the case with methane as the reacting gas and iron as the catalyst, there will always be a positive relationship between the growth temperature and the CNT wall thickness. When E_a is less than E_{sb} there may be a negative correlation between the growth temperature and the CNT wall thickness. This phenonomon has been observed when more reactive carbon sources such as acetylene have been used in the growth of carbon nanotubes [72]. The full theoretical model, therefore, indicates that care must be taken when applying the design equations derived in Chapter 3 to other CNT growth systems.

Chapter

5

CNT-Based Device Design

5.1 Introduction

Design equations for growing CNTs with specific geometric characteristics were formulated and verified theoretically in Chapters 3 and 4. The use of these equations should enable the design and creation of CNT's that possess desired stiffness and natural frequency characteristics for target applications. There are three unknown variables and only two design equations. There are therefore many variable combinations that will produce the desired CNT geometry and therefore stiffness and/or natural frequency. This chapter will present the (i) design rules for picking the best growth conditions for a desired CNT property and (ii) the results of test growths that were made by using the preceding design rules and the design equations from Chapter 3. The accuracy of the equations and rules will be discussed. The design equations are reprinted below as a convenient reference for the following sections.

$$D = 43.72\ln(F) + 0.0484T \tag{5.1}$$

$$t = -38.28 + 0.307D + 0.0316T + 0.166C \tag{5.2}$$

$$N_w = -112.58 + 0.904D + 0.0931T + 0.487C \tag{5.3}$$

5.2 Design of CNTs with Specific Geometry

A growth was performed with the intent to create CNTs that possessed a diameter of 58 nm and a wall thickness of 15 nm (about 44 walls) so that the accuracy of the design equations could be assessed.

As there are three variables – catalyst film thickness, growth temperature, and methane concentration – but only two desired outputs – CNT diameter and wall thickness. There are many possible combinations of the growth parameters which will produce a desired CNT geometry. It is generally best to start by selecting the catalyst film thickness because the catalyst film thickness is the dominate term in the CNT outside diameter equation. Once the catalyst thickness is selected, the temperature is set using Equation 5.1 because the CNT diameter and the catalyst film thickness are known. Finally, the methane concentration is set using Equation 5.2 because the CNT diameter, the temperature and the desired thickness are known. The possible growth conditions for a CNT with a diameter of 58 nm and a wall thickness of 15 nm (44 walls) are listed in Table 5.1.

Table 5.1. Possible Growth Conditions for 58 nm CNT with 44 Walls

Condition Number	Catalyst Film Thickness (nm)	Temperature (°C)	Concentration (%)
1	1.4	894	43.2
2	1.5	832	55.1
3	1.6	774	66.2
4	1.7	719	76.7

From these growth conditions, the 3rd condition was selected and then characterized. The 3rd condition was chosen because the temperature and concentration values were close to the center of the parameter range. This is important because the central composite inscribed experimental method is designed be most accurate at the center of the parameter space. The results of this growth are listed in Table 5.2.

Table 5.2. Results of Growth for Condition Number 3

	Desired	Measured	Experimental Error
Outside Diameter	58 nm	61.2 nm	7.4 nm
Wall Thickness	15 nm	16.0 nm	3.3 nm
Number of Walls	44 walls	47 walls	10 walls

The measured results were within the experimental error of the predicted values for the diameter, wall thickness, and number of walls. Also, the average error between the measured and predicted results was less than 7%. This design method offers a great

improvement over the traditional guess and check methods which typically take at least five iterations before satisfactory CNT geometry results may be achieved.

5.3 Design of CNTs for a Linear Flexural Bearing

In many cases devices must be designed with a specific stiffness in order to satisfy force or range requirements. In these cases, as opposed to the case in which CNT with a specific geometry are desired, many different combinations of CNT diameters and wall thicknesses may be used to achieve the desired stiffness. The number of desired outputs therefore decreases from two – diameter and wall thickness – to one – stiffness. The number of variables remains constant at three – catalyst film thickness, growth temperature, and methane concentration. This means that there are fewer constraints on the growth conditions and, therefore, many more possible growths may be used to produce CNTs with the desired stiffness.

In such cases, where the device stiffness is the main concern, it is often helpful to set the catalyst film thickness and then adjust the other two parameters so that the stiffness requirements are satisfied. This reduces the number of possible growth conditions and makes it possible to select an optimal growth by using the thermodynamic theory that was presented in Chapter 4. The catalyst film thickness is the best process parameter to initially set because the deposition of the catalyst film is the most expensive and time consuming step in the growth process. A standard film thickness is therefore often made, and used, many times. This reduces the cost and time necessary for each growth. By setting the catalyst film thickness to one of the prefabricated standard thicknesses it is possible to select a set of optimal growth conditions that satisfy the stiffness requirements at a low cost, and with a quick turnaround time.

An example where stiffness is of great importance is the linear flexural bearing that is shown in Figure 5.1. This type of bearing is a ubiquitous machine element that permits one rotation and two translation degrees of freedom. Simulations have shown that a CNT–based bearing is capable of deformations that are 25% of its characteristic size [73]. In contrast, a micro–scale silicon bearing of geometrically similar design would only be capable of deformations that are less than 1% of its characteristic size.

The small size, relatively large stroke, and fine resolution of this type of CNT–based flexural bearings are of interest to applications in probe–based manufacturing and metrology at the nano–scale.

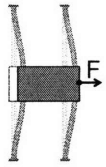

Figure 5.1. Carbon Nanotube Based Linear Flexural Bearing.

The following describes a hypothetical design scenario. In this example, a growth was designed to produce a linear flexural bearing that possessed a stiffness of 2.1 N/m. The stiffness of the linear flexural bearing may be calculated by using Equation 5.4. In the equation, k is the stiffness, E is the elastic modulus of the CNT, I is the second moment of inertia and L is the flexural length of the CNTs.

$$k = \frac{384EI}{L^3} \tag{5.4}$$

The linear flexural bearing was assumed to have a 5 μm x 5 μm stage that was connected to ground by two 15 μm long CNTs. The ends of the CNTs were assumed to be rigidly grounded to the stage and to the ground and therefore the flexural length of the CNTs was 10 μm. The elastic modulus of the CNT was assumed to be 1 TPa. Given these values, the second moment of inertia was 5.47 x 10^{-30} m^4. For this value, the set of CNT diameters and wall thickness values that satisfy the stiffness requirement may be found using Equation 5.5. In Equation 5.5, D is the CNT's diameter and t is the CNT's wall thickness.

$$I = \frac{\pi}{64}\left(D^4 - (D-2t)^4\right) \tag{5.5}$$

A standard catalyst film thickness of 5 nm was selected. This thickness was selected because it was the standard catalyst film thickness that produced CNT that were

closest to the desired stiffness when using mid–range values of the temperature and methane concentration. The mid–range values that were used in this calculation were 800°C for the temperature and 68.5% for the methane concentration. These values were selected because they are at the midpoint of the range of values that were used in the growth study. Given this catalyst thickness and Equation 5.5, the set of CNT growth conditions that would create CNTs with the desired stiffness may be determined via Equations 5.1 and 5.2. The set of growth conditions that satisfy the stiffness requirement are given in Table 5.3. In this set of growth conditions, the temperature was set in 10°C increments and the methane concentration was set to satisfy the stiffness requirement. From this set of growth conditions, condition two was selected. This condition was selected because this growth condition minimized the difference in wall thickness between the predictions of Equations 5.1 and 5.2 and predictions of the thermodynamic theory. The wall thickness that was predicted by the thermodynamic growth theory may be determined from Equation 5.6. In the equation, σ is the energy required to form graphite, r_o is the outside radius of the CNT, r_i is the inside radius of the CNT, a is the graphite interplanar spacing and E is the elastic modulus.

$$0 = -\frac{2\sigma}{(r_0 - r_i)^2} - \frac{Ea^2 r_i \ln(r_o / r_i)}{6(r_o^2 - r_i^2)^2} + \frac{Ea^2}{12r_i(r_o^2 - r_i^2)} \tag{5.6}$$

The Gibbs free energy of the CNTs is minimized when the difference between the wall thickness predictions from Equations 5.2 and 5.6 is minimized. As discussed in Chapter 4, the selection of a growth(s) that minimize the Gibbs free energy should cause the growth to be centered on a thermodynamically stable point. This should minimize the variance of the CNT diameters within the growth.

Table 5.3. Possible Growth Conditions for Linear Flexural Bearing with a Stiffness of 2.1 N/m

Condition Number	Catalyst Film Thickness (nm)	Temperature (°C)	Concentration (%)
1	5	700	65.1
2	5	710	52.4
3	5	720	41.6

From Equations 5.1 and 5.2, this growth condition was predicted to produce CNTs with an outside diameter of 104.7 nm and a wall thickness of 25.0 nm. The measured results are listed in Table 5.4.

Table 5.4. Results of Growth CNTs Designed for Flexural Bearing with a stiffness of 2.1 N/m

	Desired	Measured	Error
Outside Diameter	104.7 nm	104.3 5.4 nm	0.38%
Wall Thickness	25.0 nm	25.6 1.3 nm	2.40%
Flexural Stiffness	2.10 N/m	2.11 0.40 N/m	0.48%

The maximum error between the predicted and measured results was 2.4%. This is lower than the previous example where the CNT diameter and the wall thickness were set. This is likely due to the fact that in the previous example, the thermodynamic theory could not be used to select the optimal growth conditions because there were two desired outcomes that had to be satisfied. For the example where the CNT's geometric characteristics were specified, it turned out that the growth conditions which could be used to satisfy the CNT geometric requirements were far from the thermodynamic equilibrium point. For the example described in this section, only the stiffness of the flexural bearing was set and therefore the thermodynamic theory could be used to optimize the growth design. Also, the use of the thermodynamic theory reduced the spread of the measured results by a large amount in comparison to the example where the thermodynamic theory could not be used. For example, the maximum variance in the CNT diameter and wall thickness was reduced from 20.6% to 5.2%.

The flexural stiffness calculated from the measured CNT geometry also matched the desired flexural stiffness with an average error of less than 0.5%. The spread in the predicted flexural stiffness of the linear bearing, however, was calculated to be almost 19%. This large spread in the predicted stiffness from the measured CNT geometric characteristics is due to the fact that small errors in the CNT diameter and wall thickness are raised to the fourth power in the second moment of inertia equation. In the future, it may be necessary to control the CNTs' geometric characteristics more tightly in order to precisely set the stiffness of CNT-based NEMS devices.

5.4 Design of CNTs for a Resonator

In many cases, devices must be designed with a specific natural frequency in order to satisfy bandwidth and/or vibration requirements. For example, resonators are typically used as frequency–determining elements in signal processing devices. It is therefore necessary to set the natural frequency of a resonator in order to ensure proper function. CNTs are ideally suited for high–bandwdith resonators because the combination of their high elastic modulus and their small mass enables them to operate with high–bandwidths. CNT–based resonators could increase the bandwdith of signal processing devices if the CNTs for such devices could be accurately designed and fabricated. An example of a CNT–based resonator is given in Figure 5.2. In this CNT-based resonator, the CNT is about 1.5 μm long and 1-3 nm in diameter [4]. The resonator has a bandwidth of 300 MHz and a Q-factor of 300 [4].

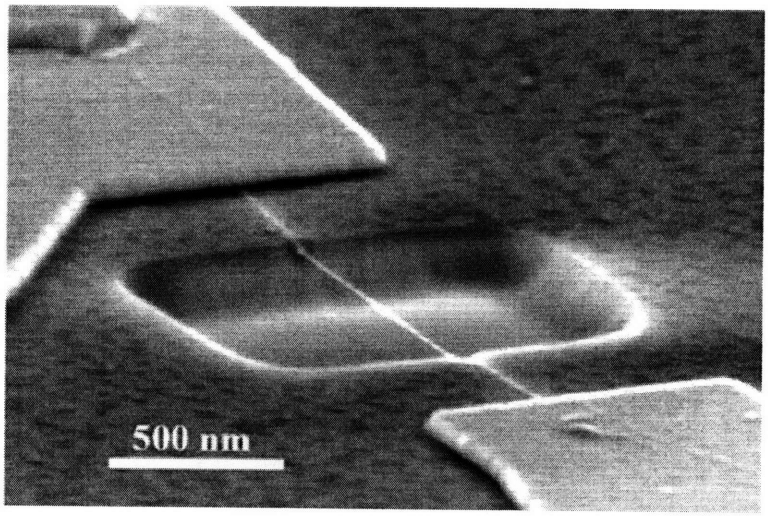

Figure 5.2. CNT-based Resonator [4].
Reprinted with permission from the American Chemical Society Copyright 2006

The following provides a synopsis of a hypothetical design scenario for a CNT-based resonator. As in the example where the CNT-based linear flexural bearing stiffness was set, there are many possible combinations of CNT diameters and wall thickness that could be used to achieve the desired natural frequency of the CNT-based resonator. As such, it is best to eliminate the catalyst film thickness as a variable by setting it to one of

the standard film thickness that has already been deposited. This thickness may be selected by setting the temperature and methane concentration to their midrange values and then selecting the standard catalyst film that produces CNTs which have natural frequencies that are the closest to the desired natural frequency.

In this example, the desired frequency of a 100 nm long resonator was 183 GHz. The natural frequency of a resonator is given in Equation 5.7 [2] where β is a constant that is equal to 4.73 for a doubly clamped beam, E is the elastic modulus of the CNT that is assumed to be 1 TPa, L is the length of the CNT resonator, D is the outside diameter of the CNT, t is the CNT wall thickness, and ρ is the density of the CNT.

$$\omega = \frac{\beta^2}{2\pi}\sqrt{\frac{EI}{mL^4}} = \frac{\beta^2}{8\pi L^2}\sqrt{\frac{\left(D^2+(D-2t)^2\right)E}{\rho}} \tag{5.7}$$

The set of possible growths that achieve the desired frequency is given by Table 5.5.

Table 5.5. Possible Growth Conditions for Resonator with a Natural Frequency of 183 GHz

Condition Number	Catalyst Film Thickness (nm)	Temperature (°C)	Concentration (%)
1	3	900	66.6
2	3	890	64.0
3	3	880	61.5
4	3	870	59.2
5	3	860	57.0
6	3	850	54.9
7	3	840	53.0
8	3	830	51.2
9	3	820	49.4
10	3	810	47.8
11	3	800	46.2
12	3	790	44.7
13	3	780	43.3
14	3	770	41.9
15	3	760	40.7
16	3	750	39.4
17	3	740	38.3
18	3	730	37.2
19	3	720	36.1
20	3	710	35.1
21	3	700	34.1

Equations 5.1, 5.2, and 5.7 were used to determine that the standard catalyst film thickness. The equations showed that a film thickness of 3 nm would produce CNTs that possessed natural frequencies that were closest to the desired natural frequency. Given the value of film thickness, the set of possible growths that would satisfy the frequency requirement was determined. The temperature was set in 10°C increments and the requisite methane concentration was determined via Equations 5.1, 5.2, and 5.7. From these possible growth conditions, condition number three was selected because it was the growth condition that has the lowest Gibbs free energy. The CNT diameter and wall thickness were predicted to be 90.6 nm and 27.6 nm respectively. The measured values are contrasted with the predicted values in Table 5.6.

Table 5.6. Results of Growth CNTs Designed for Resonator with a Natural Frequency of 183 GHz

	Desired	Measured	Error
Outside Diameter	90.6 nm	91.9 6.6 nm	1.43%
Wall Thickness	27.6 nm	27.6 1.7 nm	0.00%
Resonator Frequency	183 GHz	186 15 GHz	1.64%

The maximum error in the CNT geometric characteristics was less than 2%. Also, the variance in the measured geometric characteristics was 7.2%. The relatively low magnitude of variance may be attributed to the use of the thermodynamic theory optimization. The resonator frequency that was estimated from the measured CNT geometry differed by 1.6% from the desired value. The experimental error for the resonator frequency was about half of what it was for the stiffness of the linear flexural bearing. This is likely due to the fact that the errors in the resonator's geometry were only squared whereas the errors in the flexural bearing were taken to the fourth power. In the example of the resonator frequency, the change in mass that was associated with the errors in geometry helped to offset some of the error in the stiffness that was caused by errors in geometry. The variance in the resonator frequency was therefore much lower than the variance in the stiffness of the linear flexural bearing.

5.5 Linear Flexural Bearing with Specified Natural Frequency

For high–speed metrology and manufacturing applications at the nano–scale, it is often the natural frequency of the flexure, and not the stiffness of the flexure, that is of concern for the linear flexural bearing. For example, in probe–based nanomanufacturing applications, such as nano-electrical discharge machining (nano-EDM) or nano-dip pen lithography, the rate at which features may be written is proportional to the natural frequency because the writing rate is set by how fast the probe tip may engage and disengage the substrate surface. The frequency at which features may be written via a probe–based nanomanufacturing system that is equipped with CNT–based flexural elements is given in Equation 5.8 [2]. In the equation, k is the stiffness of the CNTs as given in Equation 5.4, m is the mass of the positioning stage plus the mass of the probe, and f is the natural frequency in Hertz.

$$f = \frac{1}{2\pi}\sqrt{\frac{k}{m}} \tag{5.8}$$

Equations 5.1, 5.2 and 5.4 may be used with Equation 5.8 to design a linear flexural bearing that possesses a specific natural frequency. In this example, the goal was to create a linear flexure bearing that possessed a natural frequency of 27 kHz. The linear flexural bearing was assumed to have a 5 μm x 5 μm stage that was connected to ground by two 15 μm long CNTs. The ends of the CNTs were assumed to be rigidly grounded to the stage and to the ground and therefore the flexural length of the CNTs was 10 μm. The stage mass is a few orders of magnitude greater than the mass of the CNTs, therefore the device mass was assumed to equal the mass of the center stage. The volume of the 5μm x 5μm x 500 μm silicon stage multiplied by the density of silicon – 2330 kg/m^3 – is 2.9 x 10^{-11} kg.

As in the previous two examples, it is helpful to eliminate one of the process variables as this reduces fabrication time/costs and the number of growth solutions to a manageable number. The catalyst film thickness was set by finding the standard film thickness that minimizes the difference between the desired and predicted natural

frequencies when the mid-range values of temperature and methane concentration are used. In the example where the natural frequency was to be 27 kHz, the standard film thickness of 3 nm was selected. Given the 3nm thickness value, the set of possible growth conditions that satisfy the frequency requirement was found. The set of possible growth conditions is shown in Table 5.7. The temperature is set in 10°C increments and the methane concentration is obtained via Equations 5.1, 5.2, 5.4, 5.5, and 5.7.

Table 5.7. Possible Growth Conditions for Flexural Bearing with a Natural Frequency of 27 kHz

Condition Number	Catalyst Film Thickness (nm)	Temperature (°C)	Concentration (%)
1	3	700	110.5
2	3	710	83.6
3	3	720	67.4
4	3	730	55.1
5	3	740	44.8
6	3	750	35.8

Growth condition two was selected because it is the condition that has the lowest Gibbs free energy. This condition should therefore produce CNTs that have the best probability of matching the desired natural frequency. The CNT diameter and wall thickness were estimated to be 84.2 nm and 23.4 nm, respectively. The predicted and measured values are listed in Table 5.8.

Table 5.8. Growth Results for CNTs for a Flexural Bearing with Natural Frequency of 27 kHz

	Desired	Measured	Error
Outside Diameter	82.4 nm	82.6 8.6 nm	0.24%
Wall Thickness	23.4 nm	23.0 3.6 nm	1.71%
Flexural Bearing Frequency	27 kHz	27.4 5.7 kHz	1.48%

The maximum error between the CNT geometric characteristics is less than 2% and all of the measured results are within the experimental error of the measurement setup. The difference between the frequency values that were associated with the modeled and measured CNT diameter was less than 1.5%. The variance in the estimated natural frequency of the linear flexural bearing was about 21%. The relatively high magnitude of the variance is likely due to the fact that any variances in the CNT

geometric characteristics increase the variance in the natural frequency of the device because errors are raised to the fourth power.

5.6 Design of a Switch with Specified Natural Frequency

There are many applications wherein the switching frequency is of great importance. For example, the bandwidth at which relays and non–volatile memory may operate is set by the switching frequency. This in turn affects the speed at which many electronic devices such as computers may operate. An example of a CNT-based switch may be seen in Figure 5.3. This switch relies upon the lateral bending of three vertical MWCNTs to create electrical contacts. The outermost CNTs have opposite potentials applied to them while the central CNT has a selected potential applied to it. The central CNT therefore feels an attractive electrostatic force to one of the outer CNTs. The attractive force between CNTs 1 and 2 causes them to come into contact thereby making an electrical connection and turning the switch on.

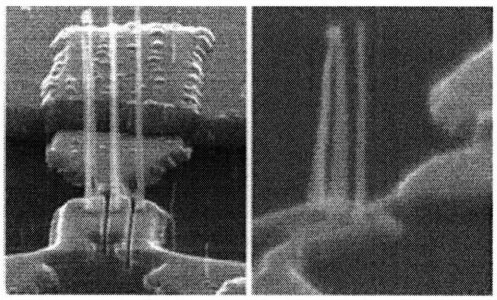

Figure 5.3. CNT-based Switch [3].
Reprinted with permission from the American Institute of Physics Copyright 2005

The natural frequency at which a CNT–based cantilever switch may operate is given by Equation 5.7. In this equation, β is equal to 1.875 for a cantilever [2]. In this design scenario, the desired switching frequency was 12 GHz for a 100 nm long cantilever switch. Equations 5.1, 5.2 and 5.6 were used to set the standard catalyst film thickness that should produce CNTs that possess a natural frequency which is closest to the desired natural frequency. For 12 GHz, a film thickness of 1 nm was selected. Given this thickness, the set of possible growths that satisfy the frequency requirement was

determined. This set of possible growth conditions is shown in Table 5.9. The temperature was set in 10°C increments and the methane concentration was obtained via Equations 5.1, 5.2, and 5.7.

Table 5.9 Possible Growth Conditions for a Switch with a Natural Frequency of 12 GHz

Condition Number	Catalyst Film Thickness (nm)	Temperature (°C)	Concentration (%)
1	1	830	101.5
2	1	820	94.8
3	1	810	90.1
4	1	800	86.5
5	1	790	83.5
6	1	780	80.9
7	1	770	78.7
8	1	760	76.8
9	1	750	75.2
10	1	740	73.7
11	1	730	72.4
12	1	720	71.2
13	1	710	70.2
14	1	700	69.3

Growth condition number nine was selected because it was the growth condition that minimized the Gibbs free energy. For this growth condition, the CNT diameter was estimated to be 36.3 nm and the wall thickness was estimated to be 9.1 nm. The measured results are listed in Table 5.10.

Table 5.10. Results of Growth CNTs Designed for Switch with a Natural Frequency of 12 GHz

	Desired	Measured	Error
Outside Diameter	36.3 nm	36.1 3.1 nm	0.55%
Wall Thickness	9.1 nm	9.2 0.8 nm	1.10%
Switch Frequency	12 GHz	11.9 1.2 GHz	0.83%

The average difference between the measured and the desired CNT diameter and wall thickness was less than 1.1%, which is within the experimental error. The maximum variance in the measured geometric characteristics of the CNTs was 8.7%. This value is relatively small given the small size of the CNTs. The small magnitude of the variance may again be attributed to the use of the thermodynamic theory.

Given the measured values of CNT diameter/thickness, the average error between the estimated switch frequency and the desired switch frequency was less than 1%. The variance in the estimated switch frequency was only 10%. This may be attributed to the fact that the variances in the geometric characteristics of the CNT were low. As in the example of the resonator, the errors in the stiffness that are caused by errors in the geometry are partially offset by the change in mass; therefore the error in the estimated frequency was relatively small.

5.7 Rules for Designing CNT Growths for Applications

The five examples in the preceding sections were used to generate several rules that may be used when designing CNT growths for specific applications. These rules are listed below as a procedure for designing CNT growths for specific applications.

1. Select the desired outcome of the growth, for example the specific CNT geometry, device stiffness, or natural frequency.

2. Eliminate catalyst film thickness as a variable by selecting a standard film thickness that should produce CNTs that closely match the desired output when the midrange growth temperature of 800°C and methane concentration of 68.5% are used. This reduces the time and cost of the growth because a standard film thickness may be used. This is important because the catalyst film deposition step is the most time consuming and costly step in the growth process.

3. Determine the set of growth conditions that will produce the desired output by calculating the required methane concentration at different values of growth temperature. Equations 5.1 and 5.2 are used to perform this calculation.

4. If possible, that is if only one CNT property such as stiffness or natural frequency is being set, select the growth condition from the set of possible growth conditions that were generated in step 3 as to minimize the Gibbs free energy. This will help

to minimize the variance in the CNT geometric characteristics as discussed in Chapter 4.

The preceding design rules and method, in combination with the design equations that were derived in Chapter 3, may be used to design and fabricate CNTs growths that produce a desired CNT geometry. The precision of the growths is affected by how tightly the process parameters are controlled. As shown in Chapter 3, the major source of variance within a CNT growth is the dewetting of the catalyst film into discrete nanoparticles. This source of variance is important because of the sensitivity of the performance to variations in the CNT diameter/thickness. Specifically, the errors in geometry that are caused by this source of error are related to the performance criteria via relationships where the errors are squared or raised to the fourth power. The preceding examples show that reasonable results may be obtained with modest control of process parameters, but it may become necessary to develop more precise methods of catalyst particle deposition for more demanding applications.

Chapter

6

Conclusion

6.1 Summary and Conclusions

The purpose of this research is to a growth method and a procedure that may be used to grow CNTs with specific performance characteristics. This research has shown that is possible to control the geometry of CNTs within 10% by tuning the process parameters that are used to fabricate them. This is important because it will enable us to design and build CNT-based compliant mechanisms such as flexural bearings, resonators and switches so that they possess specific performance characteristics. The ability to control the flexural characteristics of CNTs are envisioned to enable engineers to set process parameters, and thereby create/assemble CNTs as custom mechanical elements for nanomechanical systems. More broadly, this will enable the creation of nanoelectromechanical systems that possess the ability to run at bandwidths that exceed 10s of GHz and strokes that exceed 25% of the characteristic device size [73].

6.2 Summary

The work presented in this thesis is a first step toward a larger study that aims to ascertain how to rapidly and accurately engineer CNT-based nanoelectromechanical systems. The main findings of the work are as follows:

1. The diameter and wall thickness of CNTs that are grown by CVD may be controlled by setting the proper growth conditions as shown in Chapter 5.
2. The diameter of the CNT is set by the size of the catalyst particle that is used to grow the CNT. The size of the catalyst particle is strongly dependent upon the catalyst film thickness and weakly dependent upon the growth temperature.
3. The CNT's wall thickness increases as the CNT's outside diameter, growth temperature and methane concentration increase.
4. The dependence of the CNT's outside diameter on the process conditions was derived in Chapter 3 and is given by Equation 6, wherein D is the outside diameter, F is the catalyst film thickness, and T is the growth temperature.

$$D = 43.72\ln(F) + 0.0484T \qquad (6.1)$$

5. The CNT's wall thickness is dependant upon the process conditions that are given by Equation 6.2, wherein C is the methane concentration.

$$\text{Wall Thickness} = -38.28 + 0.307D + 0.0316T + 0.166C \qquad (6.2)$$

6. A thermodynamic growth theory may be used to explain the dependence of the CNT wall thickness on the outside diameter of the CNT.
7. The kinetic growth theory may be used to explain the dependence of a CNT's wall thickness on the growth temperature and methane concentration.
8. The variance in the CNT geometry within a sample that possesses a specific stiffness, or natural frequency, may be minimized by setting the growth conditions to minimize the Gibbs free energy of the CNTs.

This work has shown that it is possible to set the geometry of CNTs by controlling the conditions under which they are grown. This is important for the creation of nano-scale compliant mechanisms because the stiffness of the CNTs is strongly dependent upon the CNTs' geometry. It is necessary to be able to control the stiffness of MWCNTs in such mechanisms because the force, stroke, and bandwidth depend upon the stiffness. The control of the MWCNTs' stiffness enables one to design and fabricate

MWCNT-based compliant mechanisms with the desired force, stroke, stiffness, and bandwidth characteristics.

6.3 Future Work

The next major step in the development of CNT-based compliant mechanisms is to build a prototype device. This will help us to better understand the mechanics and potential limitations of CNT-based compliant mechanisms. There are several challenges, however, that must be overcome before a prototype may be built. For example, one major challenge is the bonding of the CNT to the substrate. A commonly used technique for bonding a CNT to a substrate is to use electron beam lithography to selectively deposit a thin film of gold onto the CNT and thereby create an anchor [74]. This is analogous to soldering or brazing. This technique is commonly used for device fabrication because it may be used to quickly anchor many CNTs. Unfortunately, no strength measurements have been performed on these types of bonds and so it is unknown how these anchors would affect the device performance, or if the CNT geometry would need to be adjusted to account for related effects.

Another common anchoring method is electron-beam induced deposition (EIBD) of carbon [75] or gold [76]. In this method, an electron beam is focused on to the CNT where the anchor is desired. The electrons from the electron beam then collide with hydrocarbons or organometallic molecules that have been injected into the vacuum chamber and this causes the carbon or metal atoms to split from the vapor molecules. The carbon or metal is then absorbed onto the substrate to create a bond between the substrate and the CNT [75]. This bond provides good electrical and mechanical contact between the substrate and the CNT. The bonding process is slow because the deposition rate is generally on the order of only a few nanometers per minute. The bond has been measured to be able to withstand shear stresses between the CNT and the substrate of over 200 MPa [76] and axial forces that exceed 100 μm [75]. Several other bonding techniques – such as ultrasonic welding, heat welding and the growth of silicon oxide over the CNT – have been demonstrated for CNTs. Unfortunately, each of these

techniques tends to damage the CNT, thereby having a negative effect upon their mechanical properties.

All of these techniques have been used for several years to bond CNTs to substrates, however little is known about how these bonds will effect the performance of CNT-based mechanical devices. In all of the calculations that were performed in this study, the bond between the CNT and the substrate was assumed to be perfect. It is understood that the range of motion, or the stiffness, for real devices may be strongly affected by the strength and stiffness of the bond between the CNT and the substrate. More testing of the CNT-substrate bonds must be done in order to determine how the anchoring of the CNT will affect device performance.

Another major concern in the development of CNT-based compliant mechanisms is how to accuracy and precisely place CNTs onto a patterned device structure. CNTs may be assembled into structures in one of two ways, either pick-and-place or grow-in-place. In pick-and-place, a probe is brought into contact with a CNT which then becomes attached the probe by van der Waals forces. The CNT may then be moved to the desired location and fixed in place by depositing a metal or amorphous carbon layer on top of the CNT. The probe may then be removed because the van der Waals forces are smaller than the bonding force. This method allows the CNTs to be placed accurately but this is a slow process. The pick-and-place method may be useful for building a prototype, but it is not ideal for the mass production of CNT-based compliant mechanisms.

The grow-in-place method is faster, but it is also harder to control. In general, attempts that aim to control the location and direction of the CNT growth have focused upon defining the location of the catalyst and the structure around the initial growth location. Unfortunately, even with well-defined growth locations, it is hard to control which direction the CNTs will grow. One way to overcome this is to use an electric field to direct the growth. The high polarizability of CNTs makes it possible to create a large dipole moment in the CNT when the CNT is placed in an electric field. This dipole moment produces large aligning torques and forces on the nanotube, thereby causing the CNT to align in the direction of the electric field. If an electric field is used, a CNT may be grown in place to create a nano-scale device.

While the grow-in-place method permit rapid placement of CNTs onto the substrate, it is not as precise or accurate in the placement of the CNTs as the pick-and-place method. For example, it is hard to control the number of CNTs that grow from a catalyst spot. As a result, more than one CNT may be placed at a specific location, thereby increasing the stiffness of that compliant member. It is also difficult to control the spacing between CNTs that are grown in place and this may affect the kinematics of the compliant mechanism. More research is required in order to better understand how to create a process that may be used to place CNTs into a device structure both accurately and quickly.

While there are challenges that must be overcome with regards to the placement and the attachment of CNTs to substrates, the work presented in this thesis offers an important first step in the development of CNT-based compliant mechanism. More research must be completed in order to determine how to best fit CNTs into MEMS and NEMs devices, and how the bond between the CNT and the substrate will affect the device performance. Once these questions have been answered, the path is clear for CNT-based compliant mechanisms to become important components of devices with new and/or markedly improved performance. Examples include metrology systems, nanomanufacturing systems, force-displacement transducers, nano-scale sensors and actuators, resonators, non-volatile memory, switches, and nano-scale flexural bearings.

Appendix A

Lab View Program for the Operation of the CNT Furnace

In this program, one channel is used to measure the voltage across the thermocouple and output the temperature of the furnace. Two other channels are used to measure the argon and methane flow rates so that the proper methane concentration may be maintained throughout the growth process. Finally, two channels are used to turn on and off the methane and argon flows at different points in the growth process. This allows the growth and purge times to be accurately controlled.

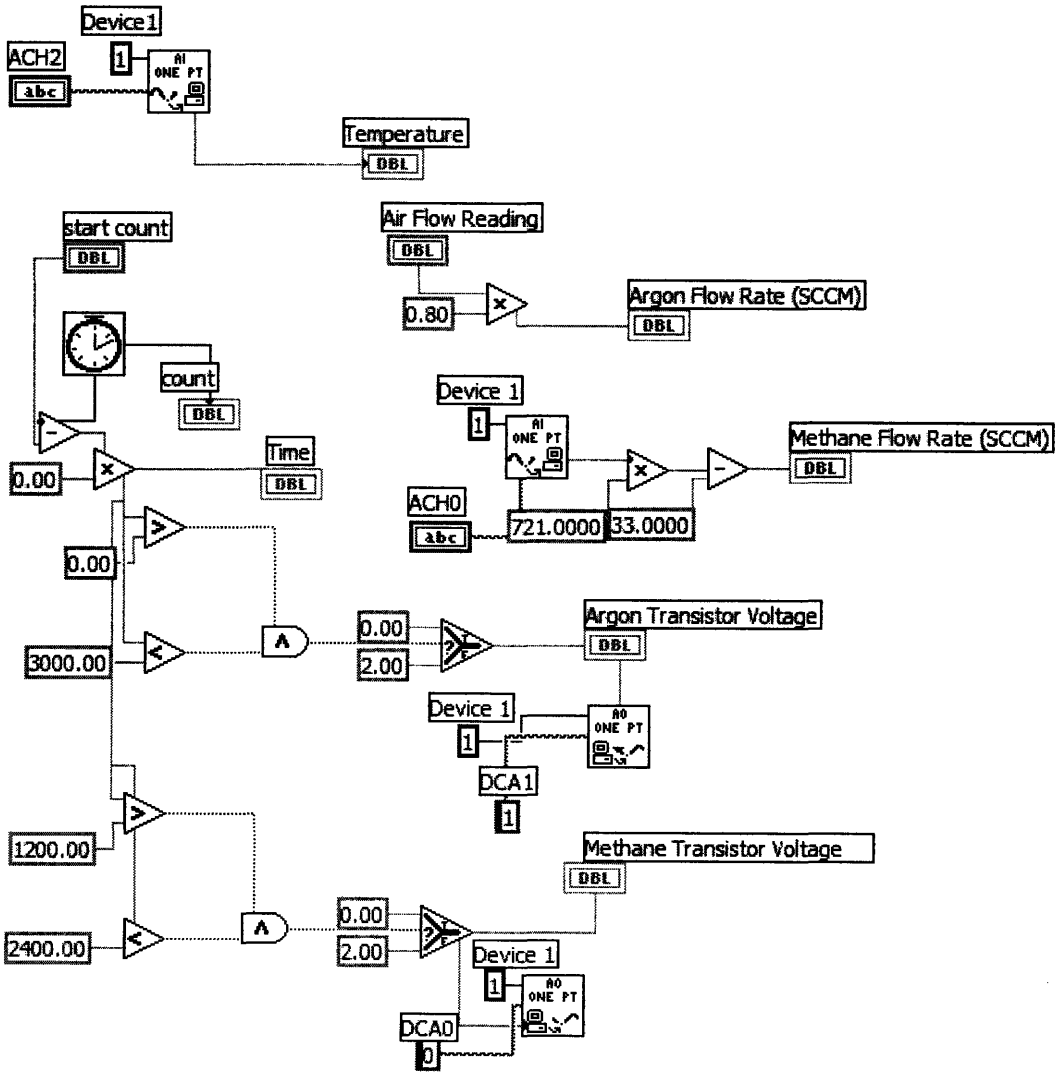

Appendix B

Data Collected on CNT Diameters and Wall Thicknesses

In this appendix, the raw data that was collected for this growth study is presented. The outside diameter and wall thickness data for each point was measured in a TEM. Over 400 data points were taken for this study. From this data, regressions were performed to extract the relationships the growth process parameters and the CNT geometry. These relationships were then used to design growths for specific applications.

Run	Catalyst Film Thickness	Temperature	Concentration	Outside diameter	Wall Thickness
1	1	740	55	46.3	10.18
1	1	740	55	38.7	9.69
1	1	740	55	23.7	5.70
1	1	740	55	33.8	8.10
1	1	740	55	36.9	9.60
1	1	740	55	42.4	11.70
1	1	740	55	50.0	13.60
1	1	740	55	39.3	10.25
1	1	740	55	38.6	9.45
1	1	740	55	35.4	7.80
1	1	740	55	46.3	10.18
1	1	740	55	38.7	9.69
1	1	740	55	23.7	5.70
1	1	740	55	33.8	8.10
1	1	740	55	36.9	9.60
1	1	740	55	42.4	11.70
1	1	740	55	50.0	13.60
1	1	740	55	39.3	10.25
1	1	740	55	38.6	9.45
1	1	740	55	35.4	7.80
1	1	740	55	46.3	10.18
1	1	740	55	38.7	9.69
1	1	740	55	23.7	5.70
1	1	740	55	33.8	8.10
1	1	740	55	36.9	9.60
1	1	740	55	42.4	11.70
1	1	740	55	50.0	13.60
1	1	740	55	39.3	10.25
1	1	740	55	38.6	9.45
1	1	740	55	35.4	7.80

2	1	860	55	34.6	3.90
2	1	860	55	24.3	3.80
2	1	860	55	29.3	10.10
2	1	860	55	35.3	10.05
2	1	860	55	34.0	10.30
2	1	860	55	33.4	8.05
2	1	860	55	26.7	8.45
2	1	860	55	27.6	7.70
2	1	860	55	29.1	7.95
2	1	860	55	29.0	7.70
2	1	860	55	37.7	12.75
2	1	860	55	39.0	12.35
2	1	860	55	31.8	9.10
2	1	860	55	32.0	4.95
2	1	860	55	38.8	6.85
2	1	860	55	47.7	15.60
2	1	860	55	35.5	8.80
2	1	860	55	28.8	5.28
2	1	860	55	31.6	6.05
2	1	860	55	35.1	10.55
2	1	860	55	30.4	7.60
2	1	860	55	21.3	4.40
2	1	860	55	21.8	5.10
2	1	860	55	38.1	11.26
2	1	860	55	34.4	9.70
2	1	860	55	33.2	8.30
2	1	860	55	38.0	8.70
2	1	860	55	29.9	7.15
2	1	860	55	31.6	7.10
3	5	740	55	122.5	20.45
3	5	740	55	139.9	41.20
3	5	740	55	132.3	19.75
3	5	740	55	114.8	29.20
3	5	740	55	104.7	20.85
3	5	740	55	92.6	26.60
3	5	740	55	83.3	16.05
3	5	740	55	134.2	31.20
3	5	740	55	122.0	34.60
3	5	740	55	81.8	16.20
3	5	740	55	112.8	18.00
3	5	740	55	113.8	16.58
3	5	740	55	107.3	15.40
3	5	740	55	130.3	34.40
3	5	740	55	133.3	41.78
3	5	740	55	111.0	25.85
3	5	740	55	125.2	35.40
3	5	740	55	126.5	27.25
3	5	740	55	102.8	17.80

3	5	740	55	112.7	24.65
3	5	740	55	105.0	31.55
3	5	740	55	57.3	17.55
3	5	740	55	81.3	19.10
3	5	740	55	96.2	19.65
3	5	740	55	110.5	15.70
3	5	740	55	123.0	33.65
3	5	740	55	122.8	28.25
3	5	740	55	106.7	22.70
3	5	740	55	143.8	51.55
4	5	860	55	149.0	43.60
4	5	860	55	105.8	19.70
4	5	860	55	138.0	44.10
4	5	860	55	138.1	41.05
4	5	860	55	122.0	35.70
4	5	860	55	75.5	21.05
4	5	860	55	176.8	63.65
4	5	860	55	98.7	29.95
4	5	860	55	115.8	38.50
4	5	860	55	137.8	47.05
4	5	860	55	109.3	37.68
4	5	860	55	139.6	49.30
4	5	860	55	153.5	50.85
4	5	860	55	138.3	42.15
4	5	860	55	109.1	30.30
4	5	860	55	161.3	53.75
4	5	860	55	109.8	32.95
4	5	860	55	177.0	62.30
4	5	860	55	134.3	44.23
4	5	860	55	94.9	36.00
4	5	860	55	145.3	40.70
4	5	860	55	117.8	39.35
4	5	860	55	140.7	42.25
4	5	860	55	81.4	25.45
4	5	860	55	157.0	51.70
4	5	860	55	97.4	23.00
4	5	860	55	115.7	28.00
4	5	860	55	102.8	22.10
4	5	860	55	138.0	45.60
4	5	860	55	81.4	22.10
5	1	740	82	35.8	10.40
5	1	740	82	37.8	9.90
5	1	740	82	48.9	11.95
5	1	740	82	32.6	9.30
5	1	740	82	52.7	14.85
5	1	740	82	37.6	9.80
5	1	740	82	40.9	10.95
5	1	740	82	39.3	8.15

5	1	740	82	35.7	10.85
5	1	740	82	34.4	8.20
5	1	740	82	32.8	8.90
5	1	740	82	48.9	13.95
5	1	740	82	40.9	11.45
5	1	740	82	36.3	9.65
5	1	740	82	37.5	11.75
5	1	740	82	35.8	10.40
5	1	740	82	37.8	9.90
5	1	740	82	48.9	11.95
5	1	740	82	32.6	9.30
5	1	740	82	52.7	14.85
5	1	740	82	37.6	9.80
5	1	740	82	40.9	10.95
5	1	740	82	39.3	8.15
5	1	740	82	35.7	10.85
5	1	740	82	34.4	8.20
5	1	740	82	32.8	8.90
5	1	740	82	48.9	13.95
5	1	740	82	40.9	11.45
5	1	740	82	36.3	9.65
5	1	740	82	37.5	11.75
6	1	830	82	52.9	13.20
6	1	830	82	28.5	6.42
6	1	830	82	39.9	9.12
6	1	830	82	34.5	7.11
6	1	830	82	47.8	13.30
6	1	830	82	38.5	10.01
6	1	830	82	42.4	12.15
6	1	830	82	33.7	11.20
6	1	830	82	28.4	9.00
6	1	830	82	49.1	12.51
6	1	830	82	45.4	13.07
6	1	830	82	35.6	10.64
6	1	830	82	53.3	15.26
6	1	830	82	27.6	6.06
6	1	830	82	41.0	8.40
6	1	830	82	33.3	9.61
6	1	830	82	45.0	11.46
6	1	830	82	34.8	6.35
6	1	830	82	33.1	8.86
6	1	830	82	29.2	8.26
6	1	830	82	37.3	7.67
6	1	830	82	31.0	6.35
6	1	830	82	36.0	8.05
6	1	830	82	42.3	10.67
6	1	830	82	29.1	5.40
6	1	830	82	25.4	9.09

6	1	830	82	47.8	12.25
6	1	830	82	39.7	12.25
6	1	830	82	40.4	11.20
6	1	830	82	28.4	7.46
7	5	740	82	79.8	21.80
7	5	740	82	89.5	27.60
7	5	740	82	86.8	35.90
7	5	740	82	114.1	47.00
7	5	740	82	98.3	21.70
7	5	740	82	77.3	29.50
7	5	740	82	106.3	31.80
7	5	740	82	100.3	36.60
7	5	740	82	112.0	12.20
7	5	740	82	89.9	17.70
7	5	740	82	98.3	27.10
7	5	740	82	90.7	19.10
7	5	740	82	90.3	28.50
7	5	740	82	82.1	26.90
7	5	740	82	113.4	27.30
7	5	740	82	89.6	25.40
7	5	740	82	101.3	42.30
7	5	740	82	77.1	20.00
8	5	830	82	119.4	49.03
8	5	830	82	107.4	38.69
8	5	830	82	103.1	38.94
8	5	830	82	97.9	35.70
8	5	830	82	122.5	45.16
8	5	830	82	114.1	44.13
8	5	830	82	127.7	45.84
8	5	830	82	113.3	43.94
8	5	830	82	102.0	32.92
8	5	830	82	128.4	41.91
8	5	830	82	123.1	48.75
8	5	830	82	116.4	41.91
8	5	830	82	115.2	37.50
8	5	830	82	121.1	46.88
8	5	830	82	108.8	42.28
8	5	830	82	119.4	49.03
8	5	830	82	107.4	38.69
8	5	830	82	103.1	38.94
8	5	830	82	97.9	35.70
8	5	830	82	122.5	45.16
8	5	830	82	114.1	44.13
8	5	830	82	127.7	45.84
8	5	830	82	113.3	43.94
8	5	830	82	102.0	32.92
8	5	830	82	128.4	41.91
8	5	830	82	123.1	48.75

8	5	830	82	116.4	41.91
8	5	830	82	115.2	37.50
8	5	830	82	121.1	46.88
8	5	830	82	108.8	42.28
9	3	700	68.5	111.6	36.82
9	3	700	68.5	45.3	9.11
9	3	700	68.5	72.6	21.79
9	3	700	68.5	75.3	12.57
9	3	700	68.5	75.2	17.69
9	3	700	68.5	92.3	26.04
9	3	700	68.5	112.7	21.87
9	3	700	68.5	99.0	29.08
9	3	700	68.5	47.7	12.00
9	3	700	68.5	73.0	17.92
9	3	700	68.5	74.6	21.26
9	3	700	68.5	73.3	18.60
9	3	700	68.5	94.9	20.80
9	3	700	68.5	109.2	23.99
9	3	700	68.5	107.8	29.00
9	3	700	68.5	92.9	26.42
9	3	700	68.5	92.5	24.41
9	3	700	68.5	41.2	10.59
9	3	700	68.5	52.2	10.78
9	3	700	68.5	67.3	20.04
9	3	700	68.5	105.1	24.83
9	3	700	68.5	63.5	23.16
9	3	700	68.5	78.4	17.01
9	3	700	68.5	71.2	17.84
9	3	700	68.5	110.2	27.49
9	3	700	68.5	66.2	22.40
9	3	700	68.5	110.9	32.27
9	3	700	68.5	69.7	15.03
9	3	700	68.5	62.7	14.35
10	3	880	68.5	105.0	35.50
10	3	880	68.5	122.2	46.04
10	3	880	68.5	101.7	35.50
10	3	880	68.5	86.8	21.30
10	3	880	68.5	64.2	17.25
10	3	880	68.5	115.3	39.60
10	3	880	68.5	74.5	21.28
10	3	880	68.5	86.7	26.30
10	3	880	68.5	111.6	32.60
10	3	880	68.5	144.8	33.53
10	3	880	68.5	94.0	32.53
10	3	880	68.5	95.8	33.25
10	3	880	68.5	73.5	21.58
10	3	880	68.5	74.2	22.80
10	3	880	68.5	91.7	19.50

10	3	880	68.5	75.2	23.85
10	3	880	68.5	73.9	20.53
10	3	880	68.5	134.3	30.38
10	3	880	68.5	52.6	18.85
10	3	880	68.5	122.8	43.93
10	3	880	68.5	61.2	21.75
10	3	880	68.5	72.3	24.48
10	3	880	68.5	89.1	22.70
10	3	880	68.5	71.0	22.38
10	3	880	68.5	59.0	17.78
10	3	880	68.5	74.1	27.30
10	3	880	68.5	61.0	16.73
11	0.5	780	68.5	17.9	3.30
11	0.5	780	68.5	12.8	3.65
11	0.5	780	68.5	14.5	3.86
11	0.5	780	68.5	17.2	3.03
11	0.5	780	68.5	14.3	3.60
11	0.5	780	68.5	18.7	5.20
11	0.5	780	68.5	18.2	4.95
11	0.5	780	68.5	14.4	4.21
11	0.5	780	68.5	9.9	3.33
11	0.5	780	68.5	17.5	5.08
11	0.5	780	68.5	17.9	3.30
11	0.5	780	68.5	12.8	3.65
11	0.5	780	68.5	14.5	3.86
11	0.5	780	68.5	17.2	3.03
11	0.5	780	68.5	14.3	3.60
11	0.5	780	68.5	18.7	5.20
11	0.5	780	68.5	18.2	4.95
11	0.5	780	68.5	14.4	4.21
11	0.5	780	68.5	9.9	3.33
11	0.5	780	68.5	17.5	5.08
11	0.5	780	68.5	17.9	3.30
11	0.5	780	68.5	12.8	3.65
11	0.5	780	68.5	14.5	3.86
11	0.5	780	68.5	17.2	3.03
11	0.5	780	68.5	14.3	3.60
11	0.5	780	68.5	18.7	5.20
11	0.5	780	68.5	18.2	4.95
11	0.5	780	68.5	14.4	4.21
11	0.5	780	68.5	9.9	3.33
11	0.5	780	68.5	17.5	5.08
13	3	800	37	82.8	15.61
13	3	800	37	79.6	13.23
13	3	800	37	59.1	12.43
13	3	800	37	87.3	15.77
13	3	800	37	83.7	14.15
13	3	800	37	70.9	10.85

13	3	800	37	94.3	12.32
13	3	800	37	102.6	12.20
13	3	800	37	113.9	18.54
13	3	800	37	117.6	17.20
13	3	800	37	76.7	13.90
13	3	800	37	79.4	14.33
13	3	800	37	63.7	14.57
13	3	800	37	71.2	10.91
13	3	800	37	54.0	8.17
13	3	800	37	75.4	11.71
13	3	800	37	102.7	17.26
13	3	800	37	51.7	6.16
13	3	800	37	61.1	10.06
13	3	800	37	62.1	13.11
13	3	800	37	94.0	12.20
13	3	800	37	58.5	16.28
13	3	800	37	63.5	10.00
13	3	800	37	98.3	12.62
13	3	800	37	98.2	8.96
13	3	800	37	98.7	9.27
14	3	785	100	54.1	17.59
14	3	785	100	77.5	25.79
14	3	785	100	129.8	29.19
14	3	785	100	80.5	27.14
14	3	785	100	102.7	39.57
14	3	785	100	81.8	24.52
14	3	785	100	31.1	10.91
14	3	785	100	102.7	31.94
14	3	785	100	81.5	25.44
14	3	785	100	35.6	11.19
14	3	785	100	131.7	36.98
14	3	785	100	108.2	43.67
14	3	785	100	105.8	28.82
14	3	785	100	102.0	22.35
14	3	785	100	79.5	22.06
14	3	785	100	87.1	31.90
14	3	785	100	81.4	25.58
14	3	785	100	128.7	37.47
14	3	785	100	75.4	21.81
14	3	785	100	107.3	31.24
14	3	785	100	59.9	20.50
14	3	785	100	84.8	22.10
14	3	785	100	84.8	22.10
14	3	785	100	62.5	20.66
14	3	785	100	66.3	20.05
14	3	785	100	67.9	18.61
14	3	785	100	128.7	32.39
14	3	785	100	56.9	16.15

14	3	785	100	61.2	16.81
14	3	785	100	54.1	14.06
15	3	780	68.5	92	25.2
15	3	780	68.5	100.4	25.4
15	3	780	68.5	84.1	30.1
15	3	780	68.5	73.3	14.45
15	3	780	68.5	90.4	19.2
15	3	780	68.5	76.2	24.7
15	3	780	68.5	72.5	23.1
15	3	780	68.5	69.3	20.8
15	3	780	68.5	105	28.1
15	3	780	68.5	71.8	17.7
15	3	780	68.5	98.3	26.75
15	3	780	68.5	78.94	25.62
15	3	780	68.5	64.8	17.2
15	3	780	68.5	71.2	22.45
15	3	780	68.5	65	24.75
15	3	780	68.5	82.2	23.3
15	3	780	68.5	91.3	32.05
15	3	780	68.5	74.4	27.2
15	3	780	68.5	79.7	25.3
15	3	780	68.5	88.7	27.95
15	3	780	68.5	96.9	31.4
15	3	780	68.5	83.7	29.75
15	3	780	68.5	65.3	21.65
15	3	780	68.5	73.6	26.95
15	3	780	68.5	90.5	30.95
15	3	780	68.5	62.5	18.95
15	3	780	68.5	81.3	26.4
15	3	780	68.5	80.9	24.7
15	3	780	68.5	95.8	29.85
15	3	780	68.5	100.8	28.8

References

[1] Beltrami I, Joseph C, Clavel R, Bacher J, and S. Bottinelli, "Micro and Nano Discharge Machining," *Journal of Materials Processing Technology*, Vol. 149, (2004), pp 263-265.

[2] Meirovitch L, Elements of Vibration Analysis. McGraw-Hill, New York, 1975.

[3] Jang J, Cha S, Choi Y, Amaratunga G, Kang D, Hasko D, Jung J, and Kim J. "Nanomechanical Switches with Vertically Aligned Carbon Nanotubes," *App. Phys. Lett.* Vol. 87, (2005), pp 163114-163114.

[4] Witkamp B, Poot M, and van der Zant H. "Bending-Mode Vibration of a Suspended Nanotube Resonator," Nano Letters, Vol. 6, (2006), pp 2904-2908.

[5] Uranga A, Teva J, Verd J, Lopez J, Torres F, Esteve J, Abdal G, Perez-Murano F, and Barniol N. "Fully CMOS Integrated Low Voltage 100 MHz MEMS Resonators," *Electronics Letters*, Vol. 41, (2005), pp 1327-1328.

[6] DiBiasio C. Design and Modeling of Carbon Nanotube Based Compliant Mechanisms. MIT Masters Thesis, Cambridge, MA, 2007.

[7] Saito R, Dresselhaus G, and Dresselhaus M. Physical Properties of Carbon Nanotubes. Imperial College Press, London, 2005.

[8] Li C, and Chou T. "A Structural Mechanics Approch for the Analysis of Carbon Nanotubes." *Int. J. Sol. and Structures*, Vol. 40, (2003), pp 2487-2499.

[9] M. Meyyappan, ed. Carbon Nanotubes: Science and Applications. CRC Press, Boca Raton 2005.

[10] Ekinci K.,Huang X, and Roukes M. "Ultrasensitive Nanomechanical Mass Detection" *Applied Physics Letters*, Vol. 84, (2004) pp 4469-4471.

[11] Ilic B, Czplewski D, Zalalutdinov, Craighead H, Neuzial P, Campagnolo C, and Batt C, "Single Cell Detection with Micromechanical Oscillators," *J. Vac. Sci. Tecnol. B.*, Vol. 19, (2001), pp 2825-2828.

[12] Huang X, Zorman C, Mehregany M, and Roukes M, "Nanoelectromechanical Systems: Nanodevice Motion at Microwave Frequencies", *Nature*, Vol. 421, (2003), pp 496-497.

[13] Yang Y, Ekinci L, Huang M, Schiavone L, Roukes M, Zorman C, and Mehregany M, "Monocrystaline Silicon Carbide nanoelectromechanical Systems," *Applied Physics Letters*, Vol. 78, (2001), pp 162-164.

[14] Yu M-F., Files B., Arepalli S. and Ruoff R., "Tensile loading of ropes of single wall carbon Nanotubes and their mechanical properties", *Physical Review Letters*, Vol. 84, Num. 24, (2000), pp 5552-5555.

[15] Lu J and Zhang L. "Analysis of localized failure of single–wall carbon nanotubes," *Comp. Mat. Sci.*, Vol. 35, (2006), pp 432–441.

[16] Petersen K. "Silicon as a Mechanical Material," *Proc. of the IEEE*, Vol. 70, (1982), pp 420-457.

[17] Demczyk B, Wang Y, Cumings J, Hetman M, Han W, Zettl A, and Ritchie R. "Direct Mechanical Measurment of the Tensile and Elastic Modulus of Multiwalled Carbon Nanotubes," *Materials Science and Engineering A*, Vol. A334, (2002), pp 173-178.

[18] Piner R, Zhu J, Xu F, Hong S, and Mirkin C. "Dip-Pen Nanolithography," *Science*, Vol. 283, (1999) pp 661-663.

[19] Hua F, Sun Y, Gaur A, Meitl M, Bilhaut L, Rotkina L, Wang J, Geil P, Shim M, Rogers J, and Shim A. "Polymer Imprint Lithography with Molecular Scale Resolution," *Nano. Lett.*, Vol. 4 (2004), pp 2467-2471.
[20] Homma Y, Kobayashi Y, Ogino T, and Yamashita T. "Growth of Suspended Nanotube Networks on 100-nm-Scale Silicon Pillars," *Applied Physics Letters*, Vol. 81, (2002), pp 2261-2263.
[21] Cassell A, Franklin N, Tombler T, Chan E, Han J, and Dai H, "Directed growth of Free-Standing Single-Walled Carbon Nanotubes" *Journal of the American Chemical Society*, Vol. 121, (1999), pp 7975-7976.
[22] Zhang Y, Chang A, Cao J, Wang Q, Kim W, Li Y, Morris N, Yenilmez E, Kong J, and Dai ., "Electric-Field-Directed Growth of Aligned Single-Walled Carbon Nanotubes," *Applied Physics Letters*, Vol. 79, (2001), pp 3155-3157.
[23] DiBiasio C., Cullinan M. and Culpepper M., "The Difference Between Bending and Stretching Moduli of Single-Walled Carbon Nanotubes Modeled as an Elastic Tube", *App. Phys. Lett.*, Vol. 90, Num. 20, (2007), pp 203116-203118.
[24] Kuo C, Bai A, Huang C, Li Y, Hu C, and Chen C. "Diameter Control of Multiwalled Carbon Nanotubes using Experimental Strategies," *Carbon*, Vol. 43, (2005), pp 2760-2768
[25] Saito K and Kuwana K. "Modeling CVD Synthesis of Carbon Nanotubes: Nanoparticle Formation from Ferrocene," *Carbon*, Vol. 43, (2005), pp 2088-2095.
[26] Kukovecz A, Mehn D, Nemes-Nagy E, Szabo R, and Kiricsi I. "Optimization of CCVD Synthesis Conditions for Single-Wall Carbon Nanotubes by Statistical Design of Experiments (DoE)," *Carbon*, Vol. 43, (2005), pp 2842-2849.
[27] Saito T and Inagaki M. "Optical Emission Studies on Chemical Species in an Arc Flame of Fullerene/Metalofullerene Generator," *Japanese Journal of Applied Physics*, Vol. 32, (1993), pp L954-L957.
[28] Thess A, Lee R, Nikolaev P, Dai H, Petit P, Robert J, Xu C, Lee Y, Kim S, Rinzler A, Colbert D, Scuseria G, Tomanek D, Fischer J and Smalley R. "Crystalline Ropes of Metallic Carbon Nanotubes," *Science*, Vol. 273, (1996) pp. 483-487.
[29] Yakobson B and Smalley R. "Fullerene Nanotubes: C1,000,000 and Beyond," *American Scientist*, Vol. 85, (1997), pp 324-337.
[30] O'Connell M. Carbon Nanotubes: Properties and Applications. Taylor and Francis, Boca Raton, 2006.
[31] Ando Y, Zhao X, Sugai T, and Kumar M. "Growing Carbon Nanotubes," *Materials Today*, Vol. 7, (2004), pp 22-29.
[32] Li W, Wang S, Yang S, Wen J, and Ren Z. "Controlled Growth of Carbon Nanotubes on Graphite Foil by Chemical Vapor Deposition," *Chem. Phys. Lett.*, Vol. 335, (2001), pp 141-149.
[33] Hofmann S, Ducati C, Roberts J, and Kleinsorge B. " Low-Temperature Growth of Carbon Nanotubes by Plasma-Enhanced Chemical Vapor Deposition," *Applied Physics Letters*, Vol. 83, (2003), pp 135-137.
[34] Meyyappan M, Delzit L, Cassell A, and Hash D. Carbon Naontube Growth by PECVD: A Review," *Plasma Sources Science and Technology*, Vol. 12, (2003),pp 205-216.
[35] Chung C, Kurtz A, Hongkun P, and Lieber C. "Diameter-Controlled Synthesis of Carbon Nanotubes," *J. Phys. Chem. B*, Vol. 106, (2002), pp 2429-2433.
[36] Choi Y, Shin Y, Lee Y, Lee B, Park G, Choi W, Lee N, and Kim J. "Controlling the Diameter, Growth Rate, and Density of Vertically Aligned Carbon Nanotubes

Synthesized by Microwave Plasma-Enhanced Chemical Vapor Deposition," *App. Phys. Lett.*, Vol. 76, Num. 17, (2000), pp 2367-2369.

[37] Chopra N and Hinds B. "Catalytic Size Control of Multiwalled Carbon Nanotube Diameter in Xylene Chemical Vapor Deposition Process," *Inorganica Chimica Acta*, Vol. 357, (2004), pp 3920-3926.

[38] Chhowalla M, Teo K, Ducati C, Rupesinghe N, Amaratunga G, Ferrari A, Roy D, Robertson J, and Milne W. "Growth Process Conditions of Aligned Carbon Nanotubes using Plasma Enhanced Chemical Vapor Deposition," *Journal of Applied Physics*, Vol. 90, (2001), pp 5308-5316.

[39] Chakrabarti S, Kume H, Pan L, Nagasaka T, and Nakayama Y. "Number of Walls Controlled Synthesis of Millimeter-Long Vertically Aligned Brushlike Carbon Nanotubes," *J. Phys. Chem. C*, Vol. 111, (2007), pp 1929-1934.

[40] Sharma R, Rez P, Brown M, Du G, and Treacy M. "Dynamic Observations of the Effect of Pressure and Temperature Conditions on the Selective Synthesis of Carbon Nanotubes," *Nanotechnology*, Vol. 18, 2007, pp 1-8.

[41] Sampedro-Tejedor P, Maroto-Valiente A, Nevskaia D, Munoz V, Rodreguez-Ramos I, and Guerrero-Ruez A. "Effect of Growth Temperature and Iron Precursor on the Synthesis of High Purity Carbon Nanotubes," *Diamond and Related Materials*, Vol. 16, (2007), pp 542-549.

[42] Lee Y, Park J, Choi Y, Ryu H, and Lee H. "Temperature-Dependent Growth of Vertically Aligned Carbon Nanotubes in the Range of 800-1100°C," *J. Phys. Chem. B*, Vol. 106, (2002), pp 7614-7618.

[43] Siegal M, Overmyer D, and Provencio P. "Precise Control of Multiwall Carbon Nanotube Diameters using Thermal Chemical Vapor Deposition." *Applied Physics Letters*, Vol. 80, (2002), pp 2171-2173.

[44] Kaatz F, Siegal M, Overmyer D, Provencio P, and Jackson J. "Diameter Control and Emission Properties of Carbon Nanotubes Grown using Chemical Vapor Deposition," *Materials Science and Engineering C*, Vol. 23, (2003), pp 141-146.

[45] Singh C, Shaffer M, and Windle A. "Production of Controlled architectures of Aligned Carbon Nanotubes by Injection Chemical Vapor Deposition Method," *Carbon*, Vol. 41, (2003), pp 359-368.

[46] Lee C, Park J, Huh Y, and Lee J. "Temperature Effect on the Growth of Carbon Nanotubes using Thermal Chemical Vapor Deposition," *Chemical Physics Letters*, Vol. 343, (2001), pp 33-38.

[47] Lu C and Liu J. "Controlling the diameter of Carbon Vapor Deposition Method by Carbon Feeding." *J. Phys. Chem. B*, Vol. 110, (2006), pp 20254-20257.

[48] Lee S, Lee D, Morjan R, Jhang S, Sveningsson M, Nerushev O, Park Y, and Campbell E. "A Three-Terminal Carbon Nanorelay," *Nano Lett.*, Vol. 4, (2004), pp 2027-2030.

[49] Rueckes T, Kim K, Joselevich E, Tseng G, Cheung C, and Lieber C. "Carbon Nanotube-Based Nonvolatile Random Access Memory for Molecular Computing," *Science*, Vol. 289, (2000), pp 94-97.

[50] Mateiu R, Davis Z, Madsen D, Molhave K, Boggild P, Russmusen A, Brorson M, Jacobsen C, and Boisen A. "An Approach to a Multi-Walled Carbon Nanotube Based Mass Sensor," *Microelectronic Engineering*, Vol. 73-74, (2004), pp 670-674.

[51] Meyer J, Paillet M, and Roth S. "Single Molecule Torsional Pendulum," *Science*, Vol. 309, (2005), pp 1539-1541.

[52] Papadakis S, Hall A, Williams P, Vicci L, Falvo M, Superfine R, and Washburn S. "Resonant Oscillators with Carbon Nanotube Torsion Springs," *Phys. Rev. Lett.* Vol. 93, (2004), pp 146101-1 – 146101-4.

[53] Hart A, Slocum A, and Royer L. "Growth of Conformal Single-Walled Carbon Nanotube Films from Mo/Fe/Al_2/O_3 Deposited by Electron Beam Evaporation," *Carbon*, Vol. 44, (2006), pp 348-359.

[54] Zhang Y, and Smith K. "A Kinetic Model of CH4 decomposition and Filamentous Carbon Formation on Supported Co Catalyst," *Journal of Catalysis*, Vol. 231, (2005), pp. 354-364.

[55] Hart A, Laake L, and Slocum A. "Desktop Growth of Carbon-Nanotube Monoliths In Situ Optical Imaging," *Small*, Vol. 3, (2007), pp 772-777.

[56] Laake L, Hart A, and Slocum A. "Suspended Heated Silicon Platform for Rapid Thermal Control of Surface Reactions with Application to Carbon Nanotube Synthesis," *Review of Scientific Instruments*, Vol. 78, (2007), pp. 083901-1 – 083901-9.

[57] Yang K. and El-Haik B., Design for Six Sigma: A Road Map for Product Development, 1st edition, McGraw Hill, (2003).

[58] Kuo C, Bai A, Huang C, Li Y, and Hu C, and Chen C. "Diameter Control of Multiwalled Carbon Nanotubes using Experimental Strategies" *Carbon*, Vol. 43, (2005), pp 2760-2768.

[59] Kukovecz A, Mehn D, Nemes-Nagy E, Szabo R, and Kiricsi I. "Optimization of CCVD Synthesis Conditions for Single-Walled Carbon Nanotubes by Statistical Design of Expiriments (DOE)," *Carbon*, Vol. 43, (2005), pp 2842-2849.

[60] Wheeler A and Ganji A. Introduction to Engineering Experimentation, Second Edition, Pearson Education, (2004).

[61] Schaffel F, Kramberger C, Rummeli M, Grimm D, Mohon E, Gemming T, Pichler T, Rellinghaus B, Buchner B, and Schultz L. "Nanoengineered Catalyst Particles as a Key for Tailor-Made Carbon Nanotubes." *Chem. Mater*, Vol. 19, (2007), pp 5006-5009.

[62] Cao G. Nanostructures and Nanomaterials: Synthesis, Properties and Applications. First Edition, Imperial College Press, London, 2004.

[63] Yamada T, Namai T, Futaba D, Mizuno K, Fan J, Yudasaka M, Yumura M and Iijima S. "Size-Slective Growth of Double Walled Carbon Nanotube Forests from Engineered Iron Catalysts," *Nature Nanotechnology*, Vol. 1, (2006), pp 131-139.

[64] Li C and Chou T. "A Structural Mechanics Approach for the Analysis of Carbon Nanotubes," *International Journal of Solids and Structures*, Vol. 40, (2003), pp 2487-2499.

[65] Tibbetts G. "Why Are Carbon Filiments Tubular?" *Journal of Crystal Growth*, Vol. 40, (1984), pp 632-638.

[66] Gilmer G. "Computer Models of Crystal Growth," *Science*, Vol. 208, (1980), pp 355-363.

[67] Zein S, Mohamed A, and Sai P. "Kinetic Studies on Catalytic Decomposition of Methane to Hydrogen and Carbon over Ni/TiO2 Catalyst," *Ind. Eng. Chem. Res.*, Vol. 43, (2004), pp 4864-4870.

[68] Gavillet J, Loiseau A, Journet C, Willaime F, Ducastelle F, and Charlier J. "Root-Growth Mechanism for Single-Wall Carbon Nanotubes," *Phys. Rev. Lett.*, Vol. 87, (2001), pp 275504-1-4.

[69] Seidel R, Duesberg G, Unger E, Graham A, Liebau M, and Kreupl F. "Chemical Vapor Deposition Growth of Single-Walled Carbon Nanotubes at 600 °C and a Simple Growth Model," *J. Phys. Chem. B*, Vol. 108, (2004), pp 1888-1893.

[70] Ding F, Bolton K, and Rosen A. "Iron-Carbide Cluster Thermal Dynamics for Catalyzed Carbon Nanotube Growth," *J. Vac. Sci. Technol. A*, Vol. 22, (2004), pp 1471-1476.

[71] Helveg S, Lopez-Cartes C, Sehested J, Hansen P, Clausen B, Rostrup-Nielsen J, Abild-Pedersen F, and Norskov J. "Atomic-Scale Imaging of Carbon Nanofibre Growth," *Nature*, Vol. 427, (2004), pp 426-429.

[72] Puretzky A, Geohegan D, Jesse S, Ivanov I, and Eres G. "In Situ Measurments and Modeling of Carbon Nanotube Array Growth Kinetics During Chemical Vapor Deposition," *Applied Physics A*, Vol. 81, (2005), pp 223-240.

[73] Cullinan M, DiBiasio C, Howell L, Culpepper M, and Panas R. "Modeling of a Clamped-Clamped Carbon Nanotube Flexural Element for Use in Nanoelectromechanical Systems," *13th National Conference on Mechanisms and Machines*, (2007), Paper # 126.

[74] Nygard J and Cobden D. "Quantum Dots in Suspended Single-Wall Carbon Nanotubes," *Applied Physics Letters*, Vol. 79, (2001), pp 4216-4218.

[75] Ding W, Dikin A, Chen X, Piner R, Ruoff R, Zussman E, Wang X, and Li X. "Mechanics of Hydrogenated Amorphous Carbon Deposits from Electron-Beam-Induced Deposition of a Paraffin Precursor," *Journal of Applied Physics*, Vol. 98, (2005), pp 014905-1 – 014905-7.

[76] Madsen D, Molhave K, Mateiu R, Rasmussen A, Brorson M, Jacobsen C, and Boggild P. "Soldering of Nanotubes onto Microelectronics," Nanoletters, (2003), pp 47-49.